Simon, Robert C.

A STUDY OF THE PHOTOCHEMISTRY AND PHOTOCATALYSIS OF GROUP VIB HEXACARBONYLS ADSORBED TO A POROUS GLASS MATRIX

City University of New York PH.D. 1984

A STUDY OF THE PHOTOCHEMISTRY AND PHOTOCATALYSIS OF GROUP VIB HEXACARBONYLS ADSORBED TO A POROUS GLASS MATRIX

by

ROBERT C. SIMON

A dissertation submitted to the
Graduate Faculty in Chemistry
in partial fulfillment of the
requirements for the degree of
Doctor of Philosophy, the City
University of New York.

1983

This manuscript has been read and accepted for the Graduate Faculty in Chemistry in satisfaction of the dissertation requirement for the degree of Doctor of Philosophy.

Dec 6 1983
date

Harry D. Gafney
Chairman of Examining Committee

29 November 1983
date

David C. Lacke
Executive Officer

Albato LaCava

T. Thomas C. Stefas
Supervisory Committee

The City University of New York

Abstract

A Study of the Photochemistry and Photocatalysis of Group VIB hexacarbonyls Adsorbed to a Porous Glass Matrix

by

Robert C. Simon

Advisor: Professor Harry D. Gafney

The Group VIB hexacarbonyls have been adsorbed onto transparent, porous Vycor glass, PVG, to investigate the photophysical and photochemical properties of the adsorbed complexes and their potential as photocatalysts of various reactions.

The bound hexacarbonyls retain spectral properties similar to those in fluid solution which suggests that the complexes are physisorbed. UV photolysis of $M(CO)_6$ads (M=Cr, Mo, and W) leads to the quantitative formation of the corresponding pentacarbonyls which have UV-visible spectra equivalent to spectra of these species generated in low-temperature matrices. The pentacarbonyls have lifetimes > 48 hours in vacuo at room temperature. Stability arises from coordination to the PVG, but does not occur at the expense of subsequent thermal and photochemical activity. The addition of either thoroughly degassed or vapor phase mono and bidentate ligands to the pentacarbonyl leads to the qualitative formation of $M(CO)_5$Lads or $M(CO)_4$Lads which were characterized by their absorption and emission spectra. Comparison of the kinetic and thermodynamic

parameters calculated from the rates of reaction of $M(CO)_5$ads with those from fluid solution studies suggest that the incoming ligand must overcome the apparent matrix bond the glass has with the pentacarbonyl.

Quantum yields for decomposition of $M(CO)_6$, which are dependent on the excitation wavelength, formation of $M(CO)_5$ads and various photoproducts were measured at 254, 310, and 350-nm.

Photolysis of $M(CO)_5$ads at 310 and 254-nm causes further CO evolution along with H_2, CH_4, and CO_2 evolution. Periodic examination of the gaseous effluent surrounding the photolyzed piece, in conjunction with spectral analysis, established that CH_4 evolution is mediated by a monomeric $M(CO)_4$ads species. The latter is irreversibly oxidized, and initially, the complex oxidized is in a 1:1 stoichiometric ratio with the CH_4 evolved. The hydrogen source is adsorbed H_2O since replacement with D_2O leads to CH_2D_2 and CHD_3 evolution. The metal complex is essential to CH_4 formation, but in contrast to what is assumed in the temperature programmed decomposition of the complexes on silica gel, isotopic labelling establishes that in these photochemical experiments CH_4 originates from carbonaceous residue in PVG rather than from coordinated CO.

The photocatalyzed isomerization and hydrogenation of olefins by these hybrid systems yields a distribution of products which contrasts with that found in solution and with other hybrid systems.

ACKNOWLEDGEMENTS

I would like to express my appreciation to my research director Dr. Harry D. Gafney for his assistance in the preparation of this thesis.

I would also like to thank the other members of the department who offered their assistance. Discussions with Dr. A. David Baker and his participation at our group meetings were helpful. Thanks to Dr. Thomas Strekas for his assistance and for the free access he granted to his instruments. To Mr. Thomas Hayden, thank-you for your generous assistance. To Mr. Hugo Shimatz and Mr. Ottmar Safferling for providing their services in the repair and construction of the esoteric glassware used throughout my work.

To my future wife and best friend Carol, thanks for helping me through the difficult times.

To my parents, thanks for helping me reach this point in my life.

TABLE OF CONTENTS

LIST OF TABLES

LIST OF FIGURES

Chapter 1

Introduction

A. General Introduction.

The search for more selective and efficient catalysts has dominated industrial research for a considerable period of time. To a significant extent, this effort has centered on the development of species which catalyze reactions of feedstocks derived from petroleum distillates. However, in recent years, particularly those following the oil embargo, research activity has grown to include the development of species which are capable of catalyzing the formation of commercially attractive organic molecules from feedstocks derived from coal, shale, and biomass. Although economically viable systems are not currently available, continued research is essential in view of the limited and constantly dwindling petroleum reserves.

Of the many avenues to new catalysts being explored, a particularly attractive approach is the use of transition metal carbonyls, which possess a number of advantages as catalytic species. First, they are commercially available or readily synthesized. Second, their structure and bonding are well characterized. Third, many form cluster compounds such that reactions requiring multiple metal sites might be accomplished. And fourth, since CO is a gas, it can be exploited as a renewable and readily labile ligand.

It is generally accepted that catalysis by transition metal carbonyls involves the absorption of a substrate

molecule to a vacant or loosely solvated site on a metal atom (1-5). In fluid solution, the coordinately unsaturated intermediate is highly reactive, and it is difficult to characterize. This is a serious disadvantage, since characterization is essential in developing a rational approach to an effective catalyst. The objective of the present research has been to explore the possibility of using a support to stabilize these reactive intermediates. In addition to stabilizing and possibly allowing characterization of these intermediates, the use of supported carbonyls has many advantages for catalytic applications. For example, these complexes have been widely used as homogeneous catalysts. In principle, homogeneous catalysis exploits the solubility of these complexes to intimately mix catalyst and reactant, but in practice suffers from the problem of separating the reaction mixture. As noted by Bailey and Langer (6) an attractive alternative is a hybrid catalyst where the catalytically active form of a metal carbonyl is bound to a support. This support must be inert to the reaction mixture, withstand the reaction conditions, and possess a large surface area. These criteria define acceptability with respect to a specific chemical reaction. However, since the intent of these experiments is to understand the immobilized species, its catalytic structure, and its catalyzed chemistry, then additional criteria must be applied. Specifically, the support must be amenable to experimental techniques which

can probe the chemistry of the immobilized species. The latter are often transient intermediates in the reaction sequence. In the past fifteen years, significant advances have occurred in instrumentation to probe surfaces and species adsorbed onto surfaces, but as yet, the surface scientist is unable to bring to bear the variety of instrumentation which has proven invaluable in characterization of species in fluid solution. Furthermore, few if any of these surface instruments have a time resolution sufficient to probe a catalytically active, coordinately unsaturated intermediate. Fast reaction techniques have proven invaluable in characterizing these species in fluid solution, but their application to supported or hybrid systems is difficult. The principle difficulty is the opacity of conventional supports such as silica gel, alumina, or metal oxides. Consequently, the support used in a hybrid system must not only satisfy criteria specific to a particular reaction system, as in the case in these experiments, but must be capable of probing reactive intermediates and their reaction pathways under a variety of conditions. For this latter reason, the present research was undertaken to explore the use of Corning's code no. 7930 porous Vycor glass, PVG, as a support.

B. A Summary of Thermally Activated Hybrid Supports.

The incorporation of a transition metal complex onto a solid support such as an organic polymer, inorganic oxide, or related material has attracted widespread attention.

Since homogeneous systems always have the problem of separation associated with them, interest in these types of systems has originated from the belief that these homogeneous catalysts could be immobilized to provide an economic competitor to traditional (7) heterogeneous systems. In addition to circumventing the problem of separation, the study of hybrid systems provides a means to explore the chemistry of an adsorbed complex and how that chemistry, perhaps through the involvement of the support, differs from its chemistry in homogeneous, fluid solution.

The advantages of incorporating a homogeneous system onto a solid support (hybrid catalyst) can best be appreciated by comparing it with homogeneous and traditional heterogeneous systems. The advantages of heterogeneous systems encompass acceptable thermal and mechanical stability, high activity for a wide range of reactions, and capacity for use in fluidized beds as well as ready separation of substrates and products. The disadvantages, which have provided the impetus to seek better systems, are that the nature of the active site is ill-defined, making rational design difficult, and severe and costly reaction conditions (i.e. high temperatures and pressures such as in the Fischer-Tropsch synthesis) which are typically associated with heterogeneous reactions. Homogeneous systems, on the other hand, are characterized by well-studied and interpreted catalytic activity, established activity under mild reaction conditions, efficient and

reproducible use of the metal atom, and controllable electronic and steric properties. In principle, these advantages can be carried over into a hybrid system along with the potential advantages that can be gained from immobilizing homogeneous catalysts. The latter include the introduction of preferred orientations, an altered stereochemistry, a changed equilibrium between the metal atoms and their ligands, stabilization of catalytically active but normally unstable coordinately unsaturated intermediates, and the prevention of the formation of dimeric species which frequently poison catalytic reactions. Therefore, the immobilization of transition-metal complexes onto solid supports to form hybrid systems offers not only the advantages of homogeneous catalysts, but also those found with traditional heterogeneous systems.

The desired characteristics of a hybrid system are that the support must possess an acceptable surface area and be inert to the required reaction conditions while the metal complex must be suitable for the desired catalytic reaction. Furthermore, the active portion of the catalyst must be stable under the reaction conditions while being accessible to the substrate molecule. It is for these reasons that our work involves an inorganic supported metal carbonyl and the ensuing discussion offers a brief survey of the literature in this field.

1. Thermal Activation of Group VIB Hexacarbonyls Adsorbed onto Inorganic Supports.

An inorganic support, offers the advantage of greater rigidity than an organic support, thereby preventing the possibility of deactivating catalytic sites via intermolecular condensation or polymerization (8). Moreover, organic polymer supports typically have an upper thermal stability of 433°K, whereas, inorganic supports have a much higher thermal stability limit (1,000°C).

Howe (9) has reported that $Cr(CO)_6$ supported on alumina would undergo complete decarbonylation in vacuo above 283°K to form dispersed metallic particles. This was established by infrared analysis, and by the observation that treatment with CO (6.6×10^3 N/m^2) at 318°K partially restores the $Cr(CO)_6$ bands. Presumably, the percentage not recovered was oxidized. Subsequent work by Brenner and Hucul (10) using a temperature programmed decomposition technique, TPDE, demonstrated that in the presence of flowing helium, temperatures in excess of 573°K were required to complete decarbonylation. The TPDE profile illustrated two distinct regions of decarbonylation, the first occured between 50-200°C and the second between 200-500°C. CO evolution at the latter temperatures is accompanied by hydrogen evolution, derived from surface hydroxyl groups, suggesting that the originally zerovalent metal has been oxidized.

Kazusaka and Howe (11) have shown that the adsorption of NO on $Cr(CO)_6$/alumina above 200°C results in the formation of species identical with those formed on convential

chromia-alumina catalysts (7), where the originally zerovalent chromium has been oxidized to Cr^{2+} and Cr^{3+}. When the catalysts are pretreated at higher temperature, the chromium is oxidized by surface hydroxyl groups (10) and the NO adsorbs directly onto oxidized sites to form Cr^{2+} and Cr^{3+} nitrosyl compounds.

Alternatively, when $Cr(CO)_6$ is bound to silica somewhat different results are obtained. Temperature programmed decomposition of $Cr(CO)_6/SiO_2$ in flowing helium established that all the carbonyl ligands are lost in rapid succession over a narrow temperature range (12). Similar to the results obtained on alumina, hydrogen evolution accompanied by metal oxidation during the decarbonylation is observed. After a temperature of 873°K is reached, the number of equivalents of hydrogen evolved establishes that chromium is in a +4 oxidation state. EPR studies (13) indicate that $Cr(CO)_6$/alumina catalysts activated at 473°K and then exposed to oxygen generated Cr^{+5} ions in square-pyramidal and tetrahedral coordination.

Although the majority of available data have focused on changes in the adsorbed metal carbonyl, some examples of their use as catalysts have been reported, Banks (14,15) has observed the polymerization of ethylene to form polyethylene when $Cr(CO)_6/SiO_2$ is activated at 394-400°K. Brenner, Hucul, and Hardwick (12) have observed propylene hydrogenation, in the presence of external hydrogen, when

$Cr(CO)_6$/alumina is thermally activated with a maximum activity observed at 468°K.

Howe, Davidson, and Whan (16) report that activation of immobilized $Mo(CO)_6$ catalysts involved complex decomposition, the extent of which was a function of the basicity and/or hydroxylation of the support. In general, supports that did not readily stabilize subcarbonyl species by coordination to the vacated sites induce rapid decarbonylation of the adsorbed complex. Kinetic and infrared studies indicated that a stabilized subcarbonyl species of unknown stoichiometry, i.e., $M(CO)_x$, on alumina and magnesia did not catalyze propylene metathesis (17). It was postulated that following decarbonylation, the initially dispersed metallic Mo(0) subsequently oxidized to form a metal oxide which was an active metathesis catalyst.

Smith, Howe, and Whan (18) investigated the metathesis of propene using catalysts prepared from $Mo(CO)_6$ supported on silica, alumina, silica-alumina and magnesium oxide. The activity of these catalysts was found to be dependent on the temperature at which the support was outgassed prior to $Mo(CO)_6$ adsorption and the activation temperature the catalyst was subjected to. The temperature at which a support is outgassed determines the extent of hydroxylation, i.e., the higher the pretreatment temperature, the larger the extent of dehydroxylation. This study suggests that fully dehydroxylated supports showed metathesis activity.

Surface bonded $Mo(CO)_6$ has been the subject of extensive spectroscopic examinations. Davie, Whan, and Kemball (19) have correlated the metathesis of propylenes, i.e.,

$$2\ CH_3CHCH_2 \longrightarrow CH_2CH_2 + \text{butenes} \quad (1)$$

with infrared characterization of the active catalytic species. They observed propene metathesis activity after the catalyst was treated for one hour at 373°K in vacuo. Prior to treatment, the infrared spectrum of the unactivated catalyst displayed a single sharp absorbance at 1985 cm^{-1} corresponding to adsorbed molybdenum hexacarbonyl. Once activated the single sharp peak is replaced by two broad bands at 1880 and 2020 cm^{-1}. The species responsible for these bands was not fully characterized, but on exposure to O_2 all carbonyl bands disappeared. An attempt to characterize the active species by complexation with cycloheptatriene suggests that the active catalyst has lost at least two or more carbonyl ligands. Similar results were found from X-ray photoelectron analysis of $Mo(CO)_6/\gamma$-alumina (20). These results indicate that the active metathesis catalyst is not the original hexacarbonyl, but a lower subcarbonyl of unknown stoichiometry. Moreover, the catalyst lost substantial activity after it had been exposed to air indicating that fully oxidized molybdenum does not show disproportionation (metathesis) activity.

EPR studies (21) of supported $Mo(CO)_6$ were reported by Howe and Leith. Thermal activation, >293°K, of a silica and alumina supported $Mo(CO)_6$ leads to the appearance of a signal attributed to Mo(V) in a square-pyramidal coordination.

The temperature programmed decomposition of $Mo(CO)_6$ bound to alumina was reported by Brenner and Burwell (22), who proposed the following scheme (ads is used throughout this thesis to designate an adsorbed species).

Scheme I

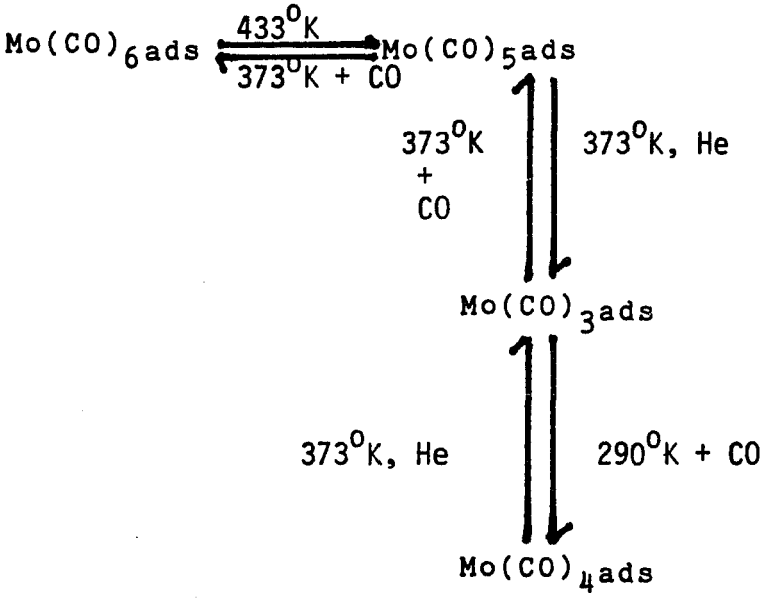

A species with an average stoichiometry, based on reactor effluent analysis of $Mo(CO)_3ads$, was isolated and found to be moderately active in the propene metathesis at 326 °K. Treatment of the catalyst at higher temperatures in flowing helium resulted in further decarbonylation and

higher catalytic activity. $Mo(CO)_3$ads was found to absorb one molecule of O_2 while ejecting a molecule of CO to form an $Mo(CO)_2O_2$ species which has been found to be 15 times more active for metathesis than adsorbed $Mo(CO)_3$ (23,24).

Brenner and coworkers (10,22) investigated the possibility of oxidized species forming during the TPDE of Group VIB hexacarbonyls bound to γ-alumina and silica. The measure of oxidation activity is the evolution of hydrogen. The low temperature portion of the TPDE profile displayed decarbonylation without hydrogen evolution. At higher temperatures, however, decarbonylation is accompanied by hydrogen evolution. It was proposed that the evolved hydrogen originates from H^+ in the surface hydroxyl groups of the alumina and is reduced to hydrogen gas, accompanied by an equivalent amount of transition-metal oxidation.

Using IR spectroscopy, Howe established (9) that when $Mo(CO)_6$ is exposed to SiO_2 or Al_2O_3, the complex is physisorbed onto the surface. However, the physisorbed $Mo(CO)_6$ is not stable in vacuo at a temperature as low as -10°C and immediately loses CO to form $Mo(CO)_5$ads. The latter then decomposes further to give a stable subcarbonyl species of unknown stoichiometry. Upon exposure to CO ($<1.33 \times 10^4$ N/m^2), however, this stable carbonyl species, $M(CO)_x$, can be reversibly carbonylated to $Mo(CO)_5$ads and at higher CO pressures

(>6.67 x 10^4 N/m^2) $Mo(CO)_6$ads slowly reappears. Identical results were obtained for $Mo(CO)_6$ on a fully hydroxylated silica surface and with both $W(CO)_6$ and $Cr(CO)_6$ on both alumina and silica.

Although Howe (9) concluded that the decarbonylation of the Group VIB hexacarbonyls was complete and reversible, subsequent work by Brenner and coworkers (12) established that following partial decarbonylation, on a fully hydroxylated support, additional CO could no longer recarbonylate the metal primarily due to the formation of an oxidized metal species.

Conflicting results were reported by Adams, Gardner, and Parkyns (25) where $Mo(CO)_6$ was adsorbed onto silica and examined by Raman spectroscopy. However, to obtain intense Raman scattering, it was necessary in these experiments to adsorb up to four layers of the complex. Under these conditions, no subcarbonyl was formed on adsorption, but a comparison with previous results is tenuous because of the necessity to use multilayer surface coverages.

Brenner and Burwell (26) reported that sweeping $Mo(CO)_6/\gamma$-alumina with a flow of ultrapure helium at 373°K results in the loss of carbon monoxide and the formation of a material with catalytic activity and an empirical composition of $Mo(CO)_3$ads. Sweeping at higher temperatures (> 473°), resulted in further decarbonylation and the formation of a "$(\sigma\text{-}O^-)_2Mo$" at 543°K, where $\sigma\text{-}O^-$ represents a surface bound

oxygen. Prolonged heating to 773°K resulted in the decarbonylated metal having an oxidation state of about 5.6 as determined from hydrogen evolution. Under the same conditions, however, Mo remains in the zerovalent state if it is bound to fully dehydroxylated alumina.

Olefin metathesis has been studied extensively by Bailey and Banks (27) using activated $Mo(CO)_6$/alumina. With propene feed at 395°K, the molybdenum catalyst produced 42% ethene and 55% 2-butene, and 3% higher molecular weight hydrocarbons at 25% conversion. A similar result was obtained for surface bound $W(CO)_6$.

Davie, Whan, and Kemball (28) observed the metathesis of propene using $Mo(CO)_6$ on alumina in a static reactor system between 273 and 353°K and propene pressures between 0.5 and 20.0 kN/m^2 in periods of 15 minutes to several hours. Infrared spectra suggest that the active species is $(C_3H_6)_2Mo(CO)_4L_{4-x}$, where x is either 3 or 4 and L is a propene molecule or a surface site (σ-O^-).

Although olefin metathesis has been studied quite extensively (27), some effort has been devoted to the study of other catalytic reactions. Brenner and coworkers (12,29) report that $Mo(CO)_6$ads exhibits greater activity for olefin hydrogenation than conventional MoO_3/alumina catalysts, and they find that $Mo(CO)_6/SiO_2$ is more active than $W(CO)_6/SiO_2$. Interestingly, the turnover frequency for the hydrogenation activities are much

lower for silica supported catalysts than for alumina supported catalysts, which is opposite what is observed in propene metathesis. Supported $Mo(CO)_6$ has also been found useful in the polymerization of unsaturated hydrocarbons (14), the desulfurization of thiols (30), and the dehalogenation of α-halo ketones (31).

During the thermal decomposition of all surface-bonded group 6 hexacarbonyls, small quantities of CH_4 are evolved, suggesting the potential of these species as Fischer- Tropsch catalysts in the reduction of CO to CH_4 (26,32,33). Bowman and Burwell (34) observed a turnover frequency of 0.04 sec^{-1} for the methanation at 573°K for $Mo(CO)_6$ supported on fully dehydroxylated alumina. Partially dehydroxylated derived catalysts show a propensity for CH_4 formation, however, lower turnover frequencies were observed.

$W(CO)_6$ bound to inorganic supports has received less attention than its molybdenum analog. In an early attempt to elucidate that nature of zerovalent metal carbonyls immobilized on an acidic solid, Bilhou et al. (35) investigated $W(CO)_5L$ (L=CO, PPh_3, $P(n\text{-}C_4H_9)_3$). Infrared spectroscopy suggest that the rupture of the W-C bond occurs through a W-C=O-Al complexation with a linear carbonyl ligand coordinated to Al, a Lewis center. This serves to increase the d_π - p^*_π back-donation of tungsten d_π electrons to the p^*_π orbitals of CO. The net decrease of tungsten electron density favors the departure of ligand, L.

Early studies (9) of the $W(CO)_6$/alumina system suggested that no stable subcarbonyl species is formed during thermal activation up to -10°C. However, Brenner and Hucul (36) have demonstrated that $W(CO)_3$ads is formed at 408°K in the TPDE systems. A temperature of 673°K is required to produce complete decarbonylation; W^{6+} is formed on highly hydroxylated supports whereas W^{o} is formed on highly dehydroxylated supports. This behavior is similar to that for the corresponding $Mo(CO)_6$/alumina system (26), and silica-supported $W(CO)_6$ also resembles $Mo(CO)_6/SiO_2$ (12).

Adsorbed $W(CO)_6$ generally catalyzes the same reactions as its $Mo(CO)_6$ counterparts. Studies of olefin metathesis (14,27,37-40), olefin hydrogenation (12), and polymerization (14) have been reported.

C) A Summary of Photochemically Activated Hybrid Systems.

The potential of preparing transition-metal catalysts from metal carbonyl complexes using photochemical techniques will now be discussed. There are a number of advantages in employing light-initiated rather than thermal processes. These complexes possess a rich and well understood photochemistry (41). The photoexcitation of any chemical system where optical energy can be selectively deposited in a specific chromophore, offers a level of control not available through thermal energy. While the photochemistry of appropriate solution species (42) can be used as a guide to the photochemistry of the surface-confined species, the

support may alter the primary photochemical events and thermal reactions of primary products. However, the opacity of many traditional oxide support materials have limited the application of photochemical methods to the preparation of supported transition-metal catalysts. The opaque nature of these supports drastically reduces the efficiency of any photochemical process due to a nearly complete loss of useful light by scattering and reflection or absorption of the support. We have circumvented this problem by employing Corning's code 7930 porous Vycor glass, PVG, as a support. Porous Vycor is a surface hydroxylated, transparent (>290-nm) glass which has a myriad of 70 $\pm$ 21 A pores or cavities interconnected throughout the glass in a random three dimensional array (43-52). The attractive feature of PVG is its transparency which allows not only the use of conventional photochemical techniques, but the spectroscopic examination of adsorbed species during the photoinduced reaction.

Because of the problem associated with the photochemical activation of supported transition metal complexes, relatively few papers describing the photoactivation of supported metal carbonyls have appeared in the literature.

Jackson and Trusheim (53) have investigated the photochemistry of silica-adsorbed $Fe(CO)_5$. Their results indicate that the starting complex, $Fe(CO)_5$, oligomerizes to $Fe_3(CO)_{12}$, rather than $Fe_2(CO)_9$, which is the product observed following

irradiation of $Fe(CO)_5$ in the gas or liquid phase or in solution.

Wrighton and coworkers (54) have reported the synthesis and photochemical behavior of $LRu(CO)_4$ and $L_3Ru_3(CO)_9$ confined to the surface of high surface silica. The results illustrate that immobilization of precursors to coordinately unsaturated species prevents cluster formation when the surface coverage is sufficiently low. Further, photodeclusterification of anchored $L_3Ru_3(CO)_9$ is reversible due to immobilization of the fragments.

Wrighton and Reichel (55-57) have described the functionalization of silica and alumina by first treating the solids with $(EtO)_3SiH$, Me_2ClSiH or Cl_3SiH in order to introduce $[S]\rightarrow SiH$, where S denotes a surface site, functionality followed by reaction with $Co_2(CO)_8$. Derivatized surfaces have been characterized by photoacoustic IR spectroscopy and compared to solution analogues to confirm the presence of $[S]\rightarrow SiH$ and $[S]\rightarrow SiCo(CO)_4$ groups on the surface. The primary photoprocess associated with these systems is loss of CO, producing an unsaturated intermediate which is exploited in the hydrosilation, hydrogenation, and isomerization of 1-pentene.

Wrighton, Kazlauskas, and Klein (58) report that when surface-confined $(\eta^5\text{-}C_5H_5)W(CO)_3R$ (R=Cl, CH_3, C_2H_5, $CH_2C_6H_5$) is photolyzed

with 355nm radiation, efficient dissociation of CO is observed as the primary photoreaction. These results are consistent with what is found for the analogous solution reaction. Direct spectroscopic evidence for the photogeneration of surface-confined, 16-valence-electron intermediates was obtained from infrared analysis of Nujol suspensions of SiO_2-$SiMe_2$-(η^5-C_5H_4)$W(CO)_3R$ (R=CH_3, C_2H_5) irradiated at 77°K. Unlike the analogous complex in solution, prolonged irradiation of the SiO_2-$SiMe_2$(η^5-C_5H_4) $W(CO)_3R$ does not yield W-W bonded products, consistent with the immobilized centers remaining anchored sufficiently far apart that W-W bonds cannot form.

To appreciate how the photochemical behavior of adsorbed group VIB hexacarbonyls differs from that found in fluid solution, the photophysics, photochemistry, and photoinduced catalytic behavior of these metal carbonyls in fluid solution is summarized below.

D. The Photochemistry and Photophysical Properties of Group VIB Hexacarbonyls.

1. Molecular Orbital Description of Octahedral Metal Carbonyls.

The coordinate system adopted for the case of full σ- and π-bonding in the octahedral symmetry is described (59). The metal valence orbitals are nd, (n+1)s, and (n+1)p. The carbon 2s and $2p_z$ orbitals will be used for σ-bonding; for π-bonding, both the ligand π-bonding (π^b) and π-antibondinng (π^*) molecular orbitals will be combined

with the d_{π} and p_x metal orbitals to form the π-molecular orbital system for the complex. The σ-molecular orbital system utilizes the $nd_{x^2-y^2}$ and nd_{z^2} (e_g), (n+1)s (a_{1g}), and (n+1)p_y, (n+1)p_z (t_{1u}) metal orbitals with the proper linear combinations of ligand σ-orbitals to form six bonding and six antibonding σ-molecular orbitals.

The pure π-molecular orbitals are composed of the nd_{xy}, nd_{xz}, and nd_{yz} (t_{2g}) metal orbitals and the t_{2g} combinations of π^b and π^* ligand molecular orbitals. The instability order of the combining π-orbitals is always $\pi^b(L) < nd_{\pi} < \pi^*(L)$. Thus there are formed three (degenerate) strongly bonding π-molecular orbitals localized on the carbonyl ligand; three virtually non-bonding molecular orbitals principally localized on the metal; and three strongly antibonding molecular orbitals principally localized on CO. The molecular orbital energy scheme expected for the bonding situation described above is shown in Figure 1.

In general, the most stable metal carbonyl complexes are highly covalent due to the ability of zerovalent metals to delocalize electron density onto the CO ligand, i.e. back bonding. Therefore, any electronic transitions which change this electron configuration will have a dramatic effect on the bonding of these complexes, providing a rationale for the photosensitivity of these complexes.

2. Electronic Structure of $M(CO)_6$.

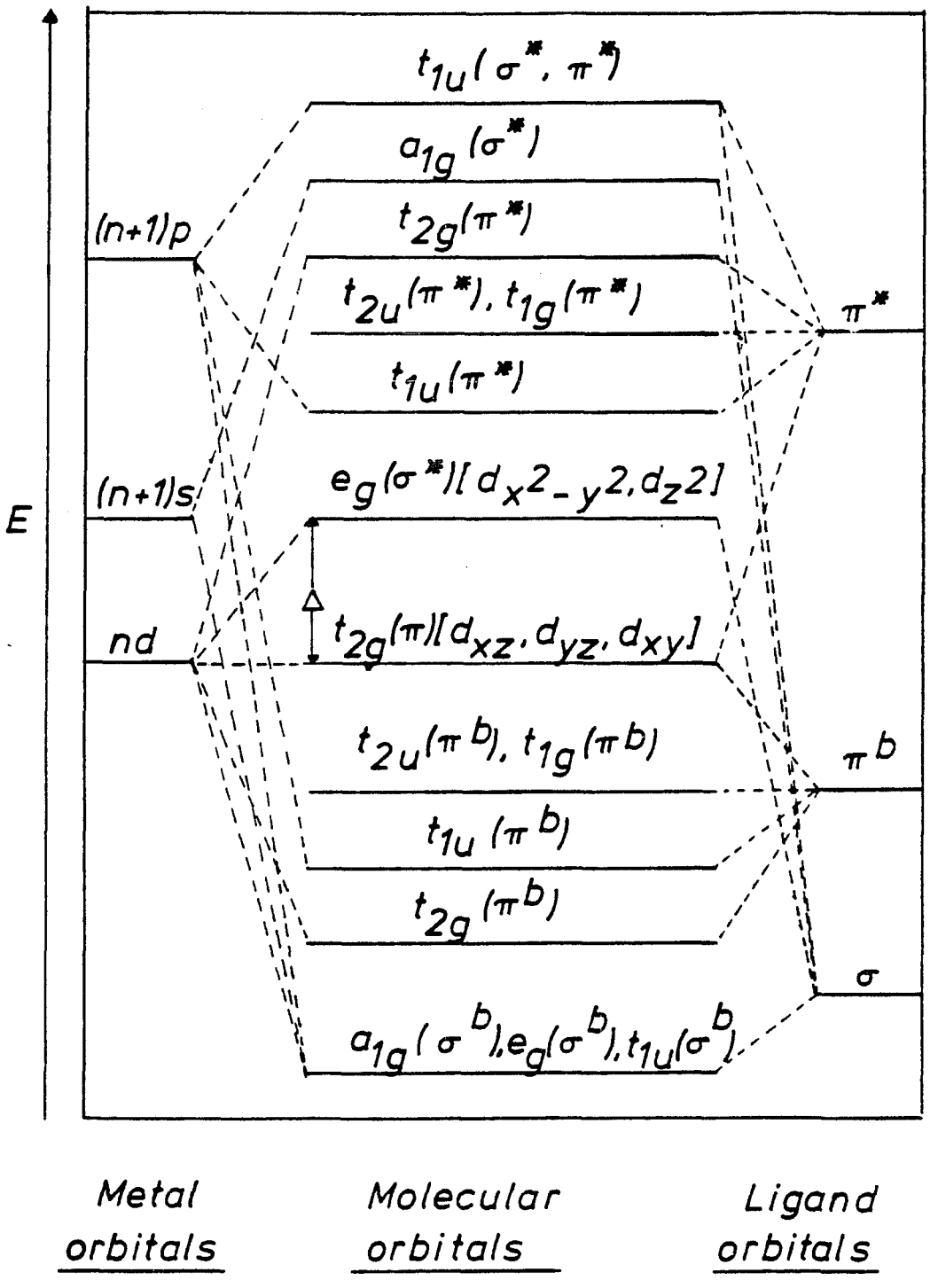

Figure 1. Molecular orbital energy level dagram for Group VIB hexacarbonyls.

A typical spectrum of $M(CO)_6$ (M=Cr, Mo, and W) in the low energy region is illustrated in Figure 2 and the transitions have been assigned by Gray (59). The lowest energy absorption at ~ 30,000 cm^{-1} is assigned as the $^1A_{1g} \longrightarrow {}^1T_{1g}$ LF absorption. This band appears as a shoulder on the more intense $M \rightarrow \pi^*$ CO charge transfer absorption at ~ 35,000 cm^{-1}. The second ligand field band, $^1A_{1g} \rightarrow {}^1T_{1g}$, predicted for d^6 O_h complexes, can be observed as a shoulder in the vicinity of ~ 37,500 cm^{-1} on the most prominent band at ~43,000 cm^{-1}, which is assigned the second component of the $M \rightarrow \pi^*$ CO charge transfer absorption. The tungsten and molybdenum complexes exhibit a low energy, spin forbidden, $^1A_{1g} \rightarrow {}^3T_{1g}$ ligand field absorption at 28,300 cm^{-1}, as a consequence of the spin-orbit coupling associated with these heavier atoms (56). The value of 10 Dq remains constant in going from Cr to W due to a balance between diminishing σ-bonding and increasing π-bonding (60). As a result of the unusually large covalency within these complexes, the ligand field absorptions, although formally Laporte forbidden, are unusually intense. This occurs because the molecular orbitals have substantial contributions from both metal and ligand atomic orbitals, thereby lifting the Laporte-forbidden restrictions which reduce the intensity of typical "d-d" transitions (41).

The one electron energy diagram is shown in Figure 3b. The ground electronic state $^1A_{1g}$, t_{2g} electronic

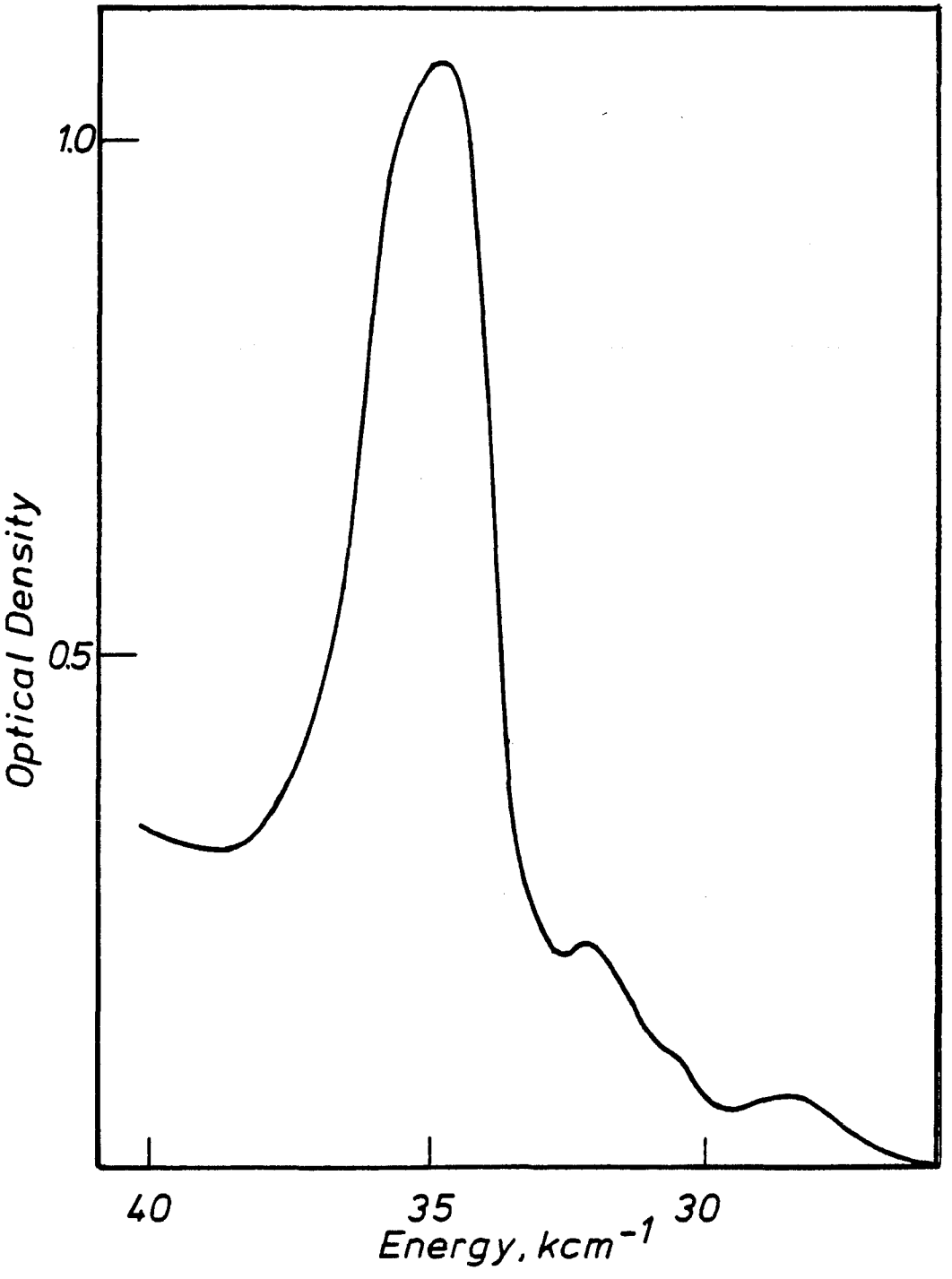

Figure 2. Electronic absorption spectrum of 8.0×10^{-5}M $W(CO)_6$ in EPA at 77°K. Note the presence of the band at 28,900 cm^{-1} which is the spin forbidden $^1A_{1g} \longrightarrow {}^3T_{1g}$ transition.

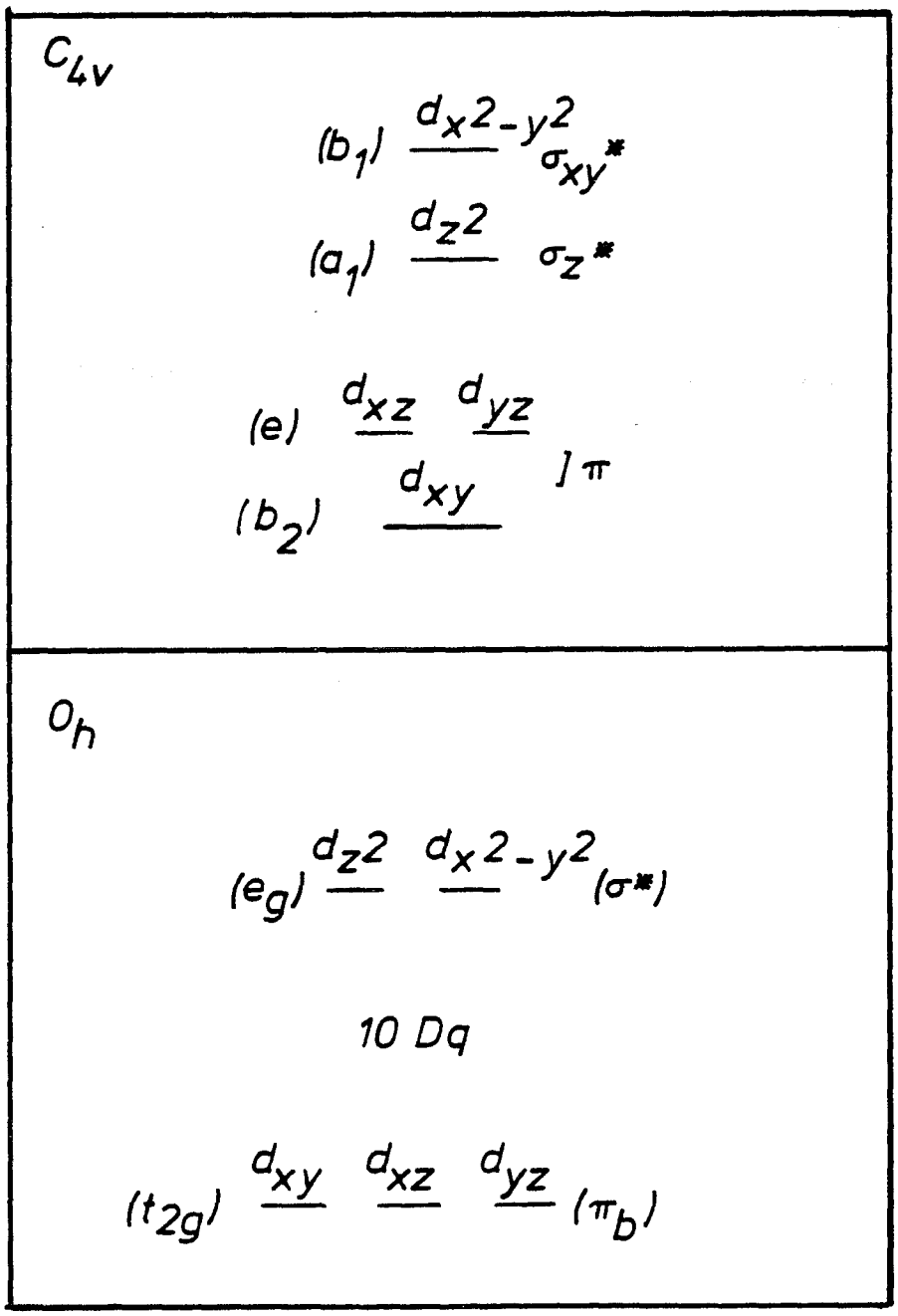

Figure 3a. One electron energy diagram of $M(CO)_5L$.
Figure 3b. One electron energy diagram of $M(CO)_6$.

configuration and the one-electron excitation to $t_{2g}e_g$ yields the $^{1,3}T_{1g}$ and $^{1,3}T_{2g}$ excited states (62). One electron excitations associated with this scheme will result in dramatic changes in the substitutional lability of $M(CO)_6$ since both σ- and π-bonding are diminished upon population of an e_g (σ^*) orbital (63).

When the symmetry of these complexes are reduced from O_h to C_{4v}, which occurs upon ligand substitution, substantial changes occur in the one-electron energy levels (64). The orbital ordering of $M(CO)_5L$, where L is a weaker ligand than CO, is shown in Figure 3a.

In C_{4v} symmetry, the relative energy of the first ligand field absorption, $^1A_1 \longrightarrow {}^1E$, is highly dependent on the nature of X. For various ligands the relative splitting of the d orbitals are in the order: CO>alkenes $\backsim$ PPh_3>pyridine $\backsim$ amine $\backsim$ oxygen donor. For $W(CO)_5$(1-pentene) the lowest energy band appears at 27,780 cm^{-1} while for $W(CO)_5(NH_3)$ the corresponding band appears at $\backsim$ 24,875 cm^{-1}. These two complexes represent the extremes in the balance between σ-donation and π-acceptancy, with amines being good σ-donors and alkenes good π-acceptors. Moreover, since 1-pentene is a good π-acceptor, the energy level diagram for $W(CO)_5$(1-pentene) is similar to $W(CO)_6$, while for $W(CO)_5(NH_3)$, the energy gap between the b_1 (σ_{xy}^*) and a_1 (σ_z^*) is sufficiently large to yield

"localized" antibonding charactor along the x and y axes or the z axis depending on which transition is excited. The lowest energy absorption in the d^6, C_{4v} complexes is the $^1A_1$ $(e^4 b_2^2) \longrightarrow {}^{1,3}E(e^3 b_2^2 \ a_1^1)$ (65-67).

The pentacarbonyl analogues, $M(CO)_5$ (M=Cr, Mo, and W), have been prepared and spectroscopically examined in low temperature matrices (68-71). The spectral data suggest that the complex has C_{4v} symmetry, and the spin-allowed, ligand field band $^1A_1 \longrightarrow {}^1E$ is highly sensitive to the nature of the matrix material. For example, $Cr(CO)_5$ generated in a neon matrix exhibits an absorption maximum at 624-nm, but shifts to 490-nm when generated in a xenon matrix. The shift is attributed to a weak metal matrix bond which occupies the sixth coordination site. The larger extent of coordination leads to a higher energy ligand field band.

3. Luminescence Studies.

Previous studies (65,66) have shown that the complexes of the formula $W(CO)_5X$, where X is an electron donor, will luminesce at 77°K either as the pure solid or in rigid glasses. The corresponding Cr and Mo complexes do not luminesce, or at least, their emission was not detectable under conditions used to determine spectra for the W complexes. The typical, broad emission observed for $W(CO)_5X$ is illustrated in Figure 4a. The lack of an identifiable emission band in the Cr and Mo complexes is

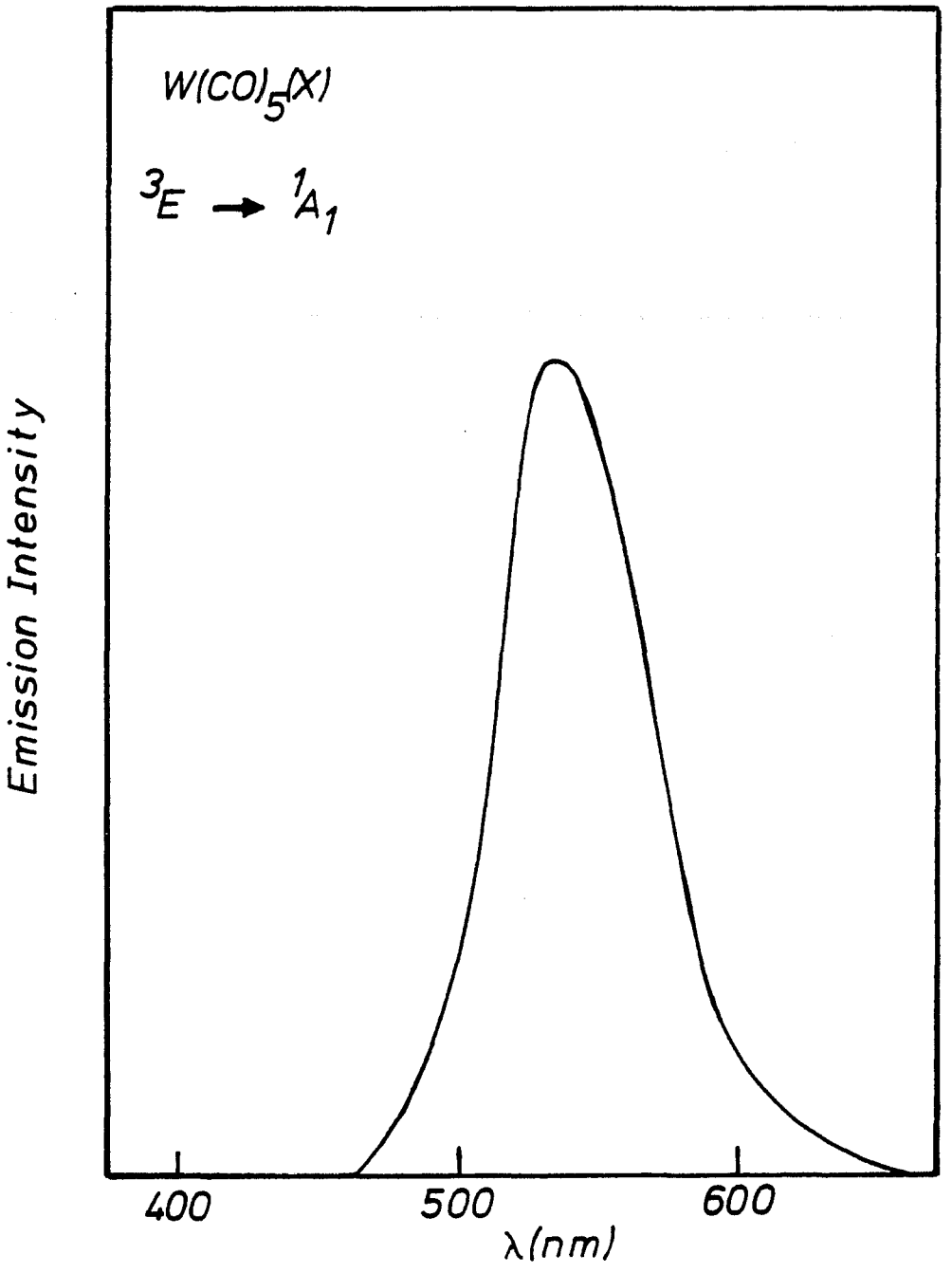

Figure 4a. Room temperature emission spectrum of $W(CO)_5X$.

correlated with the lack of an $^1A_1 \longrightarrow {}^3E$ transition, due to the limited spin orbit coupling associated with these lighter atoms. For the complexes where luminescence is observed, the lifetime of the excited state is quite long (> 10^{-6}sec). In addition, this band overlaps with the lowest energy absorption, which is assigned to $^1A_1 \longrightarrow {}^3E$ transition. The long emission lifetime and overlap of the absorption and emission bands suggest that the emission is the $^3E \rightarrow {}^1A_1$ transition.

Emission has been observed for $M(CO)_4L$ where L is a bis (nitrogen) bidentate ligand and M=Cr, Mo, and W (72,73). These emissions are highly sensitive to the nature of the solvent and are attributed to charge transfer transitions (74).

Recently, luminescence spectra have bee obtained for $M(CO)_6$ (M=Cr, Mo, and W) in argon and methane matrices at 12°K (75a). It is probable that these emissions at 340-360 nm for $M(CO)_6$ complexes correspond to fluorescence, i.e., $^1T_{1g} \longrightarrow {}^1A_{1g}$ or $^1T_{2g} \longrightarrow {}^1A_{1g}$, because of their position relative to the absorption bands and the observance of a triplet-sensitized emission for $Cr(CO)_6$ at 400 nm (75b). These data establish that other decay pathways are present in these complexes besides CO dissociation.

4. Photoreactions.

a. Substitution Reactions.

As mentioned above, excitation of the ligand field transitions of these complexes cause significant changes in the metal-ligand bond. In the ligand field excited states, CO is labilized and the photoinduced reaction is characterized by ligand substitution. The mechanism for the photoinduced substitution is proposed to be:

$$M(CO)_6 \xrightarrow{h\nu} M(CO)_5 + CO \qquad (2)$$

$$M(CO)_5 + CO \xrightarrow{\Delta} M(CO)_6 \qquad (3)$$

$$M(CO)_5 + L \xrightarrow{\Delta} M(CO)_5L \qquad (4)$$

Upon photolysis of $M(CO)_6$ in a methyl methacrylate polymer (76), a reversible photoreaction takes place. The slow thermal bleaching of the yellow intermediate is most likely due to the thermal back reaction, reaction 2. Sheline and coworkers (77) obtained IR data following photolysis of $M(CO)_6$ in methylcyclohexane glasses at 77°K, establishing that the primary photoprocess is the formation of a $M(CO)_5$ intermediate. The $M(CO)_5$ intermediate can exist as a C_{4v} square-pyramidal complex, or a D_{3h} trigonal-bipyramid. Perutz and Turner (68-71) obtained IR and UV-visible data after photolysis of group 6B hexacarbonyls in low temperature (20°K) rare gas matrices, which suggest that $M(CO)_5$ initially has a C_{4v} symmetry, but on warming to room temperature changes

Figure 4b. A comparison of d-orbital ordering of C_{4v} vs. D_{3h}.

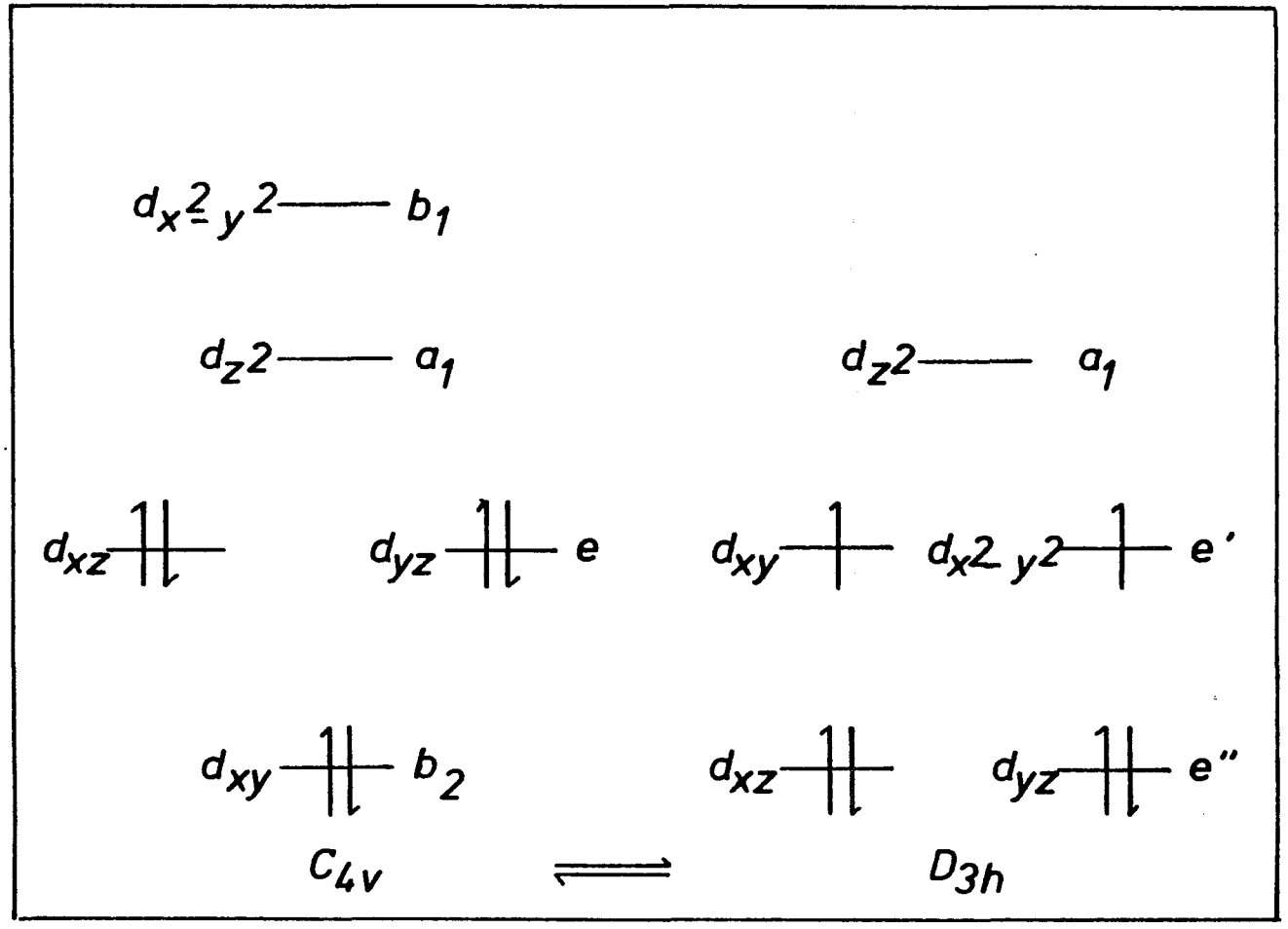

to a D_{3h} symmetry. This change in symmetry induces a change in the d-orbital ordering illustrated in Figure 4b. An important point is that a spin change also occurs. A d^6 configuration of C_{4v} symmetry is predicted to be diamagnetic, having a singlet ground state, whereas that of D_{3h} symmetry is predicted to be paramagnetic with two unpaired electrons.

The nature of the reactive excited state of $M(CO)_6$, has been investigated, and preliminary results indicate that radiative and non-radiative processes occur (75). The radiative decay is extremely short lived ($<10^{-9}$ sec), which suggests that it is a flourescence, from either a $^1T_{1g}$ or $^1T_{2g}$ excited state. Whatever the decay path is, however, it is generally accepted that the generation of an excited state, $^*M(CO)_6$, should be substantially more reactive than the ground state, since depopulation of the t_{2g} level diminishes π-back bonding and concomitant population of e^*_g diminishes σ-bonding, regardless of whether this occurs by means of ligand field or charge transfer transitions.

E. Photocatalysis of Group VIB Hexacarbonyls.

Photocatalysis is defined as the photogeneration of a catalyst from a thermally inert precursor such that substrate transformations result which are both catalytic with respect to the number of photons absorbed and with respect to the actual catalyst. Scheme II illustrates this mechanism:

Scheme II

Metal complex + Substrate $\xrightarrow{\Delta}$ No Reaction (5)

Metal Complex $\xrightarrow{h\nu}$ Catalyst (6)

Catalyst + Substrate $\xrightarrow{\Delta}$ Transformed Substrate + Catalyst (7)

Catalyst $\xrightarrow{\Delta}$ Poisoning (8)

In contrast, many catalytic reactions have been found that are accelerated by continuous photolysis (78). This type of catalysis is termed photoassisted, and is reserved for substrate transformations which appear to proceed according to Scheme II but require continuous photolysis.

In general, transformation of substrate molecule involves first the coordination of the substrate to a coordinately unsaturated metal center. It has been reported that near UV-photolysis of $M(CO)_6$ (M=Mo, W) in the presence of olefin generally leads to the isomerization of the olefin (79). Both cis-trans and positional isomerizations have been detected as indicated by examples in Table 1. All of the data reported are consistent with the first photoreaction being the formation of the $M(CO)_5$(olefin) complex with retention of the integrity of the olefin. The coordinated olefin complex, $M(CO)_5$(olefin), then absorbs additional photons to initiate the isomerization; reaction 3 in Scheme II is photoassisted. As illustrated in Figure 5, linear pentenes are isomerized using $W(CO)_6$ as a catalyst. Reaction 3

Table 1. $M(CO)_6$ photoassisted. (79)

M	Irrd λ, nm	Starting olefin	Initial product(s)
Mo, W	366	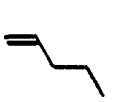	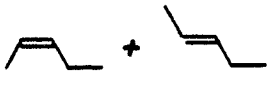
W	366, 313		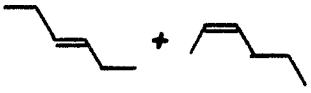
W	366, 313	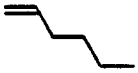	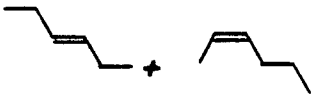
W, Mo	366	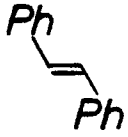	
W	366	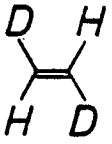	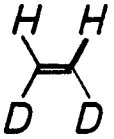
W, Mo	313, 366		

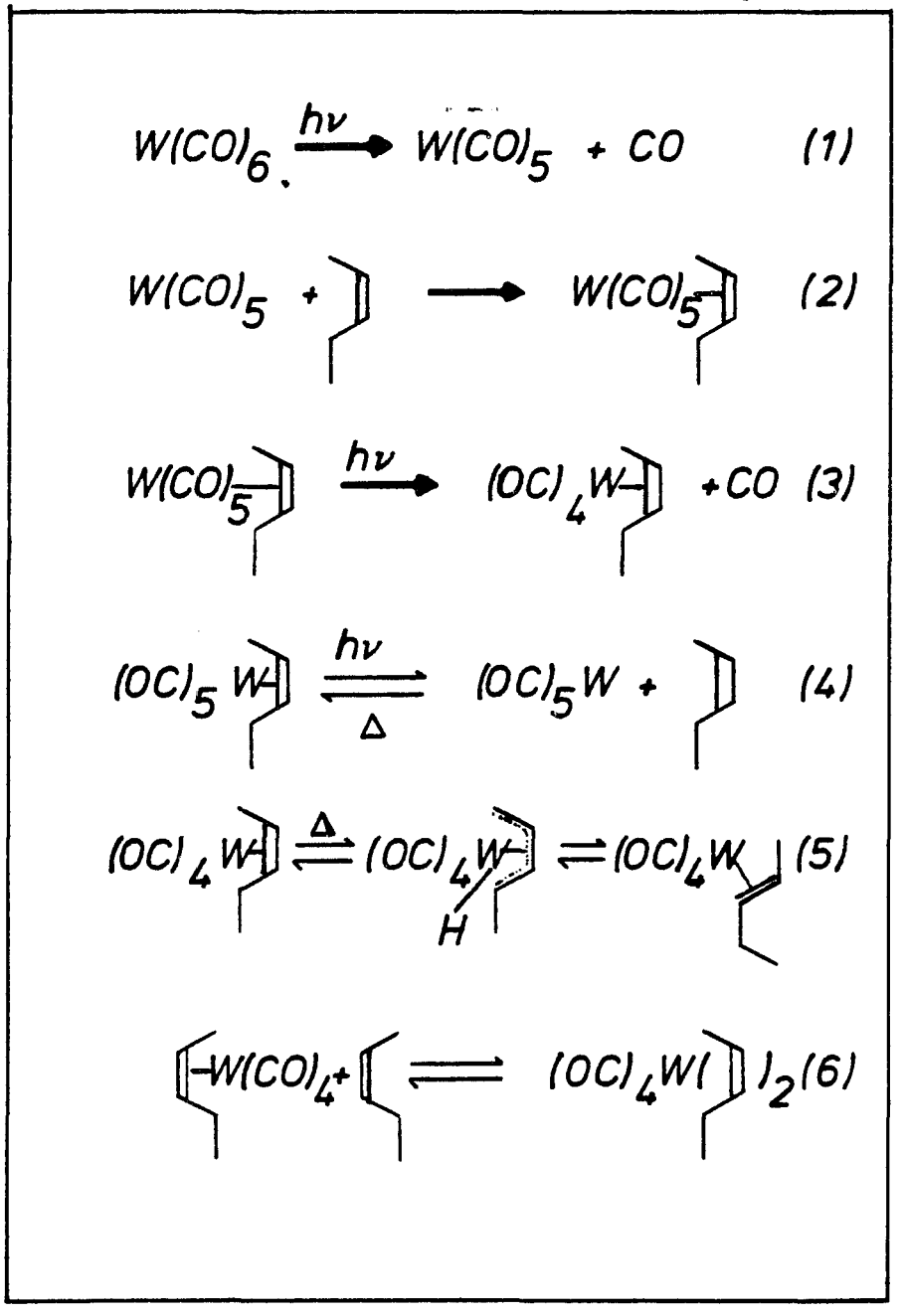

Figure 5. Mechanism of $W(CO)_6$ catalyzed isomerization of cis-2-pentene to trans-2-pentene.

in Scheme II proceeds with a quantum efficiency of 0.3 at either 313 or 366-nm (78). Loss of cis-2-pentene, reaction 4, does occur, however, cis-2-pentene coordinates immediately again since it is in high concentration. The $(OC)_4W$(cis-2-butene) leads to two possible types of products, equations (5) and (6). The thermal substitutional lability of the $W(CO)_4$(cis-2-pentene)$_2$ coupled with the possibility indicated in (5) may allow for catalytic isomerization. Oxidative addition of the alkene to $W(CO)_4$ is more reasonable than to $W(CO)_5$ since for $W(CO)_4$ there is a smaller number of ligands available to stabilize the low valent metal, providing a rationale for subsequent catalytic activity. The isomerization of cis-2-pentene to 1-pentene is thought to occur via reactions illustrated in Figure 6a. It has not been established how many CO ligands remain on the tungsten atom but it has been postulated that $W(CO)_3$ may be the truly active catalyst in the isomerization of olefins.

Other mechanisms have been suggested (78) for the isomerization reaction such as the formation of tungsten-olefin sigma bonded complexes which are then free to rotate to give the corresponding isomerized olefin (Figure 6b).

In addition to olefin isomerization, photoassisted and photocatalyzed 1,4 additions of hydrogen to 1,3 dienes have been examined.

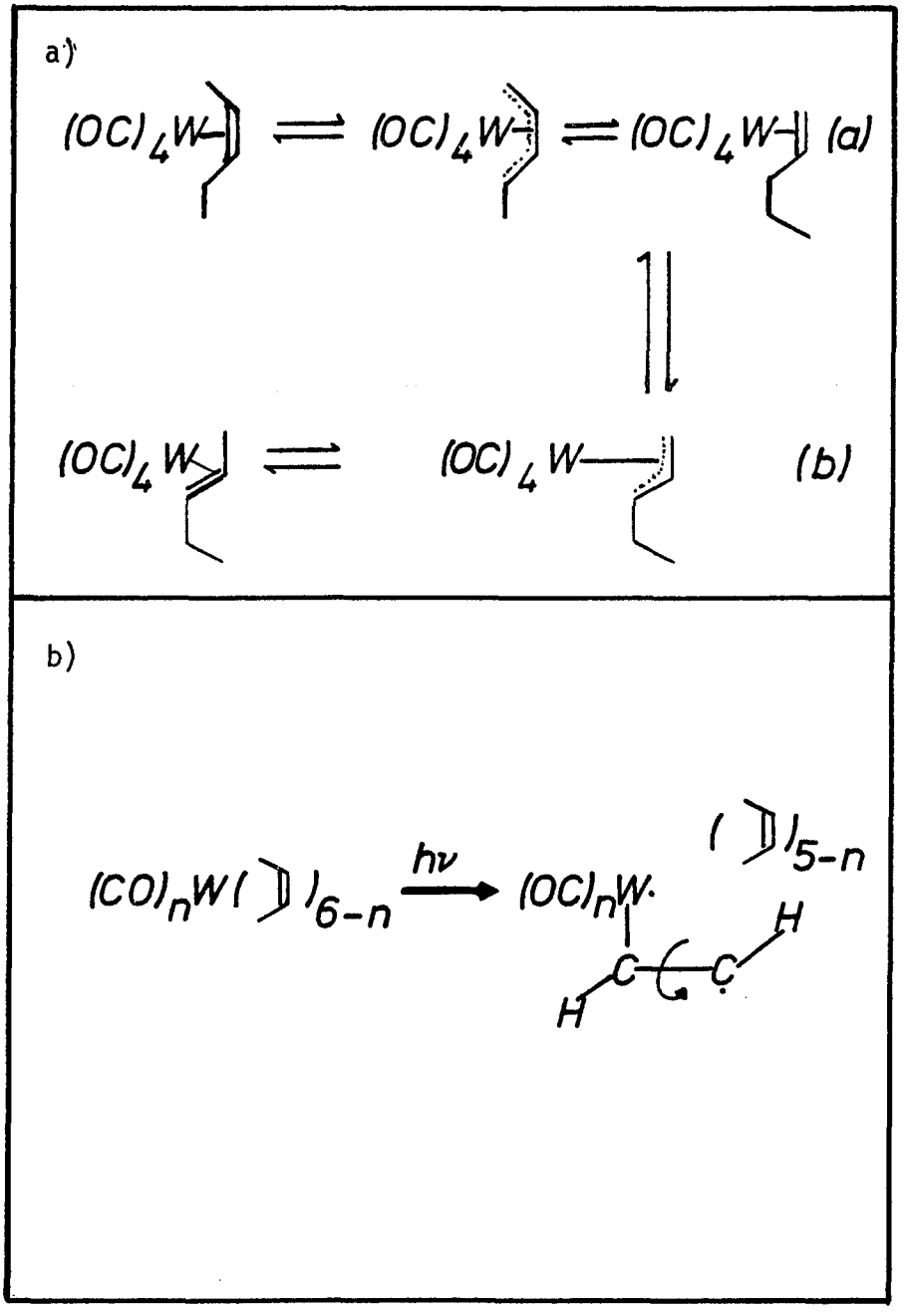

Figure 6a. Isomerization of $W(CO)_4$(cis-2-pentene) to 1-pentene.

Figure 6b. σ-mechanism for the isomerization of cis-2-pentene to 1-pentene.

Studies have shown that the photolysis of $M(CO)_6$ at 25°C in the presence of a 1,3 diene and H_2(1-atm) leads 1,4 addition of hydrogen to the diene yielding the corresponding olefin (80,81). The substrate molecules used and their corresponding products are illustrated in Table 2. The data indicate that a cis-diene is more effective than a trans diene in the hydrogenation reaction (82). Figure 7 describes the mechanism for 1,4 addition of H_2 to 1,3 dienes. Interestingly, $Cr(CO)_6$ is an effective catalyst for the hydrogenation of a diene, but does not catalyze olefin isomerization (80-82).

Photochemistry of surface-confined molecules has not received the attention that has been paid to homogeneous solution reactions. However, the impetus for research in this direction is two-fold. First, the photoexcitation of any chemical system, where optical energy may be selectively deposited into a given chemical constituent, depending on the absorption properties, provides a rational approach to selective activation of potential catalysts; a process which cannot be accomplished thermally. Second, homogeneous catalysis, whether activated thermally or photochemically, frequently gives low yield of product due to dimerization of catalytically active species. Furthermore, photochemistry of surface-confined molecules may have practical importance in imaging, weathering and corrosion inhibition, and providing new insights into reaction mechanisms. It is for these reasons that this doctoral dissertation was initiated.

Table 2. $Cr(CO)_6$ photocatalysed. (80,81)

Starting diene	Product
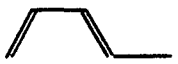	
	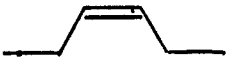
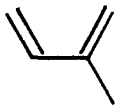	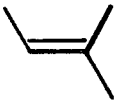
	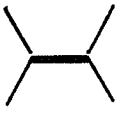
	

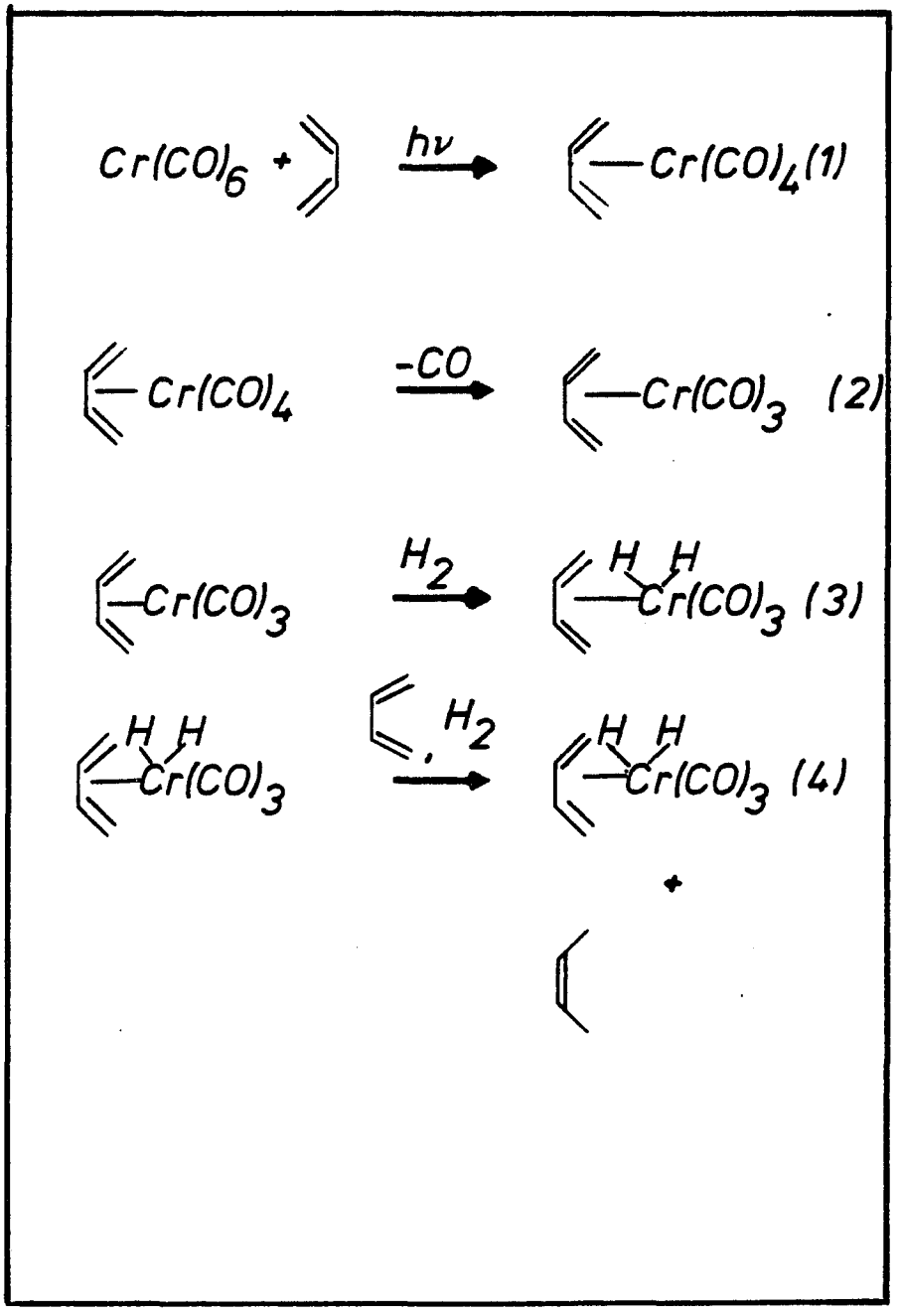

Figure 7. Mechanism of $Cr(CO)_6$ photocatalyzed 1,4 addition of H_2 to 1,3 dienes.

This thesis is a report of the experiments performed to explore 1) the photochemistry and photophysical properties of Group VIB hexacarbonyls adsorbed onto porous Vycor glass. 2) the potential of using these hybrid systems as viable photocatalysts in the transformation of substrates into more commercially attractive molecules.

Chapter 2

Experimental Section

A. Materials.

Group VIB hexacarbonyls, $Cr(CO)_6$, $Mo(CO)_6$, and $W(CO)_6$ were obtained from Pressure Chemical Company and used without further purification. UV-visible and infrared spectra of the complexes were in excellent agreement with published spectra. $W(^{13}CO)_6$ (90%enriched) was also obtained from Pressure Chemical, and the enrichment was confirmed by mass spectra and infrared spectra of the labeled material (Figures 8 and 9). All solvents used were HPLC grade (Fisher Scientific Co.) and were dried over molecular sieves. Gaseous reagents (Linde) were used without further purification since each had a purity > 99%. The only exception was CO_2 which was passed through a chromous solution to remove oxygen.

B) Preparation of $W(CO)_5(P(C_6H_5)_3)$ (83,84).

A mixture of 1.05 g (0.004 moles) triphenyl-phosphine (Alfa) phosphine (Alfa Ventron), 1.62 g (4.6 mmol) of tungsten hexacarbonyl in 10 ml of diglyme was heated to reflux for 4 hours. The hexacarbonyl, which sublimed into the condensor during the reflux, was returned to the reaction vessel by means of a copper wire ramrod. The reaction mixture was cooled, filtered, and the solvent removed on a roto-evaporator at reduced pressure. 2.1 g (89%) of green-yellow crystals were obtained and then recrystallized three times from a mixture of chloroform and

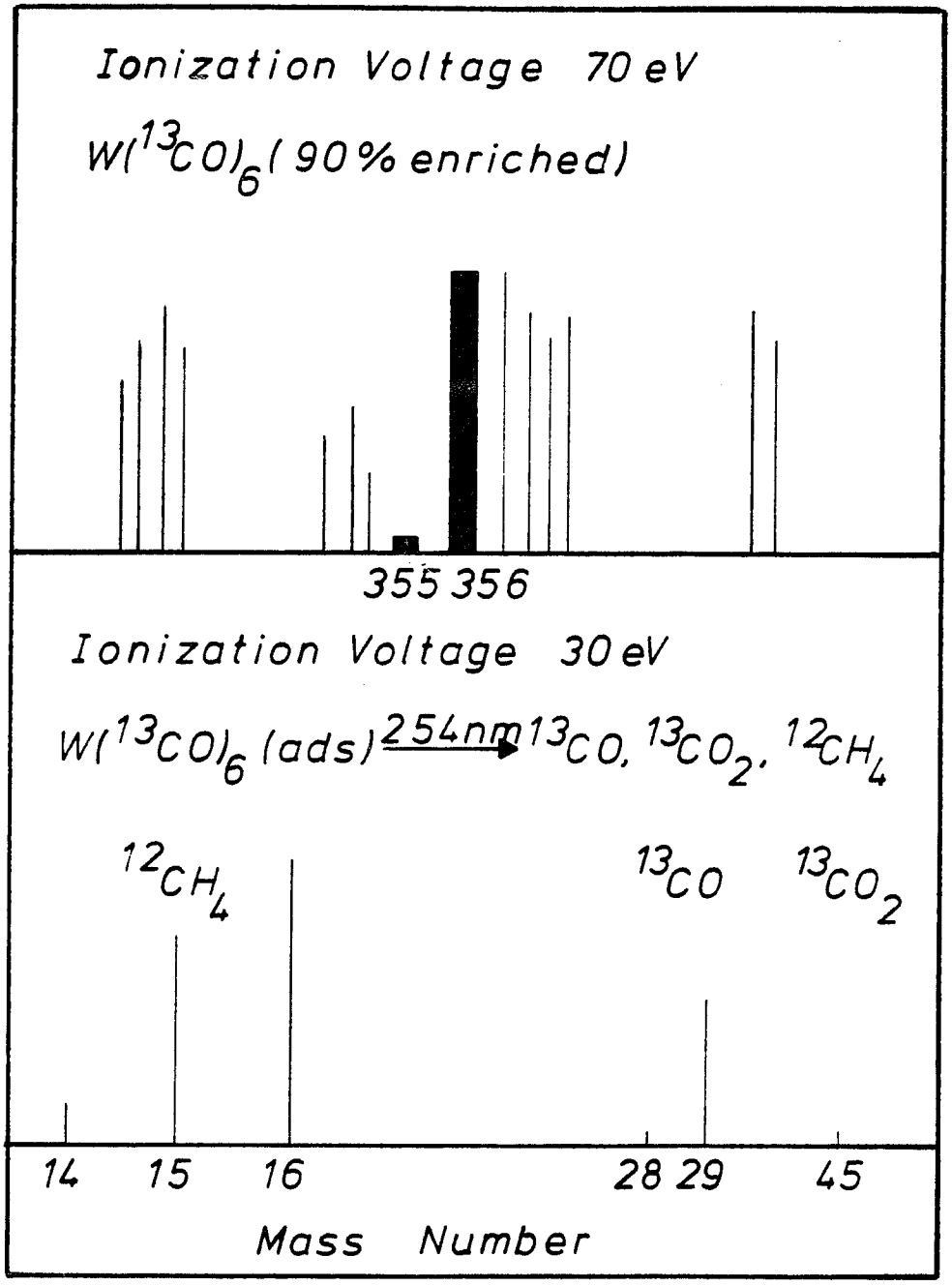

Figure 8a. Mass spectrum of $W(^{13}CO)_6$. The spectrum indicates the 90% enrichment of the labeled complex.

Figure 8b. Photolysis of $W(^{13}CO)_6$ads at 254 nm. Mass spectrum of isolated products.

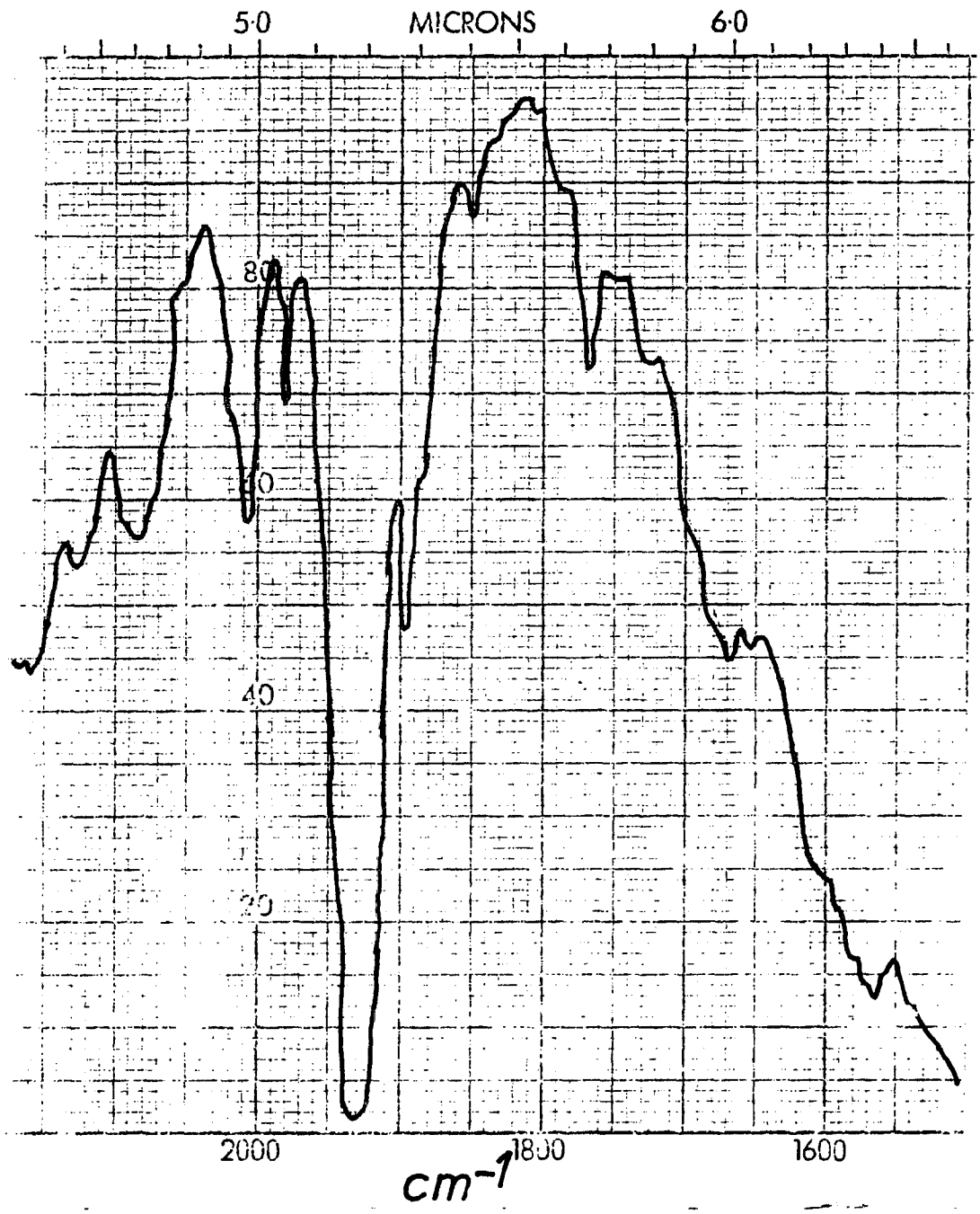

Figure 9. Infrared spectrum of $W(^{13}CO)_6$ dissolved in n-hexane. Spectrum illustrates the 90% enrichment of labeled complex.

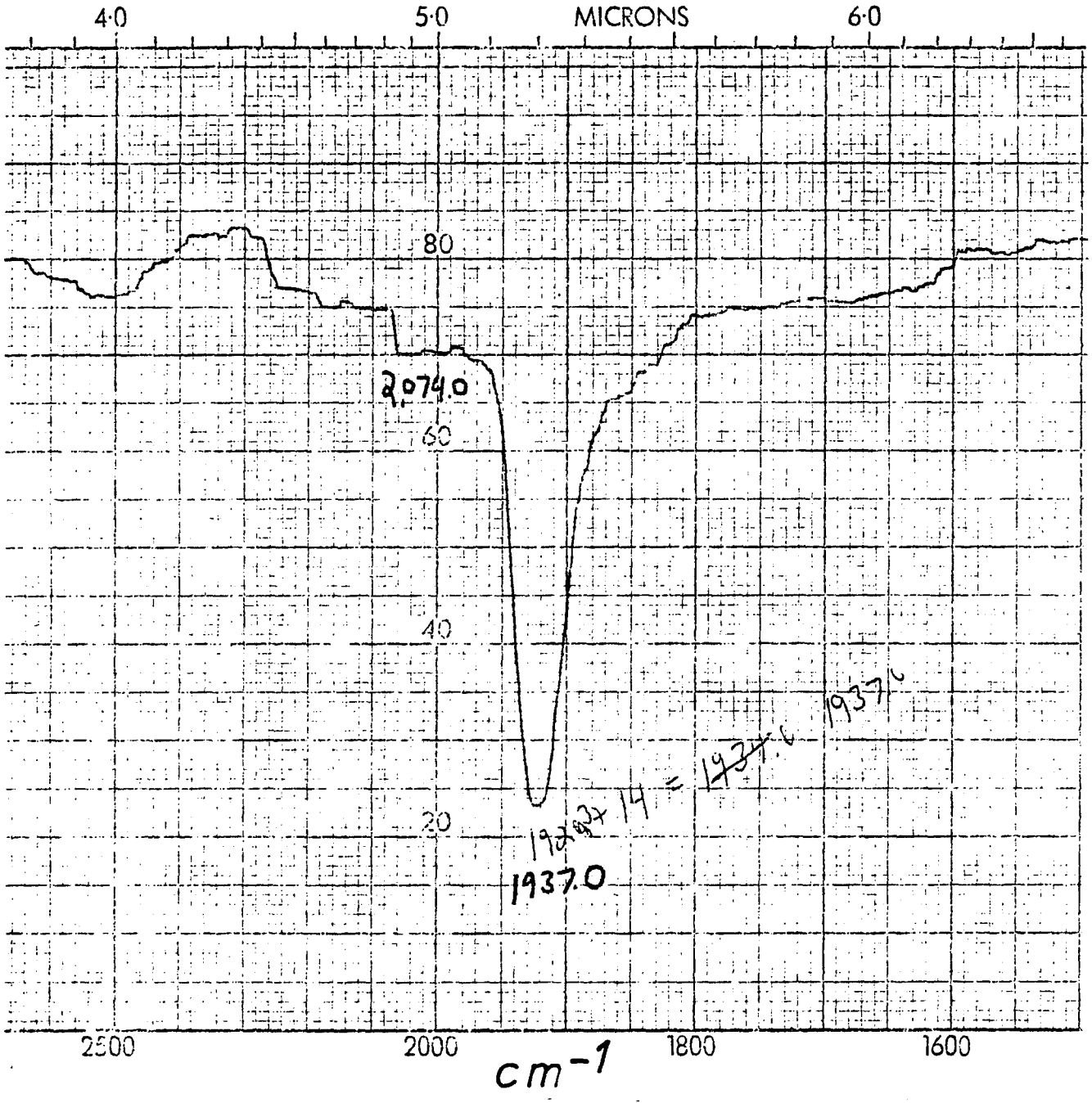

Figure 10. Infrared spectrum of $W(CO)_5P(Ph)_3$ dissolved in $CHCl_3$.

ethanol. The resulting pale yellow crystals weighed 1.6 g (68%) and melted at 145-147 °C (theoretical: 146-147°C). The UV-visible absorption spectrum of the complex in n-hexane, exhibits two absorptions; a 227-nm M π^* CO charge transfer transition, (ϵ =6.79 x 10^4 M^{-1} cm^{-1}), and at 347-nm a $^1A_1 \longrightarrow {}^1E$ ligand field transition, (ϵ =2.2 x 10^3 M^{-1} cm^{-1}). The infrared spectrum of the complex in hexane, shown in Figure 10, is in good agreement with the reported spectrum of the complex in $CHCl_3$ (84) where bands at 2075m, 1980sh, and 1938vs are observed.

C) Preparation of $(C_2H_5)_4N^+HW(CO)_5^-$ (85).

A mixture of $W(CO)_6$ (2.11g, 6.0mmol), powdered KOH (5.05g, 90mmol), and Et_4NHSO_4 (1.36g, 6mmol) was added directly under nitrogen to a three-necked 250ml flask equipped with a mechanical stirrer, reflux condensor, and a Claisen adaptor for nitrogen purging and IR sampling. Acetonitrile, 80 ml, was added to the flask followed by 0.4 ml of water under nitrogen. The mixture was heated to 60°C and stirred for one hour. During stirring, the solution gradually changes from yellow to orange and then back to yellow. IR spectra recorded after 1 hour indicated that $W(CO)_6$ had been consumed. The mixture was then cooled to room temperature, dried over $MgSO_4$, and then filtered through celite into a Schlenk vessel. The solvent was removed under vacuum, and the residue triturated with 30 ml of THF and then filtered. Hexane, 8 ml, was added to the

resulting THF solution, and this mixture was cooled in an ice bath. After cooling to room temperature, a small amount of a semisolid material was removed by filtration and its spectral properties indicated that it consisted primarily of the dianion $W_2(CO)_{10}^{2-}$: IR ν(CO)(CH_3CN) 1940 w, 1890 vs, 1865 sh, 1770 s cm^{-1} (86). The filtrate was evaporated to dryness, the solid was collected, washed several times with hexane, and dried under vacuum. 2.0 gm of the resulting yellow-orange powder was collected in 73% yield. The IR spectrum of the of the complex in hexane, Figure 11, is in good agreement with reported spectrum of the complex in CH_3CN where CO bands at 1890 (s) and 1850 (m) are observed.

D) Preparation of $W(CO)_4$(o-phen) and $W(CO)_4$(bpy)(72,88,89)

The $W(CO)_4L$ (L=1,10-phenanthroline, o-phen, and 2,2'-bipyridine, bpy) complexes were prepared by 350-nm irradiation of an N_2 purged, 25°C hexane solution of $W(CO)_6$ in the presence of one equivalent of the appropriate ligand. In hexane, the $W(CO)_4L$ complexes are sparingly soluble and immediately precipitate from the reaction mixture. The precipitate was collected and recrystallized from CH_2Cl_2 by addition of n-hexane. The complexes were characterized by their absorption spectra and IR spectra (88,89). The latter, in goo' agreement with published spectra of the CO region, shows bands at 2010 $\pm$ 10 cm^{-1} (w), 1910 $\pm$ 10 cm^{-1} (vs), 1880 $\pm$ 10 cm^{-1} (s), and 1830 $\pm$ 10 cm^{-1} (s).

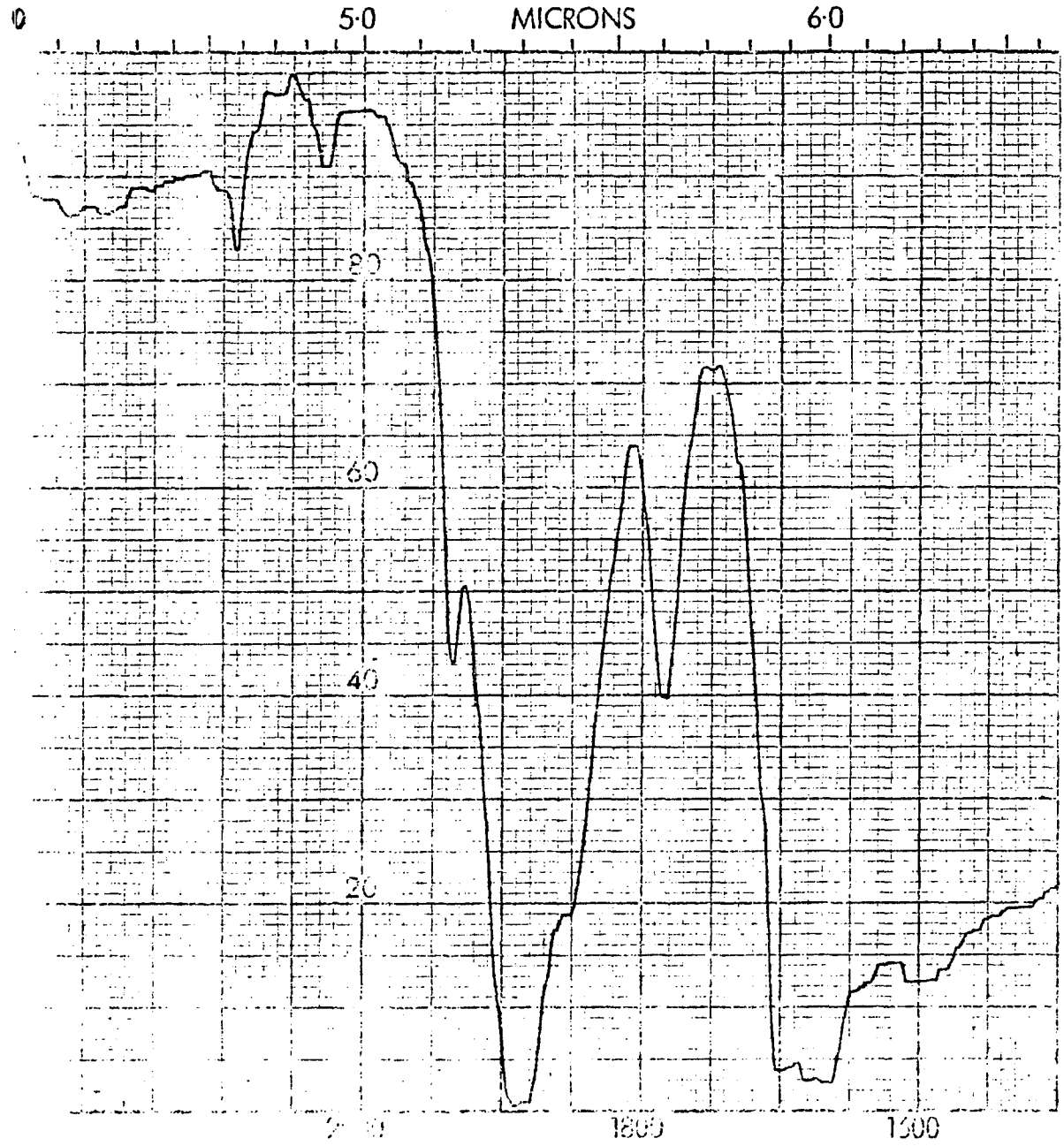

Figure 11. Infrared spectrum of $Me_4N^+HW(CO)_5^-$ in CH_3CN.

E) Impregnation Procedures.

25mm x 20mm x 4mm pieces of Corning code no. 7930 porous Vycor glass were extracted in a Soxhlet extractor with distilled water, and then dried in a vacuum oven at 50°. The dried glasses were then calcined in a muffle furnace at 600°C in air or at the same temperature in a tube oven under flowing O_2 or H_2 for > 72 hours to remove volatile carbonaceous impurities. Cleaned pieces were cooled to room temperature in a vacuum desiccator.

Impregnation was accomplished by conventional procedures (90-92). Clean, dry samples of PVG were mounted upright in an Eastman Kodak chromatogram developing jar (catalogue number 13265). 50 ml of an n-hexane solution, generally 10^{-3}-10^{-2} M in $M(CO)_6$, was added and the sample soaked for > 12 hours. The adsorption of the complex was monitored periodically by UV-visible spectroscopy to achieve the desired loading, and the number of moles adsorbed was calculated from the change in optical density of the impregnating solution.

The impregnated samples were rigidly mounted with a Teflon holder in a 1-cm x 2.2-cm x 4-cm quartz or Pyrex cell with a 7.62-cm O.D. O-ring joint. The cell was attached to a pyrex top which has a 2-mm high vacuum valve and 10/30 joint. The entire cell apparatus, illustrated in Figure 12, was then attached through the 10/30 joint to a vacuum line and the excess solvent and air was removed under vacuum ($p<10^{-3}$ torr).

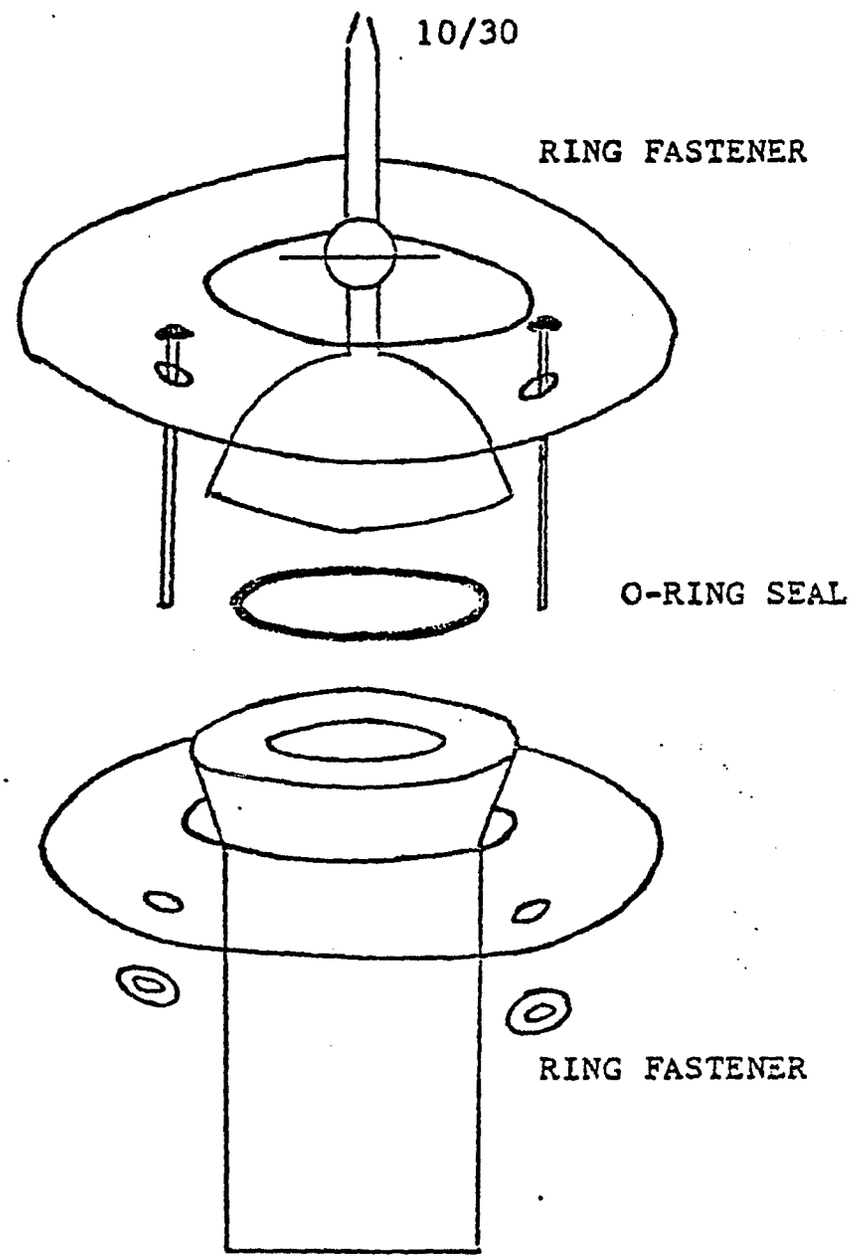

Figure 12. Cell apparatus.

F) Spectroscopic Monitoring and Instrumentation.

Difference spectra, indicative of only the adsorbate, were obtained by placing a quartz cell containing an untreated piece of PVG in the reference compartment. Using this procedure, absorption spectra were recorded on a Cary 14 or a Techtron 635 spectrophotometer adapted with rectangular mounts to accomodate the quartz cell containing the impregnated PVG. Resonance Raman spectra were obtained with a Spectra-Physics 164-08 Laser. The Raman scattering was spectrally resolved with a Spex Industries 14018 double monochromator. The transmitted light was detected with an RCA 31034A photomultiplier and Pacific Precision Instruments model 126 photometer and displayed on a Beckman model recorder. Room temperature emission spectra were recorded on a Perkin-Elmer Hitachi MPF-2A emission spectrophotometer equipped with a red-sensitive Hammamatsu R928 photomultiplier. The cell holder of the spectrometer was adapted to rigidly hold the rectangular quartz cell and the impregnated PVG in it at an angle of 50° relative to the excitation beam. The emission from the surface of the sample was monitored from 480-700-nm at right angles to the excitation. Infrared spectra were measured on a Perkin-Elmer 598 spectrophotometer. IR spectra of either nujol mulls or hexane solutions of the complexes were recorded in NaCl cells and calibrated against polystyrene.

Gaseous photoproducts were collected with a Toepler pump and quantitatively transferred to a Gow-Mac 69-100 gas

chromatograph equipped with a rhenium-tungsten thermal conductivity detector. Molecular sieve 5 Å (80/100 mesh) was packed in a 6 x 1/4" stainless steel column for the analysis of H_2, CH_4, and CO and a 6' x 1/4" column packed with Chromosorb 102 (100/120 mesh) was used for CO_2 analysis. CP grade Argon (Matheson Gas Products) was used as a carrier gas in the simultaneous detection of H_2, CH_4, and CO. In each measurement, the gas chromatographs were calibrated using CP grade CO, CH_4, CO_2, and H_2, obtained from Linde. A known volume and pressure of each gas was injected into the gas chromatograph and the resulting peak area versus number of moles of gas is illustrated in Figure 13. The different slopes for each gas reflect the difference in thermal conductivity of the solute gas relative to the carrier gas. Table 3 summarizes the slopes obtained for each gas in a variety of carrier gases. In all measurements, the gas chromatographic conditions were (except where indicated) an oven temperature of 100°, a flow rate of 40 ml/min., and a detector current of 150 mA. The detector response was displayed on a Shimadzu R-111 millivolt recorder. Retention times for the various gaseous products are summarized in Table 3 and a typical chromatogram is displayed in Figure 14.

In catalyzed olefin reactions, the gaseous products were collected in a gas tight syringe (Hamilton Company) and analyzed on a Varian 2400 gas chromatograph equipped with a

Figure 13. CO calibration curve. Helium carrier gas, Detector 200 mA, and Attn:4.

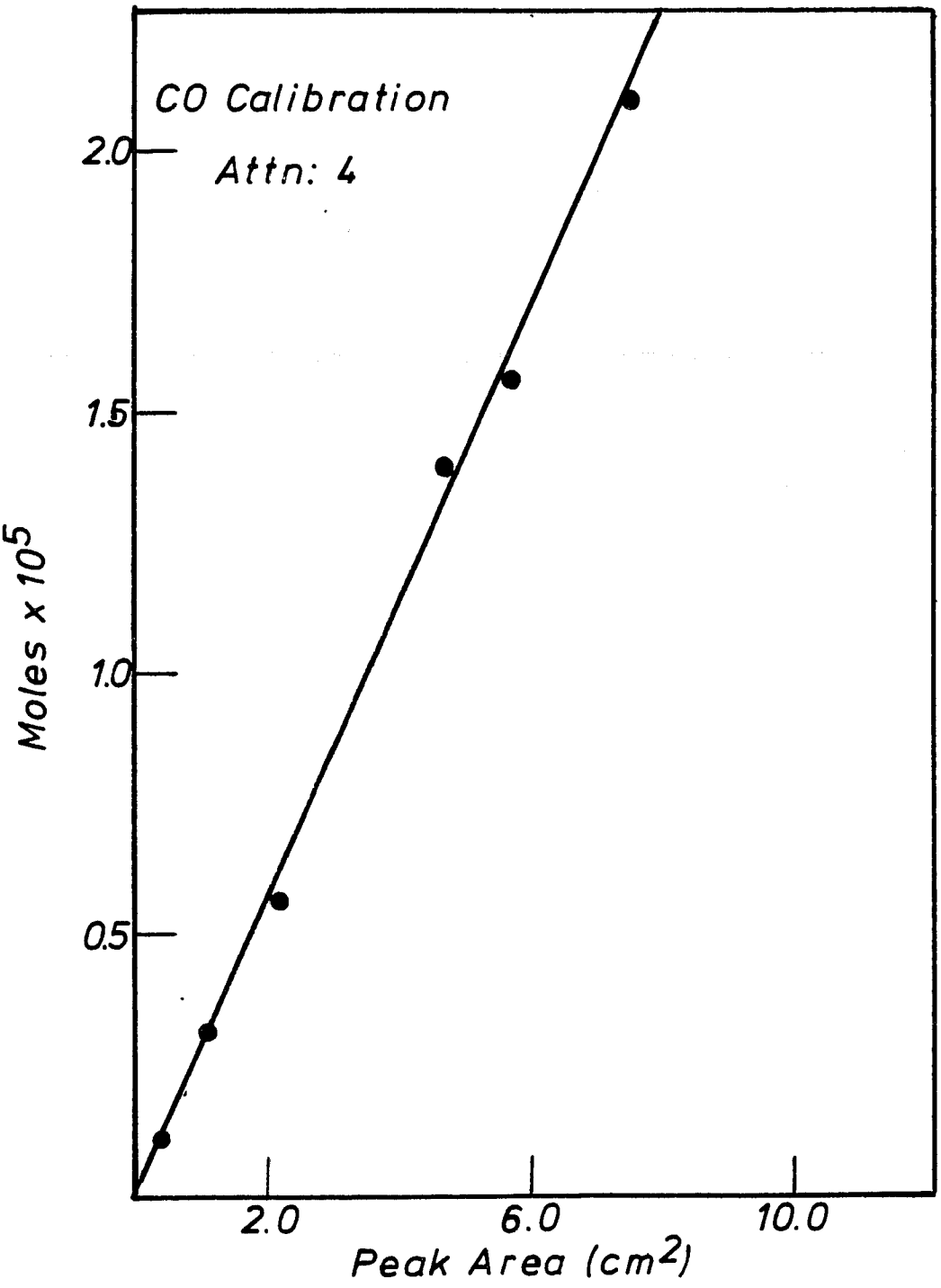

Table 3. Thermal Conductivity Detector Response for H_2, CH_4, and CO in Various Carrier Gases

Carrier Gas	Calibration Slope x 10^6		
	H_2	CH_4	CO
Nitrogen	16.9 (a)	8.74 (a)	N.R.
Helium	N.R.	1.25 (b)	1.54 (b)
Argon	1.35 (c)	3.76 (c)	13.0 (c)

a) Attn: 8 detector 150 mA

b) Attn: 4 detector 200 mA

c) Attn: 16 detector 150 mA

Retention Times

H_2 1.5 minutes

CH_4 4.8 minutes

CO 8.0 minutes

Figure 14. Gas chromatogram showing separation and simultaneous detection of: 1=H_2, 2=O_2, 3=N_2, 4=CH_4, and 5=CO.

Gas chromatographic conditions: Argon carrier gas at 40 ml/min., thermal conductivity detector at 150 mA.

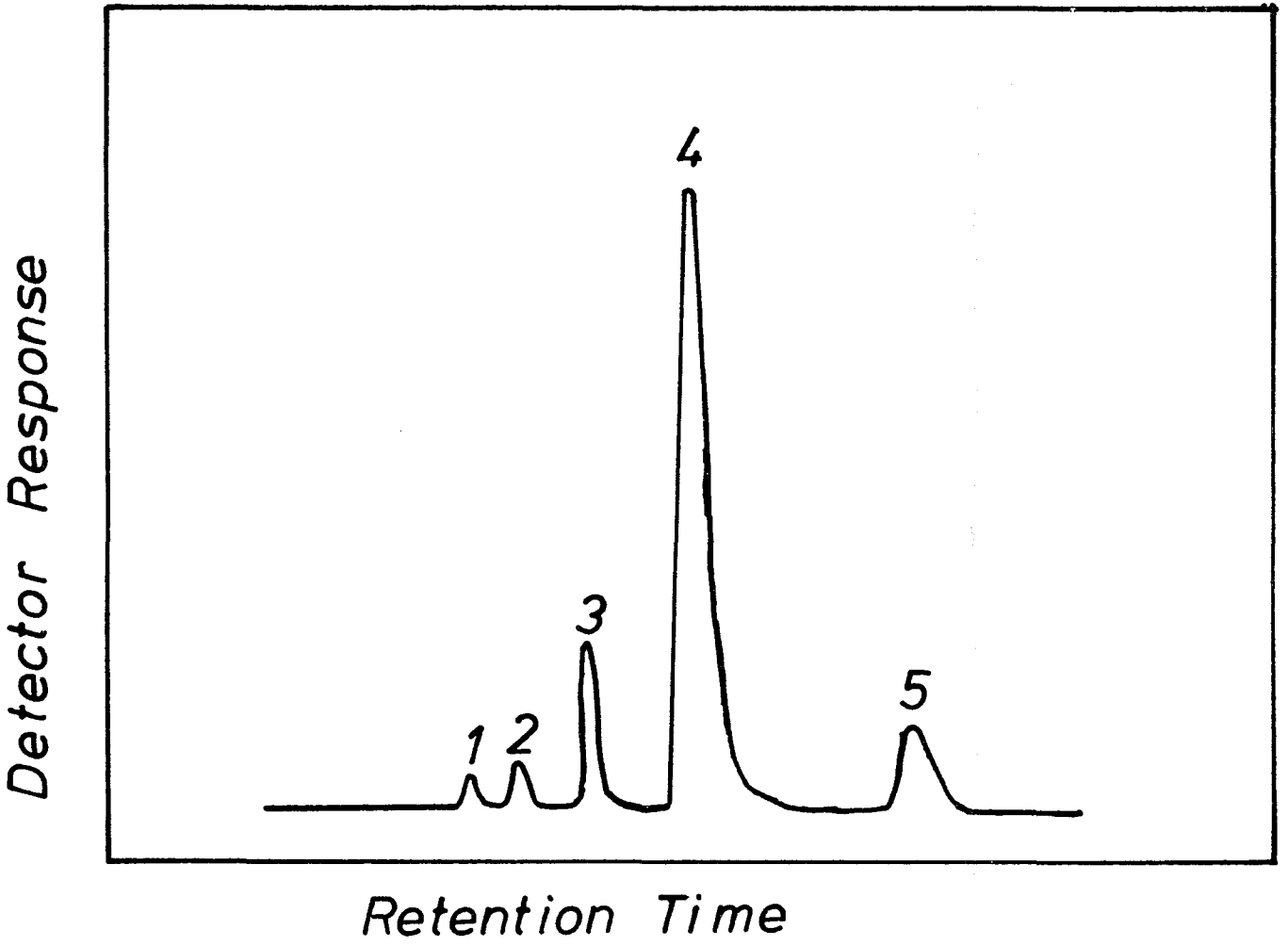

flame ionization detector. A 20' x 1/8" stainless steel column containing tricresyl phosphate as a liquid phase bonded to Chromosorb PAW (100/120 mesh) was used to separate the various olefins. A typical chromatogram, using N_2 as the carrier gas, is illustrated in Figure 15. Gas chromatographic conditions used throughtout were a flow rate of 20 ml/min., an oven temperature of 100°C, an injection temperature of 130°C, and a detector temperature of 130°C.

EPR spectra of crushed PVG (60/80 mesh) containing adsorbed complexes were recorded on a IBM-Bruker 200E-SRC spectrometer equipped with a 9.78 GHz microwave source. Room temperature NMR spectra were recorded on a 60 MHz Varian EM 360 Spectrometer. Mass spectra were obtained with a Varian MAT CH7 mass spectrometer. The instrument was calibrated against perfluorokerosene, PFK. Gas samples were isolated with a Toepler pump and transferred to the mass spectrometer. The mass spectrum was recorded on a Siemans galvanic recorder. The vacuum line was equipped with a Sargent-Welch Duo-Seal pump that was capable of a vacuum $< 10^{-3}$ torr.

Kinetic studies were done in a Techtron 635 spectrophotometer containing a thermostated cell that was connected to a Haake FK 2 temperature bath.

A Rayonet photochemical reactor (Southern New England Ultraviolet Corporation) was used to irradiate the samples. The impregnated PVG samples, mounted in evacuated 4-mm x

Figure 15. Gas chromatogram of various olefins. 1=1-butene, 2=trans-2-butene, and 3=cis-2-butene. Nitrogen carrier gas, 20 ml/min., and flame ionization detector were employed.

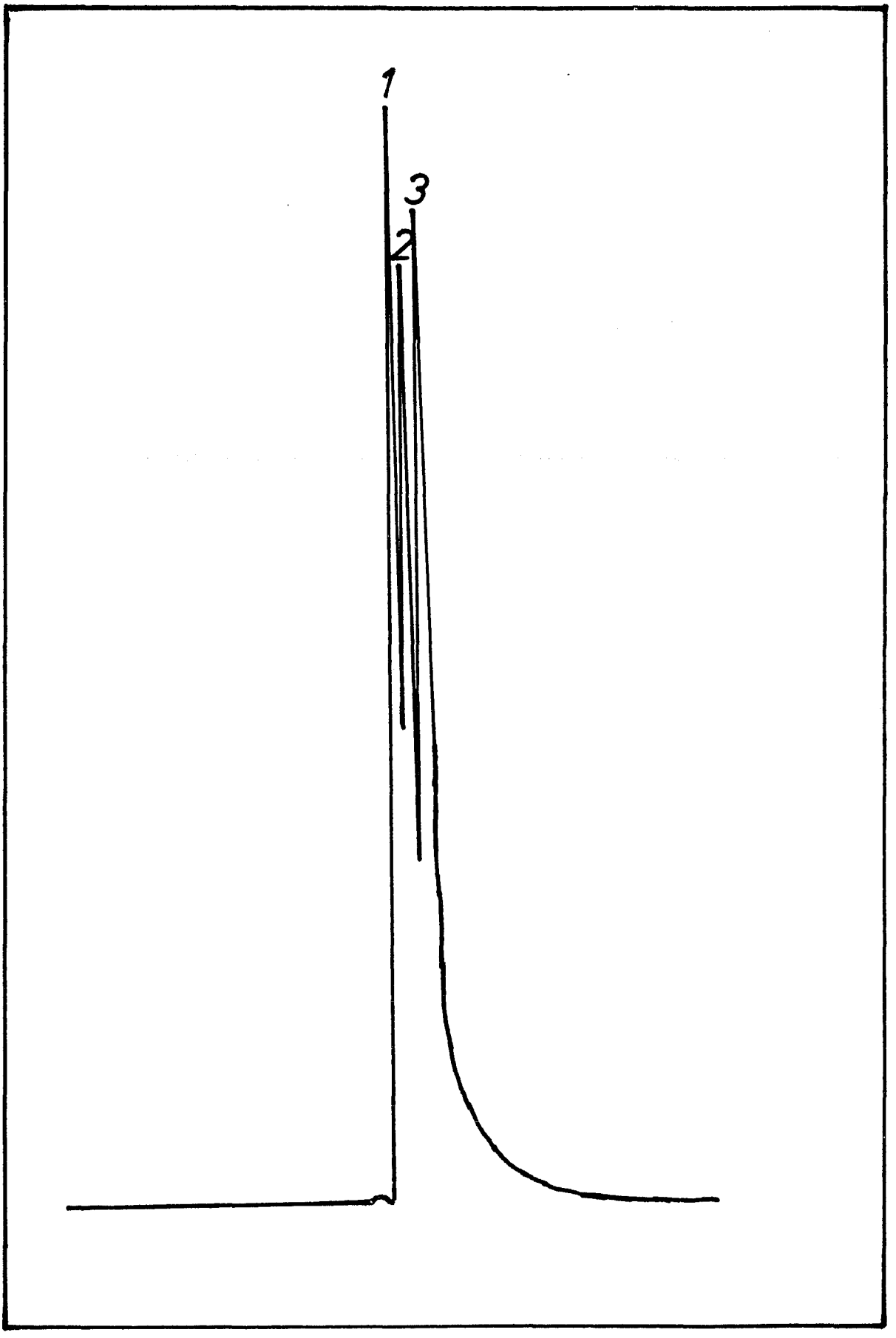
1
3
2
DETECTOR RESPONSE
RETENTION TIME

10-mm x 22-mm rectangular quartz cells, were exposed to 254, 310, or 350-nm light. The circular design of the Rayonet reactor allows each face of the PVG sample to be exposed to a uniform photon flux and light intensities impinging on the sample were measured by ferrioxalate actinometry (93a,b,c).

G) Procedures.

1) Gas Sampling.

Periodic examination of gaseous photoproducts following photolysis was accomplished by isolating the gaseous products in a Toepler pump and transferring the sample to a 4.4 ml loop which is connected to a gas chromatograph. The entire apparatus is illustrated in Figures 16 a,b.

For chromatographic analysis of olefin catalytic reactions, the pyrex cell top, was fitted with a gas sampling valve containing a rubber septum through which a gas tight syringe could withdraw 1.0 ml samples for periodic analysis.

A similar procedure was used to inject gaseous photoproducts into the mass spectrometer. The sample loop, which contained ca. 10^{-4} moles of sample, was either connected to a syringe and injected into the mass spectrometer or connected directly to a gas inlet of the spectrometer.

Isotopic labelling studies were done by treating PVG with D_2O, (>99% pure, Norrell Chemical Company) for 24 hours. Excess D_2O was removed by vacuum and the sample impregnated with $W(CO)_6$ and photolyzed. The labeled

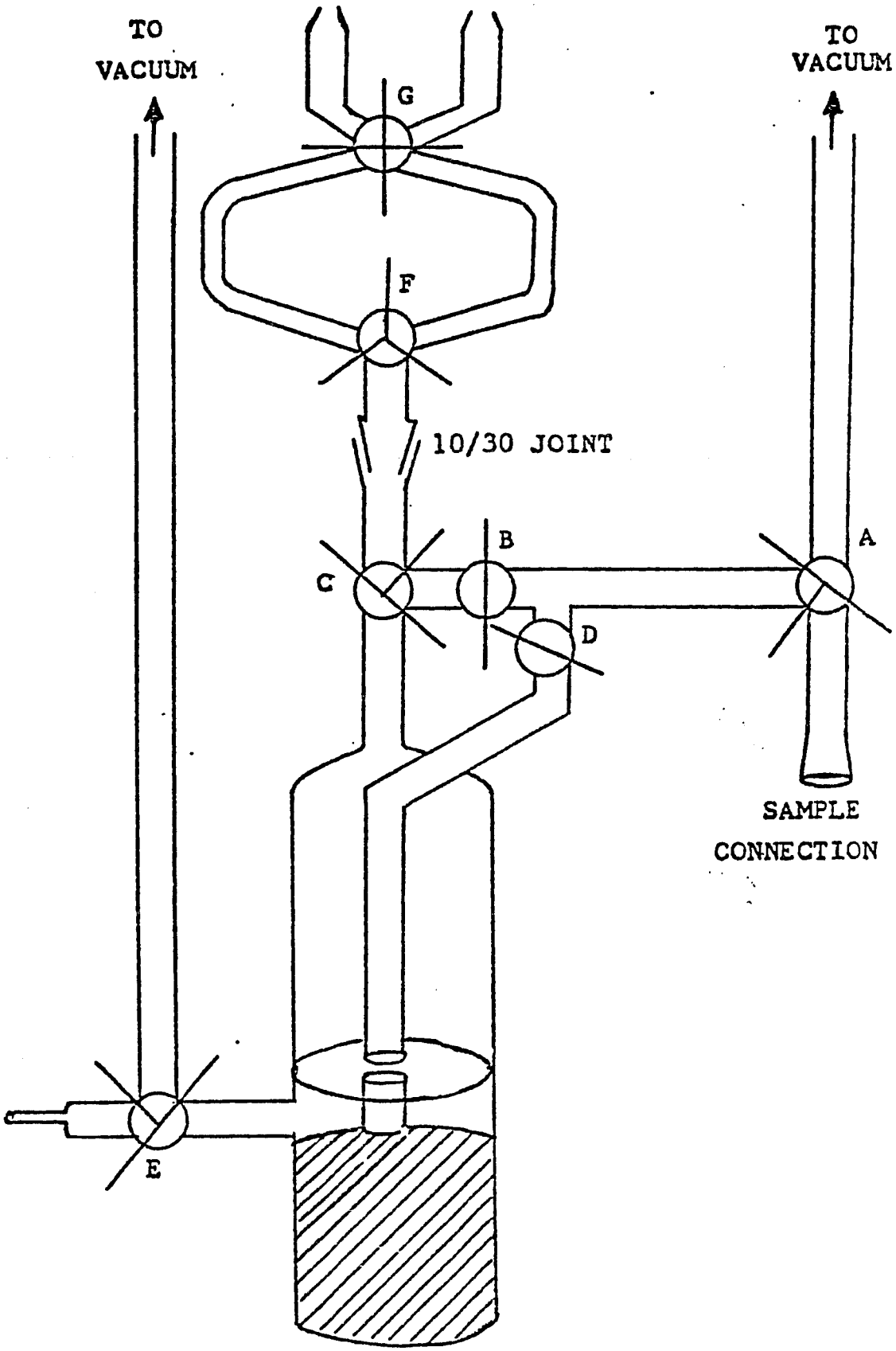

Figure 16a. Toeppler pump apparatus.

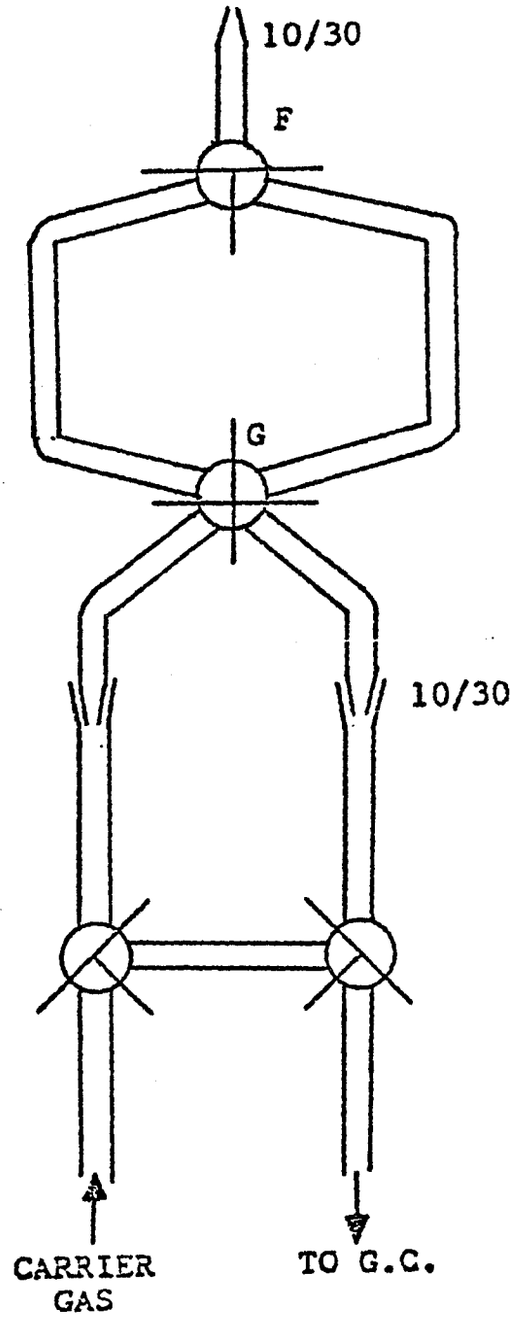

Figure 16b. Connection of gas sampling loop to gas chromatograph.

photoproducts were isolated in the same manner as described above and transferred to the mass spectrometer. In general, repetitive scans were run to ensure that true representation of the isotopic distribution was reaching the analyzing tube of the mass spectrometer.

2. EPR Studies.

All reagents were adsorbed on crushed PVG (60/80 mesh) and placed in a small capillary tube which was then placed in a cylindrical quartz cell with an attached 2-mm high vacuum valve and a 10/30 joint (Figure 17). Degassed samples were photolyzed and EPR spectra spectra recorded as a function of photolysis time. Low temperature (77°K) spectra were obtained by placing the quartz cell, containing the crushed PVG sample, into a low temperature dewar filled with liquid N_2 into the cavity of the EPR. Diphenylpicrylhydrazyl, DPPH, was used as an internal standard in all EPR experiments.

3. Distribution Experiments.

Previous studies in this laboratory (94,96) with $Ru(bpy)_3^{2+}$ adsorbed onto PVG established that most of the adsorbed complex was near the surface with little or no reagent adsorbed into the middle of the glass. To determine the distribution of the adsorbed metal carbonyls, the cross-sectional distribution across the sample was mapped.

Several pieces of PVG, whose dimensions were measured with a Vernier caliper, were impregnated as described above. The moles of complex adsorbed were determined spectrally and

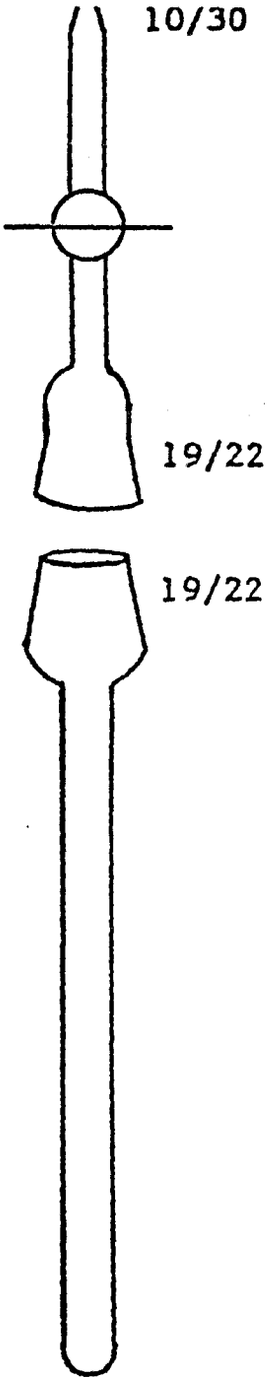

Figure 17. EPR cell.

a visible absorption spectrum of the impregnated PVG, immersed in chlorobenzene (refractive index = 1.5), was recorded relative to a blank sample of PVG. The sample was then removed from the chlorobenzene and one face was ground with very fine grade sandpaper. The ground sample was returned to the chlorobenzene and the visible spectrum recorded relative to an untreated PVG sample in chlorobenzene. The chlorobenzene was checked spectrally for possible leaching of the adsorbed complex. This process was repeated until grinding caused no further spectral change, then the process was repeated on the other side of the sample. A plot of optical density as a function of relative sample thickness, constructed from this data, is illustrated in Figure 18. Since Figure 18 shows that the complexes impregnate only the region adjacent to each surface, the fractional surface coverage is calculated in the following manner.

A 2.7 x 1.9 x 0.44-cm glass containing 2.30×10^{-5} moles of $W(CO)_6$ showed a 97% decrease in optical density when a 0.44-mm layer is removed from the front and back surface. From the volume of the layer (0.236 cm^3) and the density of the glass, 1.393 g/cm^3 (43-52), the mass of the layer is calculated to be 0.263 g. The fractional surface coverage is calculated from equation 9.

$$f_s = \text{moles adsorbed} \times N \times r^2(m^2)/\text{Surface Area} \times \text{weight} \quad (9)$$

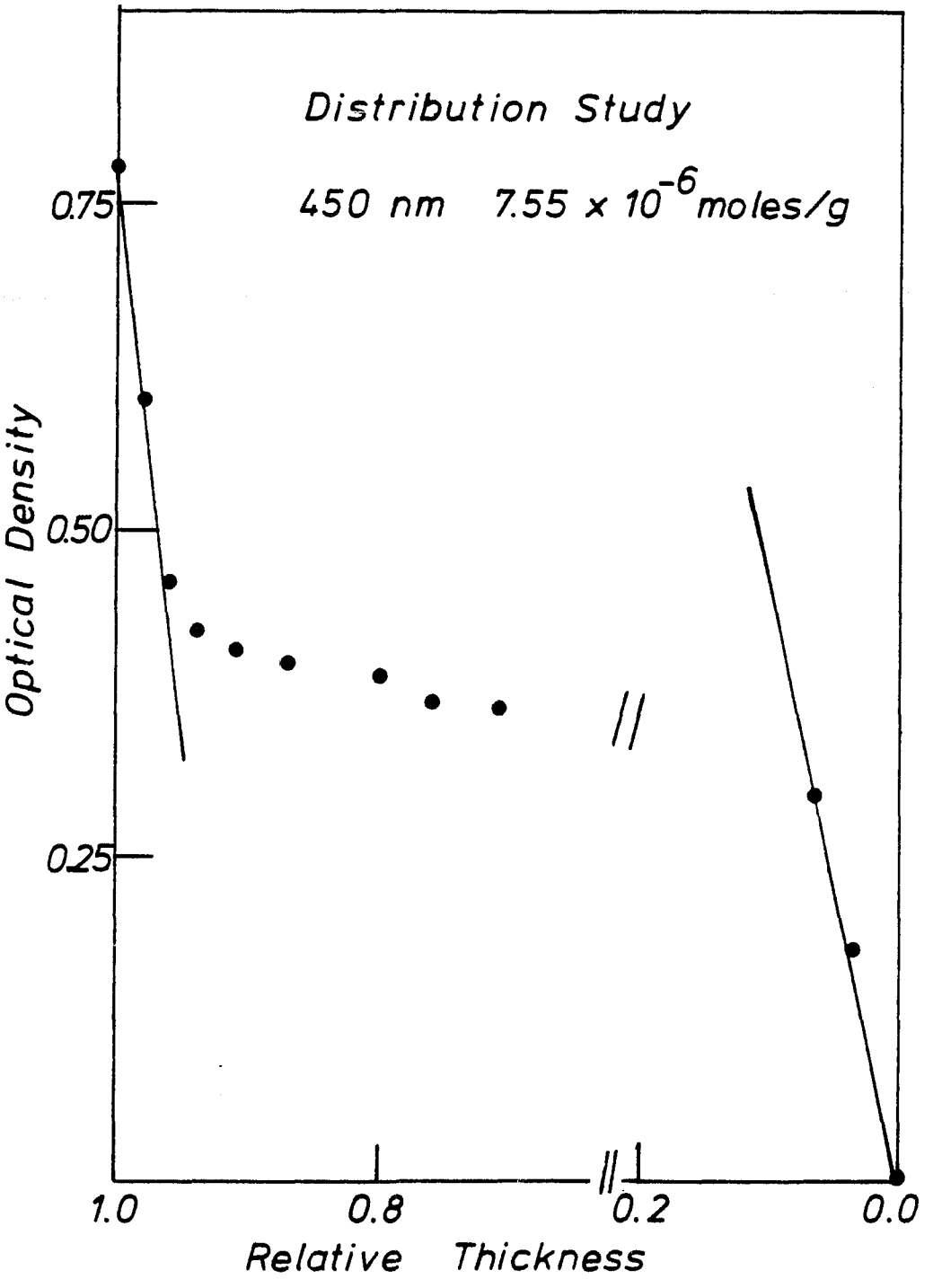

Figure 18. Distribution of $W(CO)_6$/PVG.

where N is Avogadro's number, r is the radius of the molecule, surface area is $130 m^2/g$, and the weight is the weight of the glass. Therefore, the fractional surface coverage, for this particular experiment is 3.69×10^{-2}.

4. Adsorption Isotherms.

Adsorption isotherms were determined by the methods of Ross and Olivier (97). The temperature dependence of each isotherm was determined over the range $1.0^{\circ}C$ to $79.0^{\circ}C$ by fitting an electrically heated sand bath around the cell containing the PVG sample.

Chapter 3

Results

A. Adsorption of Reagents.

Corning code no. 7930, porous Vycor glass, PVG, which is a highly porous form of silica with pore sizes in the range of many silica gels, consists of 96.3% SiO_2, 2.95% B_2O_3, and 0.72% R_2O_3 and RO_2 (43-52). The density is 1.38 gm/ml, void space 28%, and specific surface area 130 m^2/gm (43-52). The PVG used in these studies contains $1.2 \pm 0.3 \times 10^{18}$ cavities/gm, which are 70 ± 21 A in diameter, and are interconnected throughout in a random three dimensional array (43-52,94,96).

In distilled water at $25 \pm 0.1^{o}C$, PVG develops zeta potential of -26 ± 2 mV, which indicates an anionic surface (95). The adsorption onto PVG of a series of indicator dyes and their subsequent color changes, indicate a surface pH of ca. 4-5 (99). Consistent with the anionic nature of the surface, previous studies in this laboratory (94,96) have established that anionic complexes are not adsorbed onto PVG. However, neutral complexes, such as metal carbonyls, and cationic complexes are readily adsorbed onto PVG (98).

A comparison of the absorption spectrum of $W(CO)_6$ in n-hexane and $W(CO)_6$ads is illustrated in Figure 19. The UV spectrum of $M(CO)_6$, in n-hexane solution, is dominated by an intense metal to ligand charge transfer absorption (in hexane, $\epsilon = 1.42 \times 10^4$ M^{-1} cm^{-1}). Upon adsorption, a 4nm blue shift of the MLCT maximum

Figure 19. UV absorption spectra of $W(CO)_6$/n-hexane and $W(CO)_6$ads

●=$W(CO)_6$/n-hexane (9.15×10^{-4} M)

▲=$W(CO)_6$ads (8.16×10^{-7} moles adsorbed).

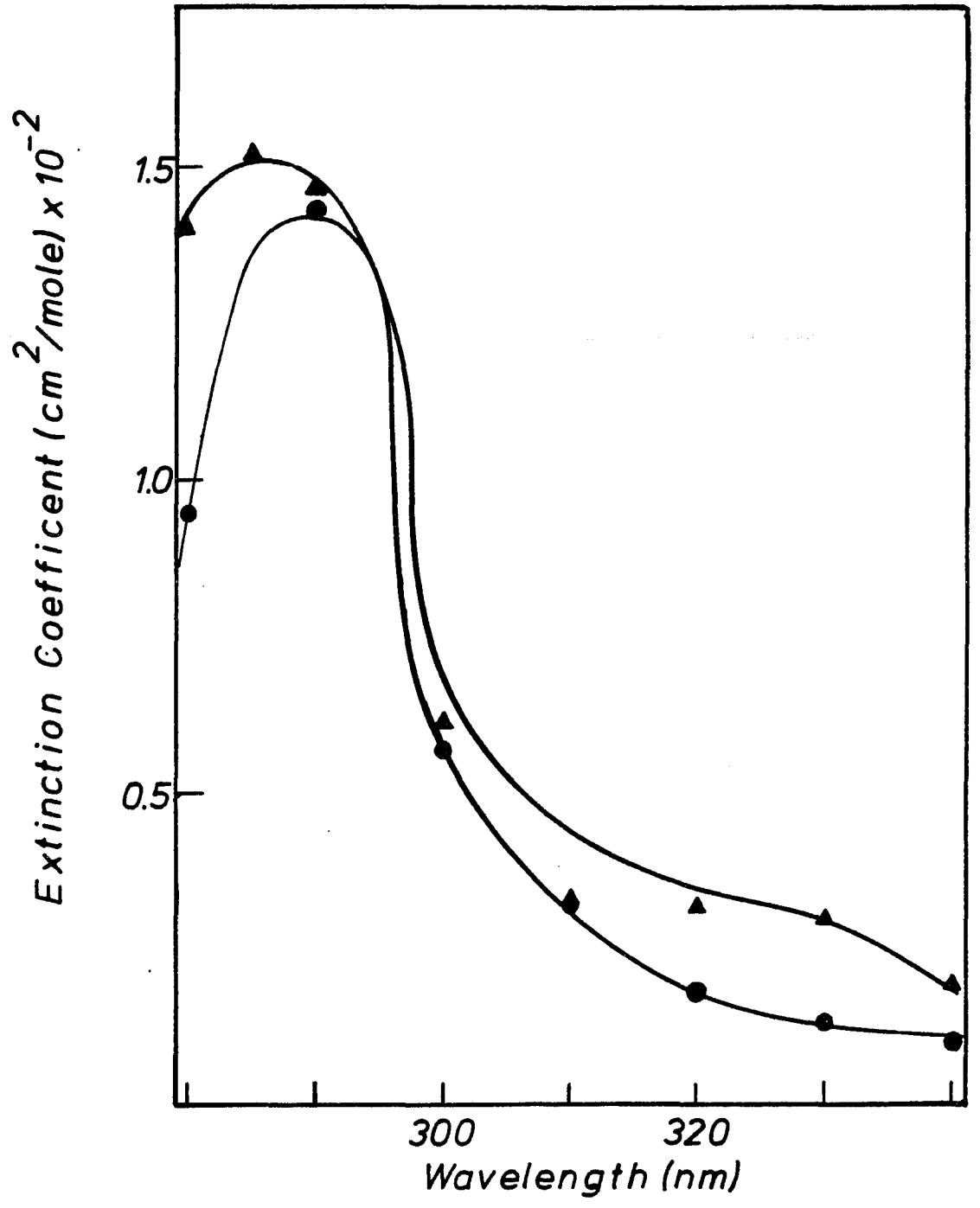

occurs. The weak ligand field bands observed in fluid solution, as well as higher energy MLCT, found at 223 nm in n-hexane are not observed in the spectrum of the adsorbed complex because of high absorption due to PVG. However, the absence of low energy ligand field bands in the 370-450-nm region, which ususally accompany substitution, indicates that the primary coordination sphere of these complexes are not disrupted on adsorption. Further support for a lack of change on adsorption, is the excellent agreement between the FTIR-PAS spectra and conventional IR spectra in n-hexane (Table 4). The similarity of these spectra as well as the absence of significant changes in the absorption spectra establish that these complexes are physisorbed onto PVG without disruption of their primary coordination spheres.

The distribution of adsorbed reagents was determined spectrally. Absorption spectra recorded at various points on the impregnated piece are within experimental error (<7% deviation) and indicate a uniform distribution of the complex over the outer geometric area of the sample. In order to quantitate the cross-sectional distribution of a known amount of a complex, the impregnated samples were ground and monitored spectrally as a function of relative thickness. A representative plot of optical density versus thickness, Figure 18, of a PVG sample impregnated with 7.55 x 10^{-6} moles of $W(CO)_6$/gm shows, in the volumes adjacent to each face, linear decreases in absorbance of the complex. Similar results are obtained with samples of PVG

Table 4.

UV-Visible and Infrared Absorptions of $M(CO)_6$ and $M(CO)_5$ Adsorbed onto PVG at Room Temperature.

	$M(CO)_6$[a]			$M(CO)_5$[b]
metal	nm	cm^{-1}	FWHM(nm)	nm
Cr	280 (280)	1999 (1980)	30 (20)	450 (489)
Mo	285 (289)	2005 (1980)	10 (20)	405 (411), 244 (247)
W	286 (290)	1986 (1980)	20 (10)	408 (413), 246 (244)

FWHM Full width at half maximum

[a]Values in parentheses are band maxima from spectra of n-hexane solution of the complexes. [b]Values in parentheses are the band maxima reported by Perutz and Turner for the $M(CO)_5$ complex in a 20°K. CH_4 matrix (68-71).

impregnated with different amounts of $W(CO)_6$ or with $Cr(CO)_6$ and $Mo(CO)_6$. The plot confirms a symmetric distribution of the complex amongst the different faces and that no reagent is adsorbed into the interior of the piece. $W(CO)_6$ penetrates 0.4 mm $\pm$ 0.02 mm in the PVG. The linearity of optical density with thickness suggests that the concentration (in moles/unit volume of PVG) $W(CO)_6$ads is constant, and that there is a uniform distribution of the complex within PVG impregnated with the complex. Furthermore, since similar penetration depths are found with different neutral and cationic complexes-the latter ionically bind to the silanol sites- we believe that the 0.4 mm penetration depth reflects the deviation in surface planarity rather than penetration into interior cavities. Scanning electron micrographs of the PVG surface has substantiated this claim (42-53).

Taking 3 Å as the radius of $W(CO)_6$ (100), 130 m^2/gm and 1.38 gm/ml as the surface area and density of PVG, respectively (42-53), impregnation of these volumes with 1.82×10^{-5} moles of complex corresponds to a surface coverage, calculated according to equation 10,

$$f_s = \text{Volume impregnated} \times \text{density} \times \text{surface area} \quad (10)$$

of <3%. Consequently, the vast majority of the surface is vacant and when exposed to the gases used in these studies, the impregnated sample acts as an adsorbent. Representative

adsorption isotherms for cis-2-butene, trans-2-butene, and carbon monoxide are illustrated in Figures 20, 21, and 22, respectively. Typically, < 1-atm of each gas was used in these measurements and the isotherms were corrected for adsorption of the gases by the cell and any residual grease present in the system. This correction was significant for adsorption of cis- and trans-2-butene. The amount of gas adsorbed/gram of untreated PVG is within experimental error of that adsorbed/gram of PVG impregnated with 7.67 x 10^{-6} moles/g of $W(CO)_6$. This suggests that the adsorption of a gas onto PVG is a random process in which the gas molecules are adsorbed onto available PVG sites rather than onto the adsorbed metal complex.

For pressures < 1-atm, the CO isotherm, Figure 22, conforms to the Langmuir derivation (115). To establish the actual adsorption onto the PVG surface, the isotherms determined for cis-and trans-2-butene were constructed from a diference plot, where adsorption onto the line was subtracted from the total adsorption. The temperature dependence of the isotherms indicates that less adsorption occurs as the temperture increases; adsorption of these gases onto PVG is an exothermic process.

The adsorption isotherm for $W(CO)_6$, illustrated in Figure 23, was measured by solution impregnation. Approximating $W(CO)_6$ as a sphere, a molecular surface area is calculated to be 28.25 m^2/gram with a PVG surface area of 130 m^2/g, monolayer coverage occurs at

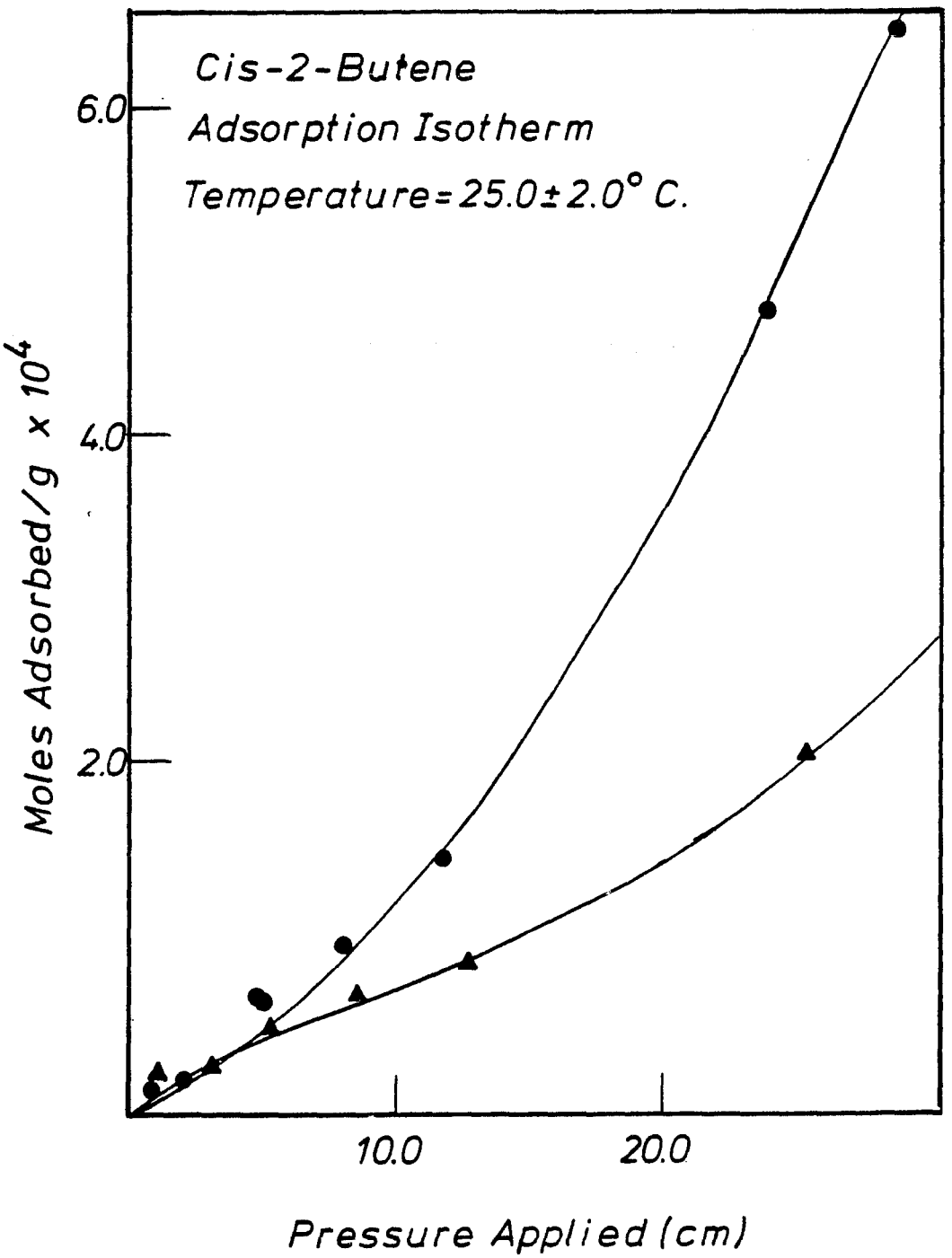

Figure 20. Adsorption isotherm of cis-2-butene. ● = in presence of PVG. ▲ = in absence of PVG. Weight of PVG = 2.9348g.

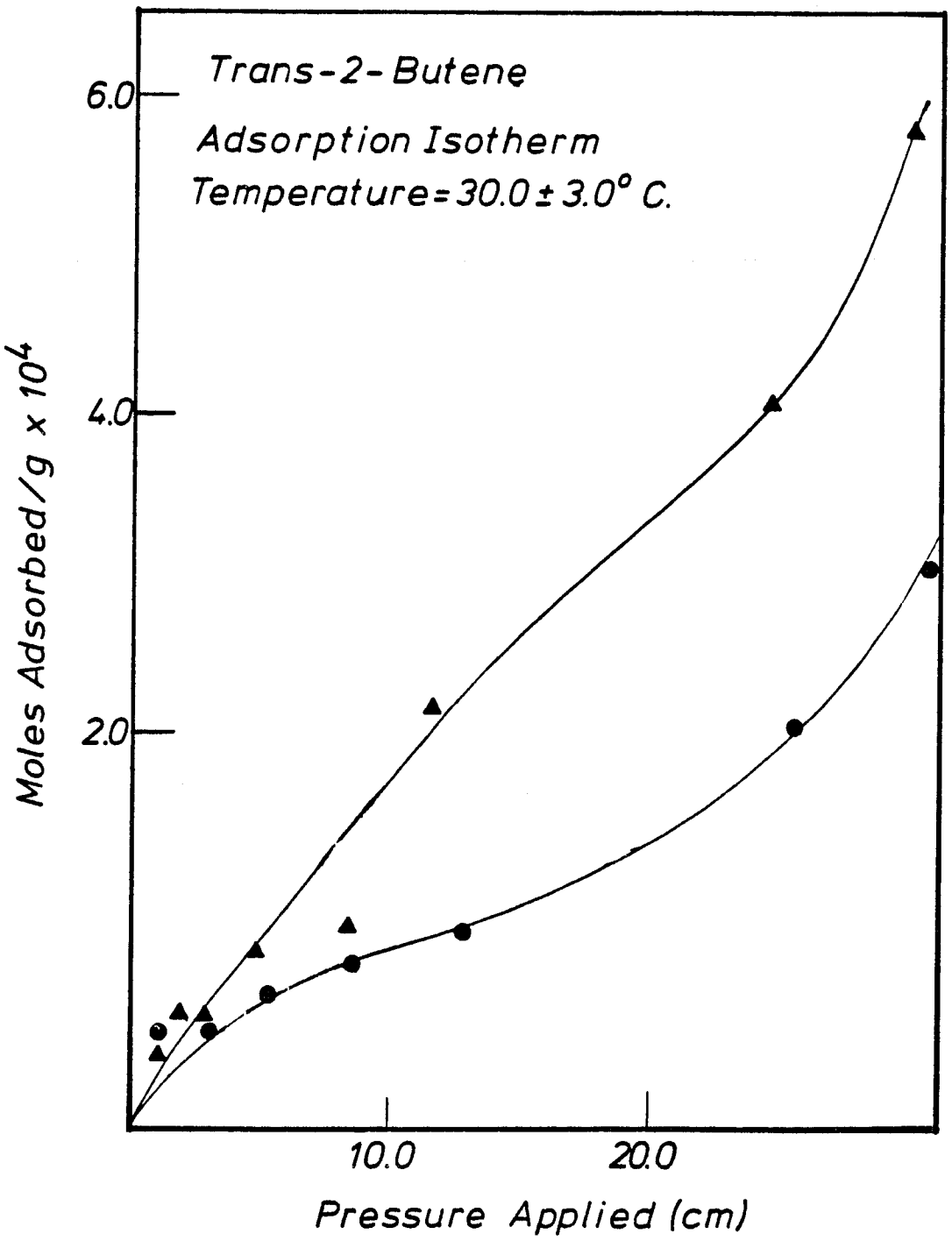

Figure 21. Adsorption isotherm of trans-2-butene. ▲ =adsorption in the presence of PVG. ● =adsorption in absence of PVG. Weight of PVG = 2.9348g.

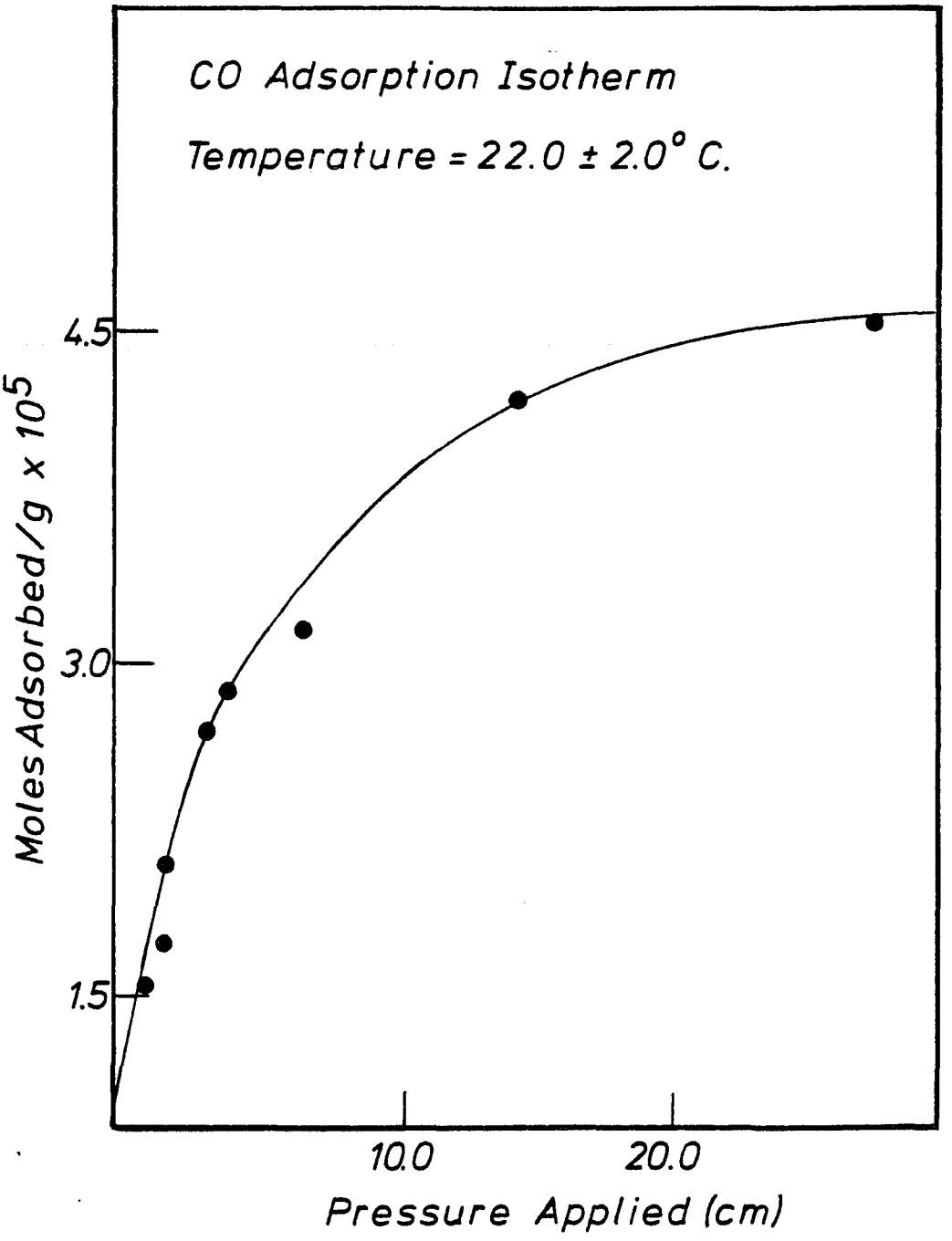

Figure 22. Adsorption isotherm of CO. Weight of PVG = 2.9348g.

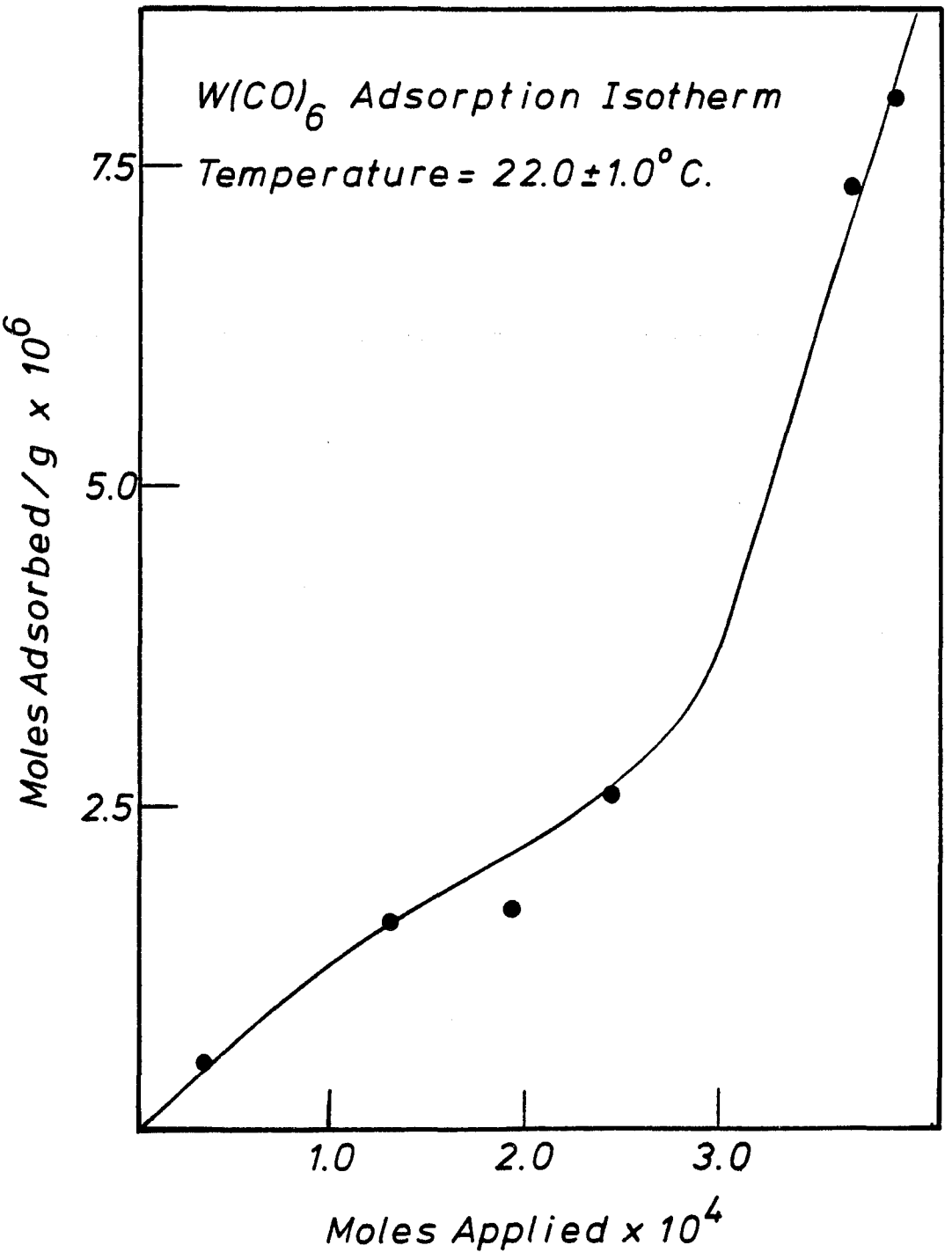

Figure 23. Adsorption isotherm of $W(CO)_6$ using solution impregnation method.

10^{-10}mol/cm^2. Comparing this with the amount of $W(CO)_6$ adsorbed from n-hexane, indicates that the solution impregnation method achieves a limit of <5% of a monolayer coverage.

The rate of adsorption of $W(CO)_6$ onto PVG was measured using 5 clean, dry pieces and immersing each of them in 40 ml of 8.26 x 10^{-3} M hexane solution at 22 ± 1.0°C. The moles adsorbed/g, was monitored spectrally and plotted as a function of time. As illustrated by Figure 24, an initial linear dependence is followed by a region in which no further adsorption occurs. At this saturation point, which occurs at 1.19 x 10^3 minutes, 8.16 x 10^{-7} moles/g are adsorbed which corresponds to a surface coverage of 0.003.

As mentioned above, the absorption spectra of $M(CO)_{6ads}$ closely resembles that found in fluid solution. Although these data indicate that the relative extinction coefficients are equivalent in both media, they do not establish their absolute values. The molar extinction coefficient, ε, is defined as the optical density at a specific wavelength of a solution of known concentration and pathlength. This definition is restricted to homogeneous solutions, but can be extended to reagents adsorbed onto PVG. As shown in Figure 18, the hexacarbonyls are uniformly distributed on the surface. In equation 11, ε, is defined in terms of a two dimensional extinction coefficient.

Figure 24. Rate of Adsorption of $W(CO)_6$ onto PVG.

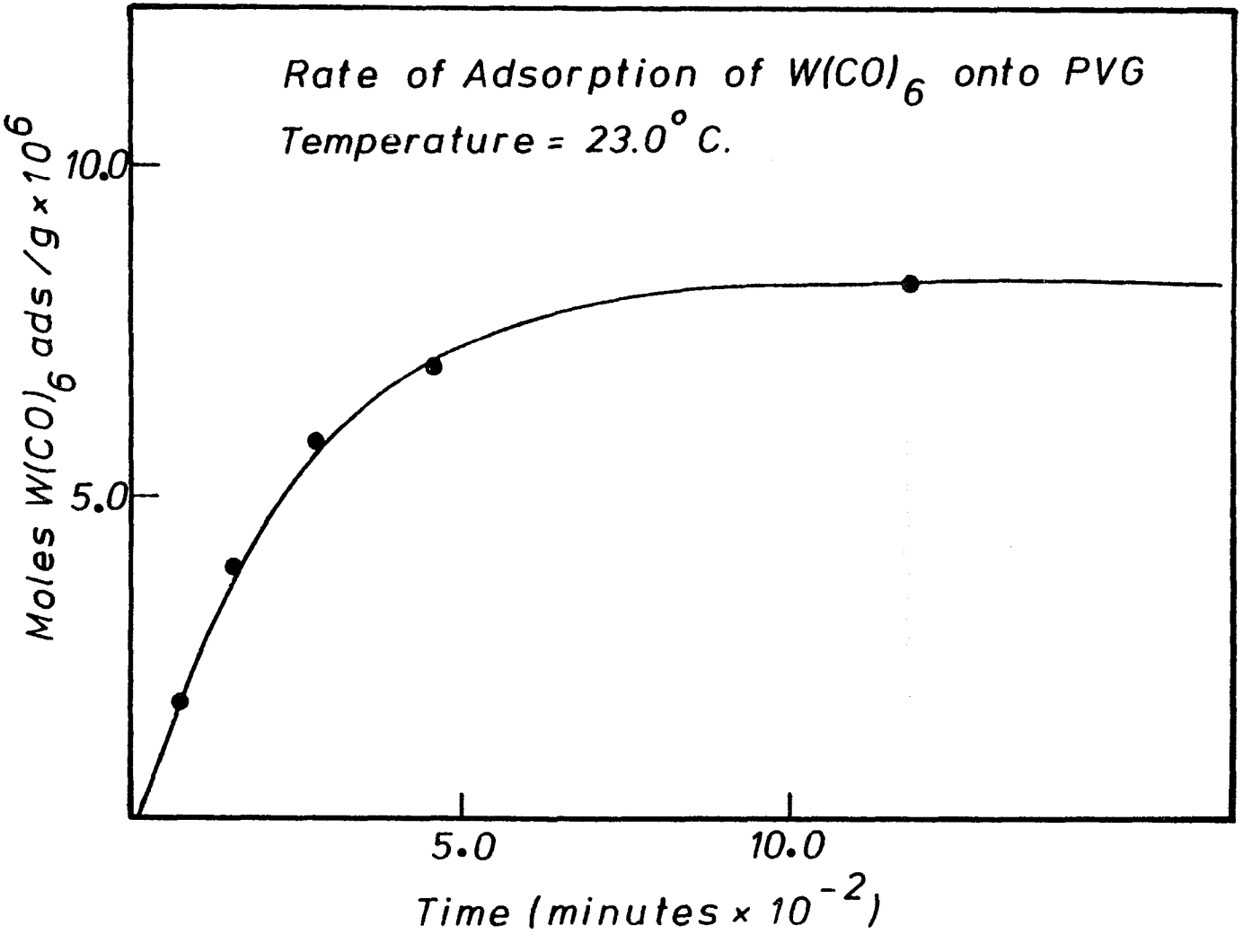

ε= Optical Density/Molar cm = O.D./moles cm/liter = O.D./moles-cm/10^3 cm^3 = O.D. 10^3 cm^2/moles adsorbed (11)

Optical density is measured and the number of moles adsorbed is calculated from spectral analysis of the impregnating solution. If the surface area of the glass is calculated from the sum of the surface areas of each face, then a value for the extinction coefficient in the glass, designated ε_{eff}, can be obtained. Figure 19 illustrates the correspondance between ε and ε_{eff}, in the 270-350-nm range, for a 10^{-3}M solution of $W(CO)_6$ in n-hexane and for a glass containing 8.16×10^{-7} moles of $W(CO)_6$. Similarly, solution spectra can be plotted in units of 10^2 cm^2 if a 1-cm path length is used. The agreement between the values of ε_{eff} of $M(CO)_6$ in solution and adsorbed onto PVG indicates that adsorption does not significantly change either the allowedness or energy of the electronic transitions. The spectral properties of the adsorbed hexacarbonyl are equivalent to those in fluid solution. Consequently, the photophysical and photochemical properties of the adsorbed complexes are expected to parallel those previously found in fluid solution. As described below, a close similarity exists in the initial photochemical event, but surprising differences occur in subsequent reactions.

B. Photolysis of $M(CO)_6$ads.

As illustrated by Figure 25, photolysis (λ_{ex} <350-nm) of the adsorbed complex at 25°C in vacuo

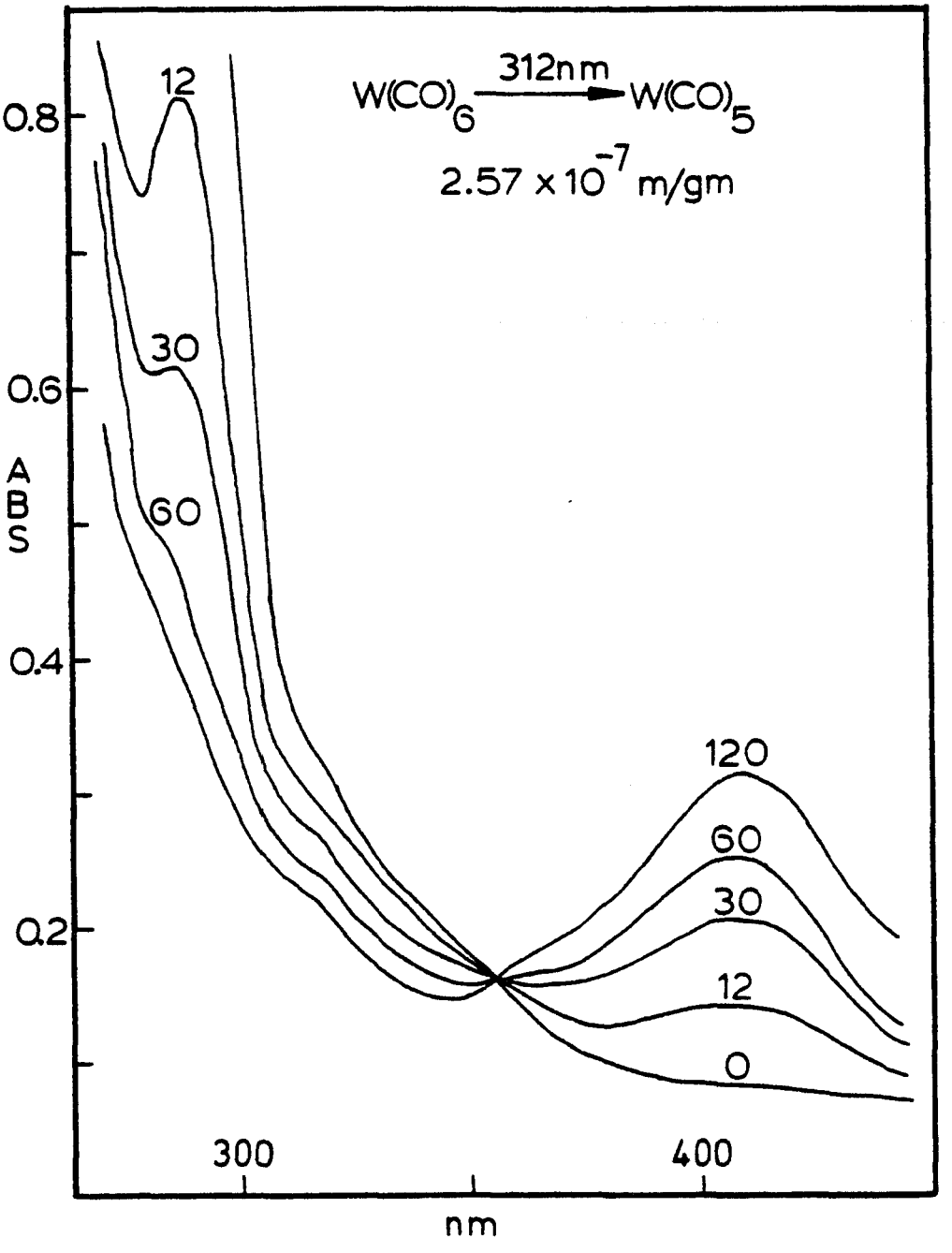

Figure 25. Photolysis of $W(CO)_6$ads at 312-nm in vacuo

Times are in seconds. Photolysis at 22.0 ± 1.0 °C.

results in the formation of a species which has an absorption maximum at 408-nm. The decline in optical density at 289-nm, characteristic of $W(CO)_6$ads, occurs with a concurrent growth of the spin allowed $^1A_1 \longrightarrow {}^1E$ ligand field absorbance, characteristic of $W(CO)_5$ads, and maintainance of an isosbestic point at 355-nm. Also, an intense MLCT band (in low temperature matrices (68-71) $\varepsilon = 6.35 \times 10^4\ M^{-1}\ cm^{-1}$), characteristic of $W(CO)_5$ads, is observed at 245-nm at low photolysis times. The similarity between the spectral maxima of the adsorbed photoproduct and those of $M(CO)_5$ generated in low-temperature rare gas matrices, Table 4, indicates formation of $M(CO)_5$ads. The spectral changes induced by photolysis of $Cr(CO)_6$ads and $Mo(CO)_6$ads are shown in Figures 26 and 27. Similar to that found with the tungsten complex, the absorption spectrum of the product closely resembles those of $Cr(CO)_5$ and $Mo(CO)_5$ generated in low temperature matrices. These spectral changes, the occurence of isosbestic points, and the quantitative regeneration of $M(CO)_6$ads when the photoproduct is exposed to 1-atm of CO establishes the initial photochemical reaction to be

$$M(CO)_6\text{ads} \longrightarrow M(CO)_5\text{ads} + CO$$

The quantum yields for the decomposition of $M(CO)_6$ads as well as the formation of $M(CO)_5$ads have been determined using the method described by Strohmeier and Gerlach (113). Representative plots of log ϕ vs. log t, for

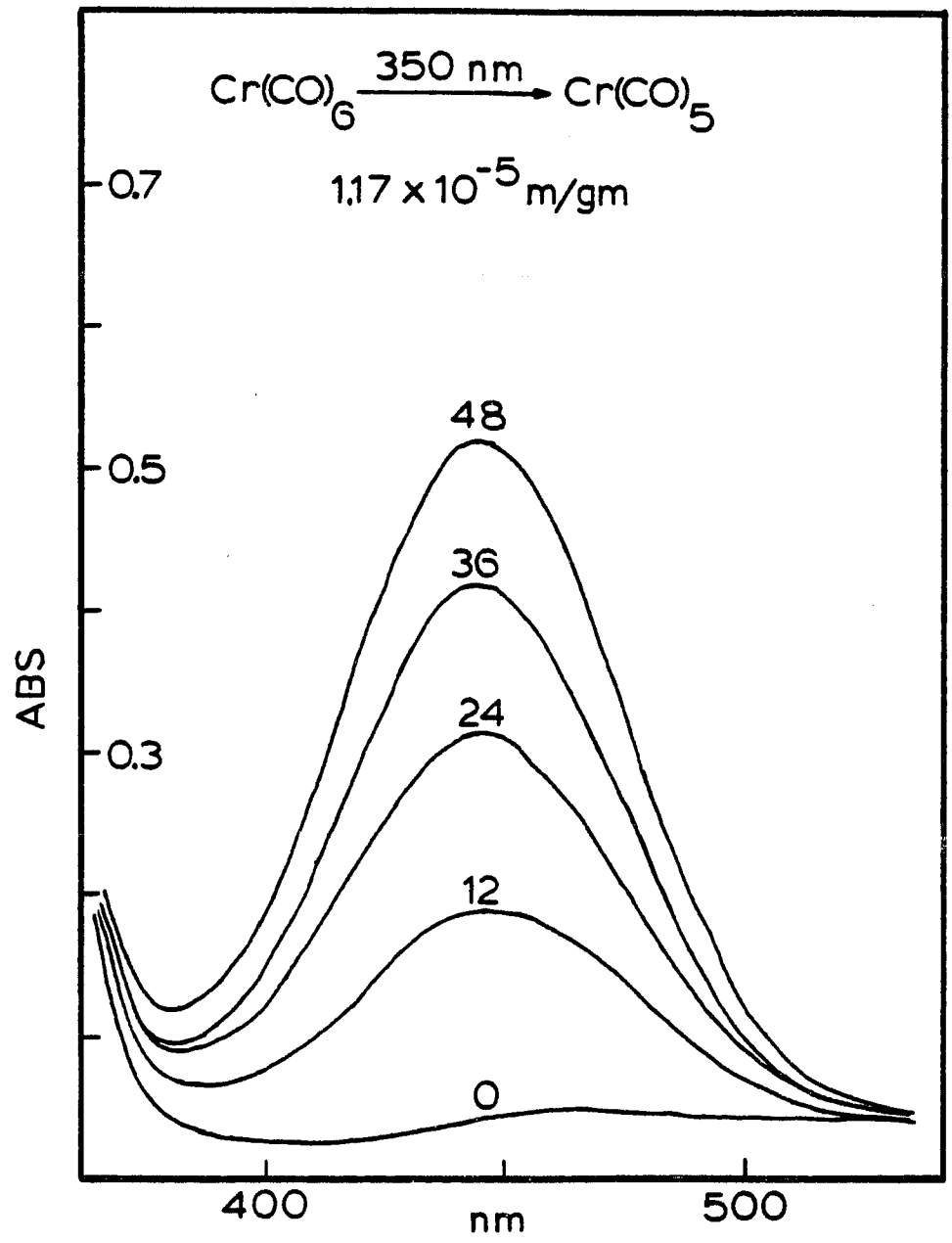

Figure 26. Photolysis of $Cr(CO)_6$ads at 350-nm in vacuo. Figure displays formation of $Cr(CO)_5$ads. Photolysis times are in seconds. Photolysis at 22.0 ± 1.0 °C.

Figure 27. Photolysis of $Mo(CO)_6$ ads at 310-nm in vacuo. Figure displays formation of $Mo(CO)_5$ ads. Photolysis times are in seconds. 1=300 sec; 2=600 sec; 3=1,260 sec. 1.06×10^{-6} moles $Mo(CO)_6$/g PVG. Photolysis at 23.0 $\pm$ 1.0 ^{o}C.

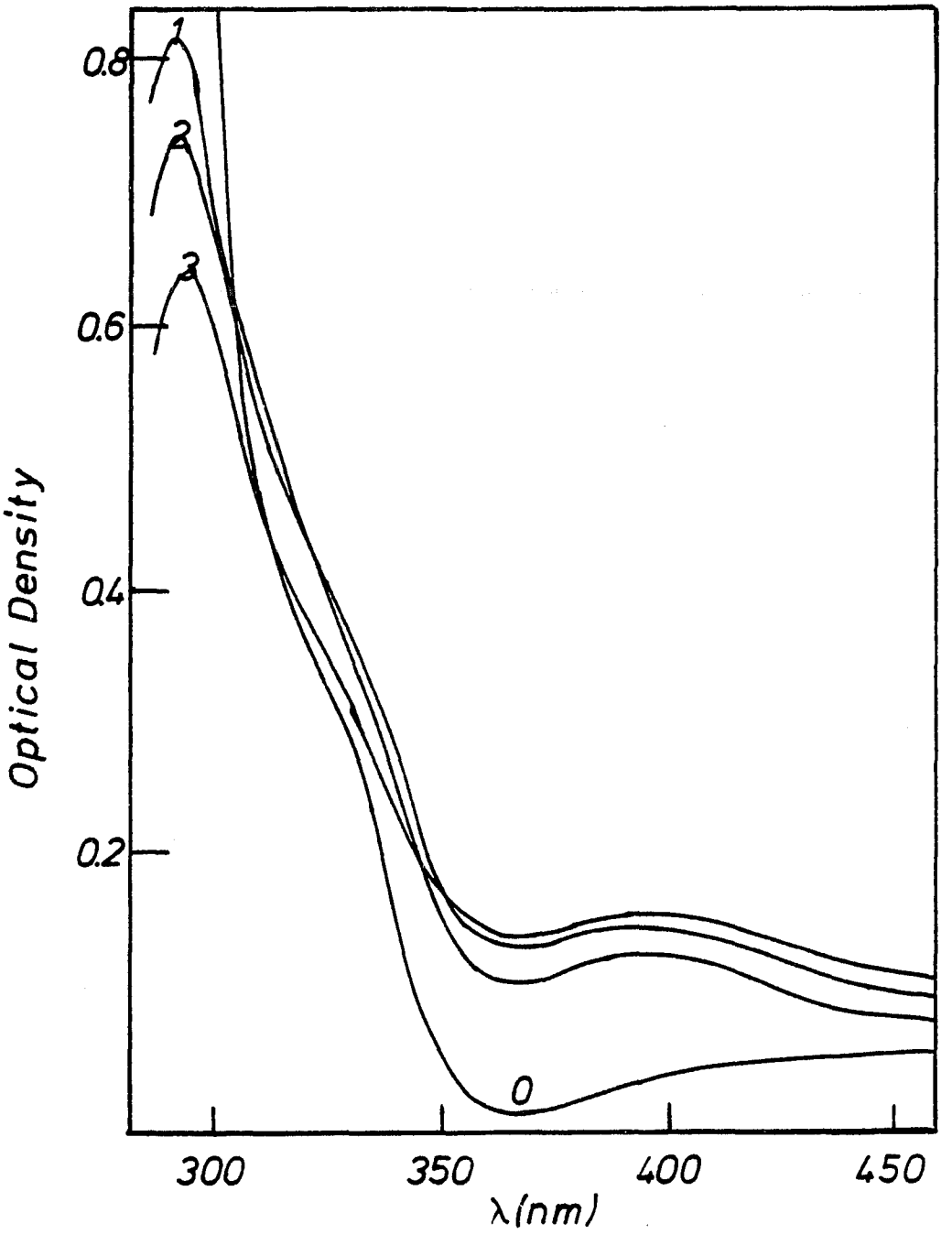

each complex, are illustrated in Figures 28, 29, and 30, and the values listed in Table 5 are obtained by extrapolation of the plots. In general, quantum yields of formation and decomposition were calculated from equation 12.

$$\phi_{for} \text{ of } \phi_{dis} = m/I_a \qquad (12)$$

where m is number of moles of photoproduct formed or starting complex decomposed/unit volume/sec and I_a is light intensity absorbed/unit volume/sec. Grinding studies have established that > 95% of the complex is near the surface which justifies our claim that ε_{eff} should be defined in terms of a two dimensional extinction coefficient. Therefore, in accordance with our adopted formalism, for adsorbed species, unit surface area will be used instead of unit volume. Incident light intensities were measured by a ferrioxalate actinometer (93a,b,c) and were corrected for actual light absorbed by the adsorbed complex using equation 13.

$$\text{Light Absorbed} = I_o(1-10^{-O.D.}) \qquad (13)$$

I_o is calculated from equations of Parker (93a,b). and is in units of quanta/unit volume/sec. The optical density is determined from the absorption spectrum for a particular excitation wavelength. To be consistent, our calculation of the quantum yields of reactions, a 1-cm path length cell is used in actinometric measurements. This simplifies the calculation by making the surface area of the cell to be equal to its volume. The number of moles of photoproduct is calculated according to equation 14.

Figure 28. Log ø vs. Log t. Quantum yield of formation of $Cr(CO)_5$ads at 350 nm. 1.18×10^{-5} moles of $Cr(CO)_6$/g. Photolysis at 22.0 ± 1.0 °C.

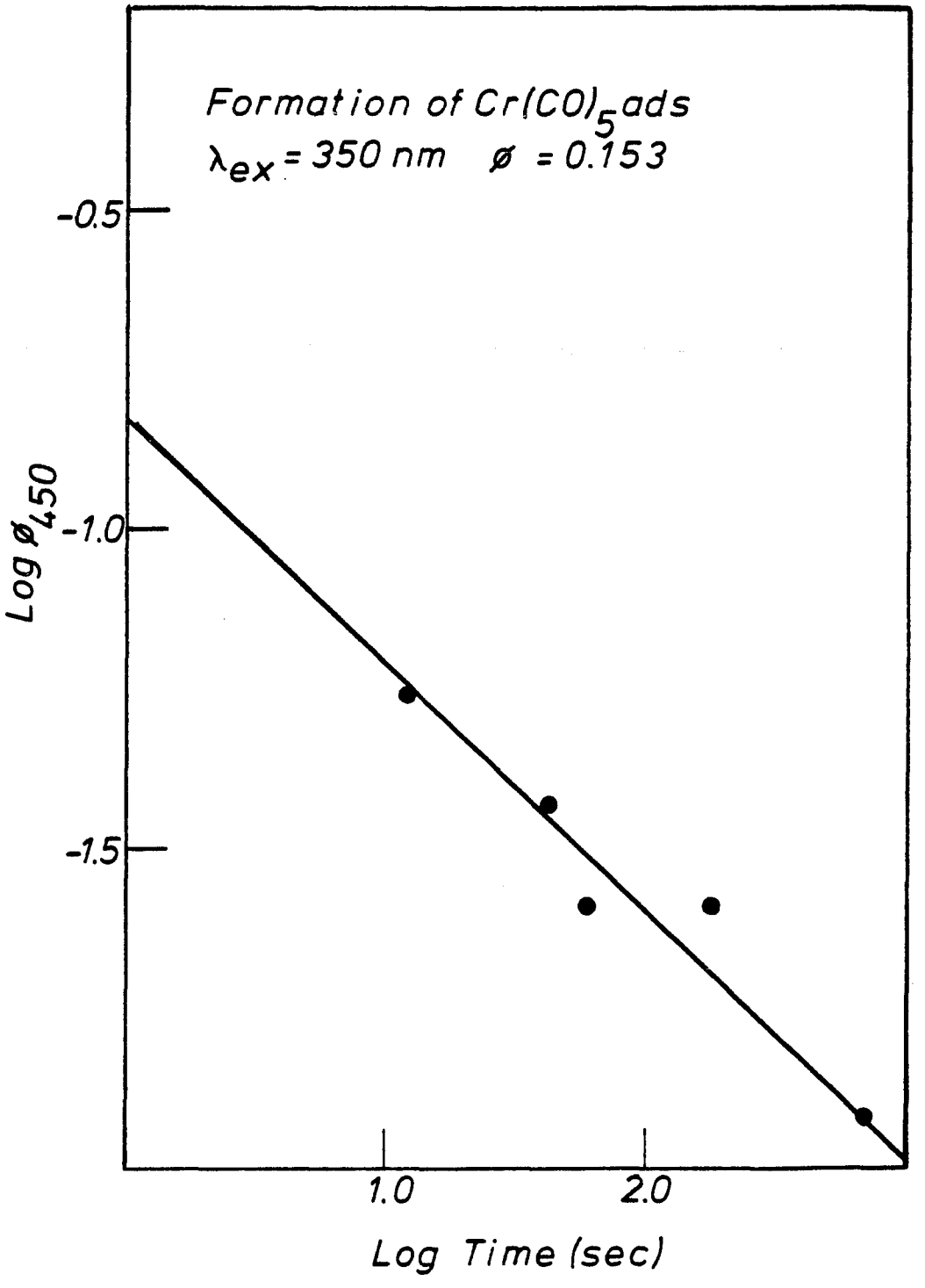

Figure 29. Log ø vs. Log t. Quantum yield of formation of $Mo(CO)_5$ads at 350 nm. 3.58×10^{-6} moles $Mo(CO)_6$/g. Photolysis at 22.0 ± 1.0 °C.

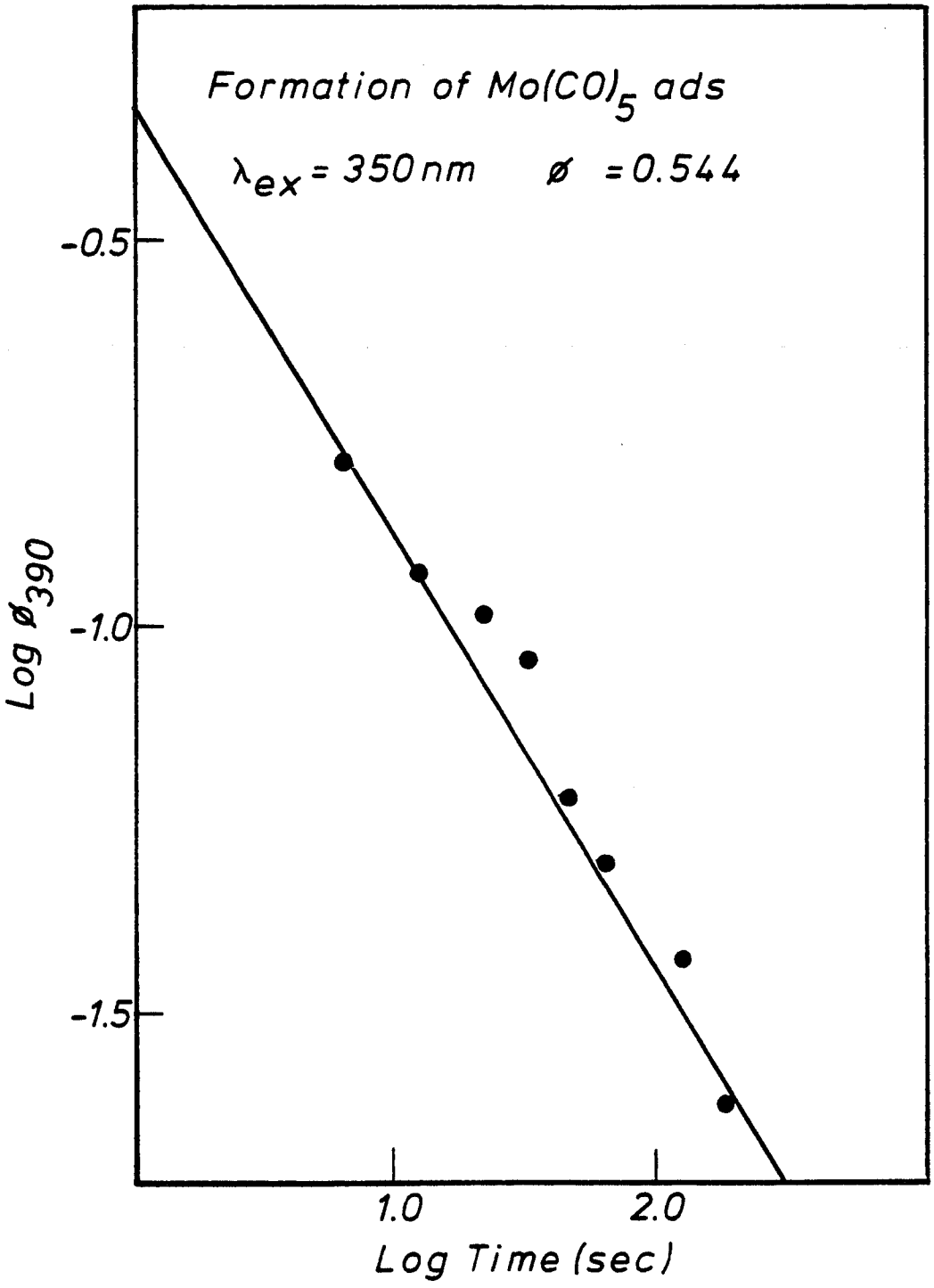

Figure 30. Log ø vs. Log t. Quantum yield of formation of $W(CO)_5$ads at 350 nm. 2.70×10^{-6} moles of $W(CO)_6$/g. Photolysis at 22.0 ± 1.0 °C.

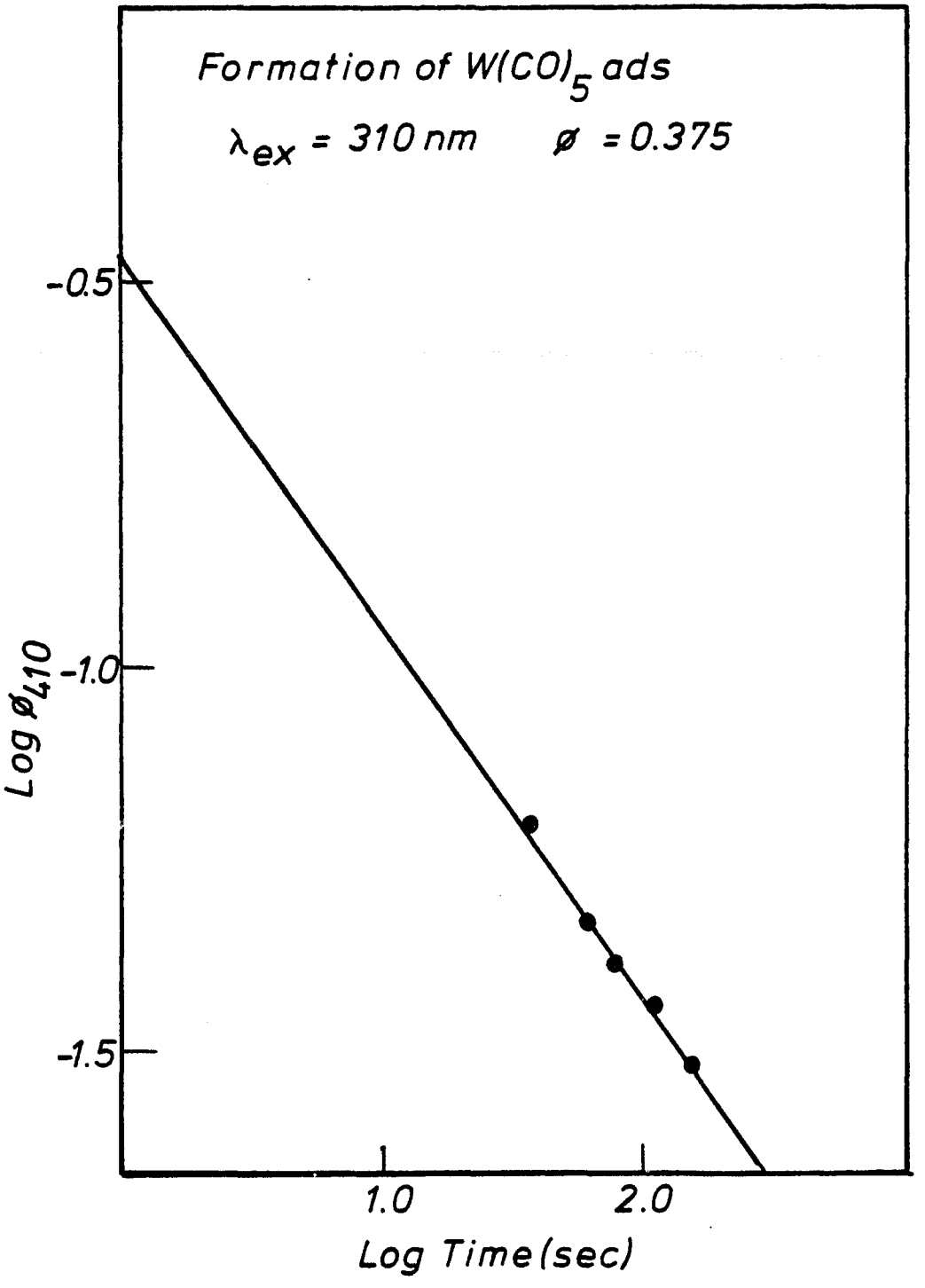

Table 5. Quantum Yield Data.

Metal	λ_{ex}	$M(CO)_6$ads (moles/gram)	Light Absorbed [a]	$\phi_{for.}$ [b]	$\phi_{decomp.}$ [b]	ϕ_{CH_4} [b]
Cr	254	1.7×10^{-7}	7.70×10^{15}	0.04	0.06	0.002
	310	N.D.	N.D.	N.D.	N.D.	N.D.
	350	1.63×10^{-7}	5.96×10^{14}	0.153	0.081	0.0
Mo	254	4.25×10^{-7}	8.13×10^{15}	0.214	0.394	0.008
	310	3.32×10^{-7}	2.87×10^{15}	0.398	0.104	N.D.
	350	3.43×10^{-7}	1.75×10^{14}	0.544	0.789	0.0
W	254	2.99×10^{-7}	2.90×10^{15}	0.33	0.207	0.01
	310	2.96×10^{-7}	1.80×10^{15}	0.375	0.115	0.002
	350	2.81×10^{-7}	6.46×10^{14}	0.822	0.839	0.0

[a] Light intensities are in units of quanta/unit volume/second.

[b] All quantum yields are $\pm$ 10%.

$$\frac{\varepsilon_{M(CO)_6}}{\varepsilon_{M(CO)_5}} = \frac{\varepsilon_{eff\ M(CO)_6}}{\varepsilon_{eff\ M(CO)_5}} \qquad (14)$$

Although equation 14 assumes that ε_{eff} is equal to ε_{hexane}, the assumption appears justified in view of close agreement of the values shown in Figure 18. For each experiment, however, a new extinction coefficient was calculated due to slight differences in the distribution of reagents, therefore, yielding slight differences in the calculated ε_{eff}. Quantum yields were calculated by the above procedure for each photolysis time. These were then plotted, by the procedure of Strohmeier and Gerlach, and linear regression analysis applied to obtain the best extrapolation to t=0. This treatment is necessary to account for the formation of secondary photolysis products and thermal back-reactions found for $Cr(CO)_5$ads and $Mo(CO)_5$ads. For these complexes, spectra recorded after photolysis indicate that unless pumped out, photodissociated CO recombines with these adsorbed pentacarbonyls and regenerates ~ 70% of the original complex within 30 minutes. Figure 31 shows the rates of the back reaction for each complex and the difference in slopes suggest difference in reversibility. If $M(CO)_6$ads is photolyzed and the photoreleased CO removed by vacuum, however each photoproduct, $M(CO)_5$ads, is stable for > 48 hours at room temperature.

The observed stability does not occur at the expense of subsequent thermal and photochemical reactivity.

Figure 31. Comparison of the rate of thermal back reaction of $M(CO)_5$ads with 1-atm CO. ● =$Cr(CO)_5$ads, ■ =$Mo(CO)_5$ads, and ▲=$W(CO)_6$ads.

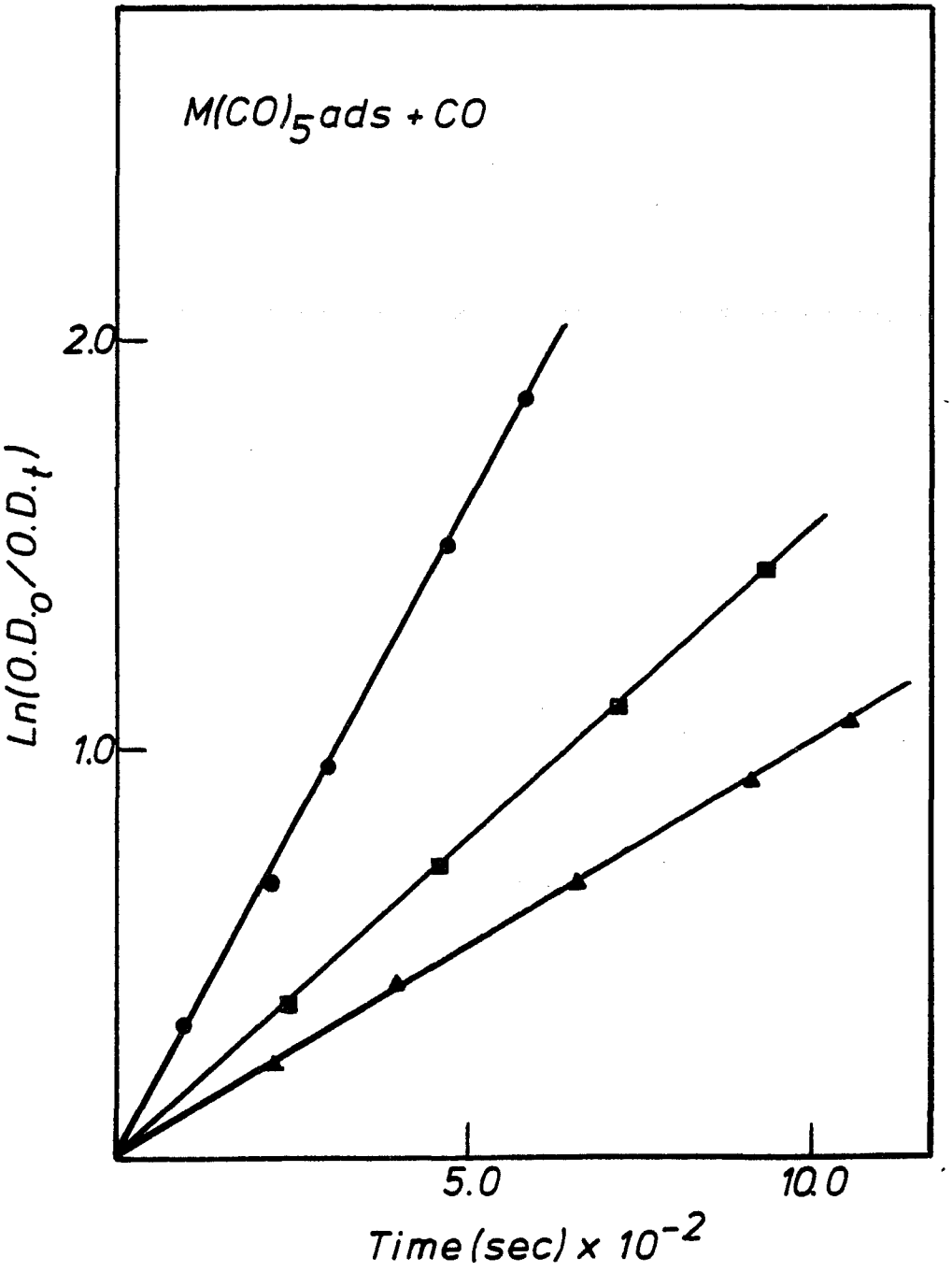

Figure 32. Reverse reaction following exposure of photogenerated $W(CO)_5$ads to 1-atm CO.

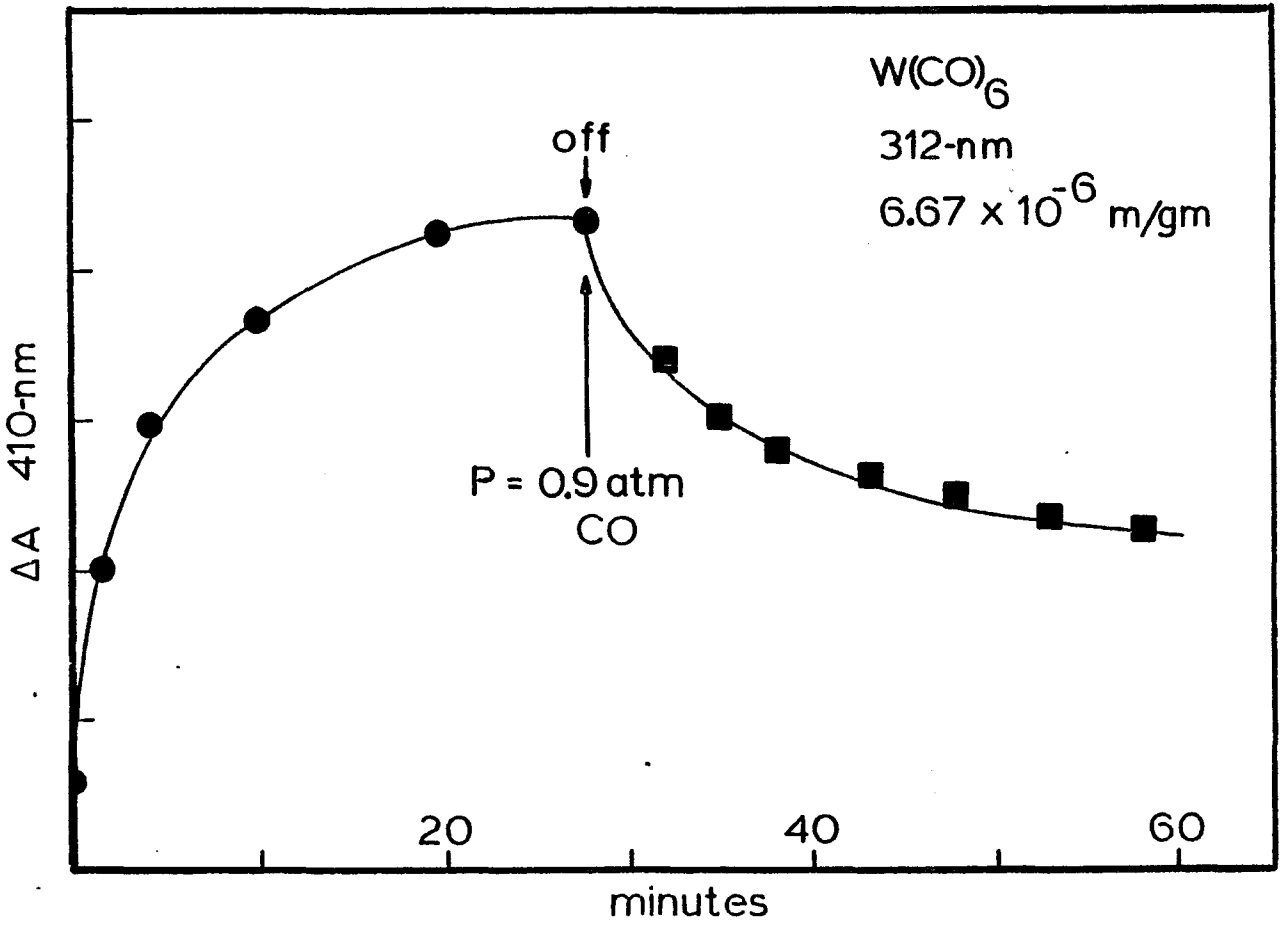

Exposing $M(CO)_5$ads to various ligands, either as gases or dissolved in degassed, non-coordinating solvents, causes rapid quantitative formation of $M(CO)_5$Lads (L=CO, NH_3, pyridine (py), cis-2-butene, trans-2-butene, CO_2, 1-butene, and 1-pentene) and $M(CO)_4$Lads (L=2,2'bipyridine, bpy, 1,10- ortho phenanthroline, o-phen, and 1,3 butadiene). Figure 32 shows the reverse reaction folowing exposure of photogenerated $W(CO)_5$ to 1-atm of CO. This sequence, 350-nm photolysis followed by exposure to 1-atm of CO, has been carried out through five successive cycles, with a >90% recovery of $W(CO)_6$ads in each cycle. However, high reversibility is dependent upon the extent of original photolysis; photolysis to <30% consumption of $W(CO)_6$ leads to high reversibility whereas >30% decreases the recovery. The decrease in thermal reversibility is attributed to a concurrent oxidation of the metal atom. I will discuss the metal oxidation later. It is sufficient to note here, however, that metal oxidation is a function of the extent of photoinduced decarbonylation and occupation of the vacated coordination sites by adsorbed H_2O and/or silanol groups.

Exposing $M(CO)_5$ads to degassed pyridine, py, leads to spectral changes consistent with the formation of $M(CO)_5$(py)ads (Figure 33a,b,c). The shift of the pyridine vibrations to higher energy than to those of adsorbed pyridine, Figure 34, establishes its coordination to the metal atom (111).

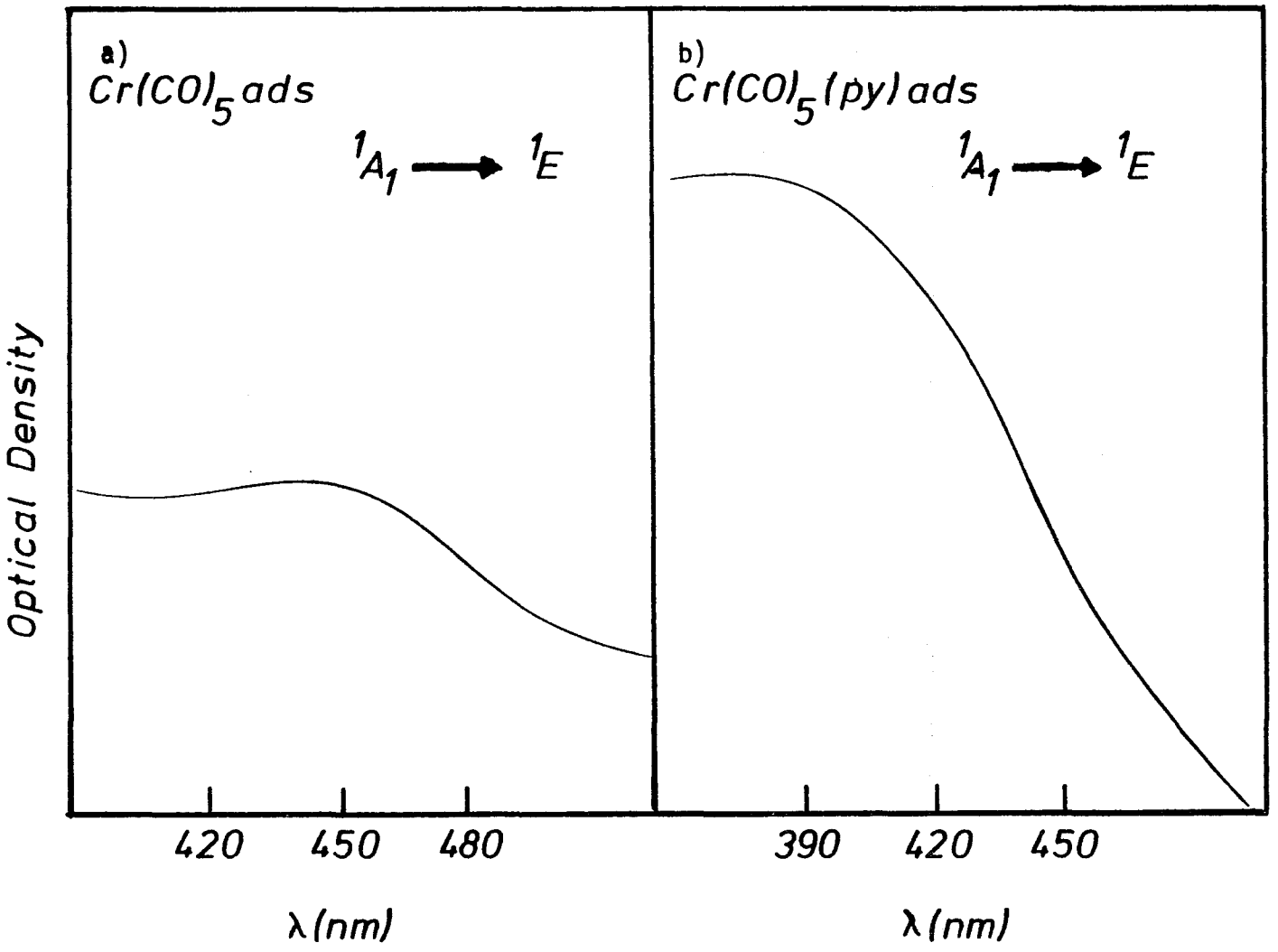

Figure 33a. Visible absorption spectrum of $Cr(CO)_5$ads.

Figure 33b. Visible absorption spectrum of $Cr(CO)_5$(py)ads.

Both figures illustrate the relative ligand field strength of pyridine and PVG.

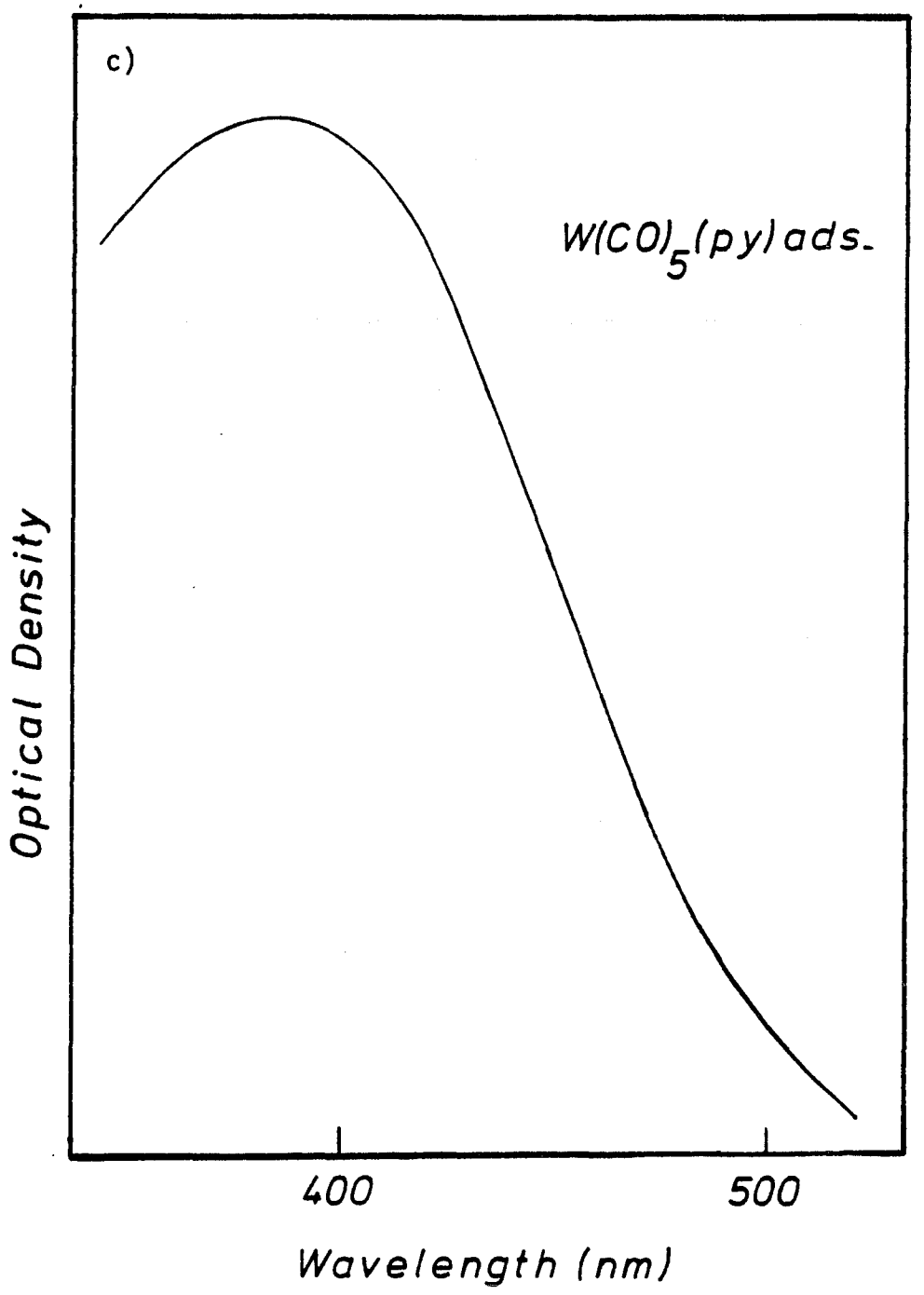

Figure 33c. Visible absorption spectrum of $W(CO)_5(py)$ads.

Figure 34. Resonance Raman spectrum of $W(CO)_5(py)$ads. Excitation wavelength is 457.9 nm. Figure illustrates shifts in pyridine breathing modes upon coordination to metal atom.

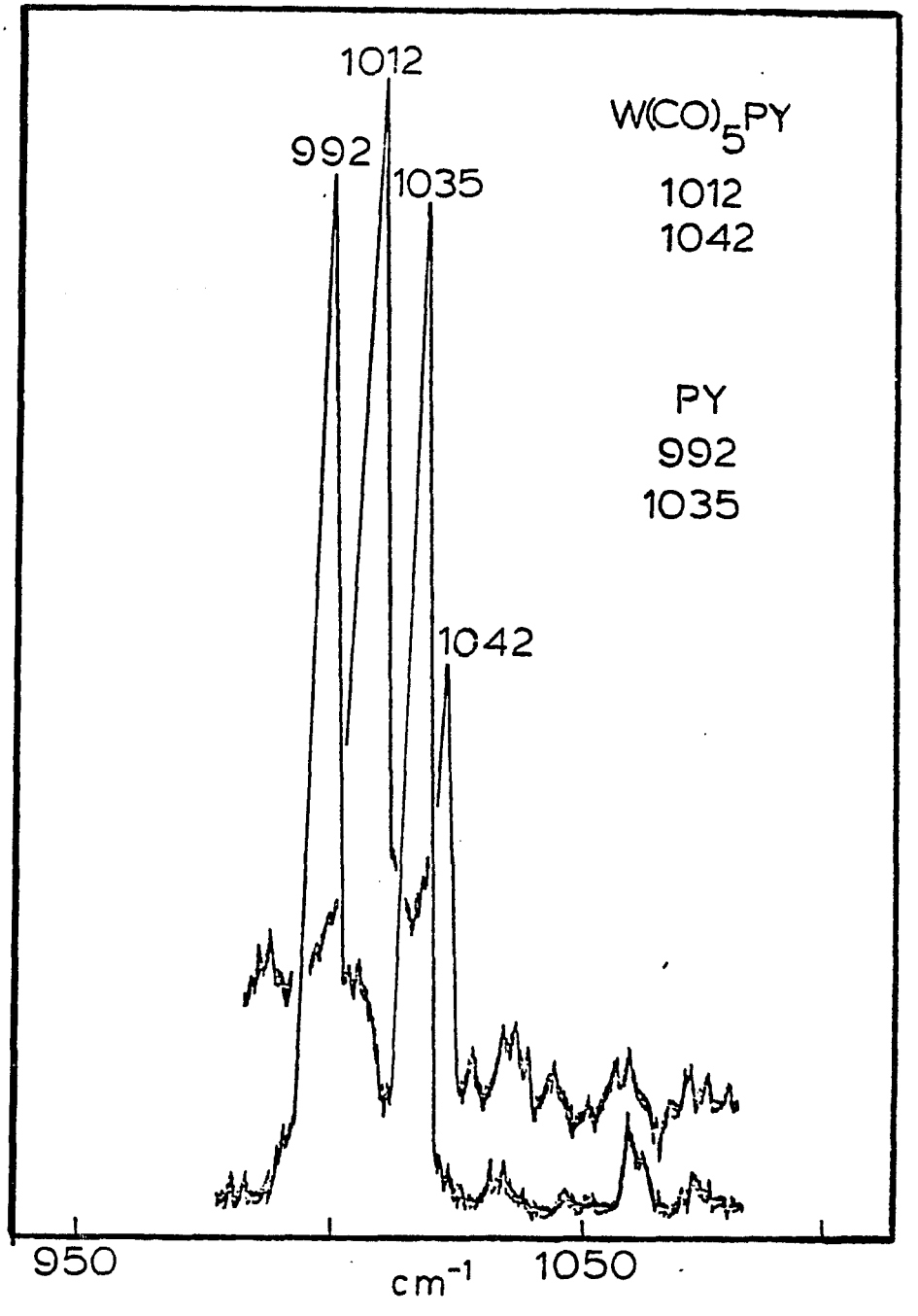

$W(CO)_5$ads was exposed to thoroughly degassed 10^{-2}M n-hexane solution of bipyridine or o-phenanthroline. Spectra recorded periodically during the bipyridine reaction showed an isosbestic point at 444 nm. The kinetic data indicate that the reaction was pseudo-first order with a calculated rate constant of 5.55×10^{-4} sec $^{-1}$. As shown by Table 6, the absorption maxima agree very well with the absorption maxima of $M(CO)_4$(bpy) and $M(CO)_4$(phen) recorded in CH_2Cl_2. However, this MLCT transition has been shown to exhibit an exceptionally large solvent dependence (73,74). To substantiate the spectral changes which indicate formation of $W(CO)_4$Lads, the $M(CO)_4$L (M=Mo,W;L=bpy, o-phen) complexes were prepared and adsorbed onto PVG. The resulting spectral changes were identical to those obtained when the complexes were made in situ.

The room temperature emission spectrum of $W(CO)_5$ads was recorded (Figure 37) and, in accordance with the higher energy absorptions of $W(CO)_5$ads, the emission maximum occurs at 510-nm, which is in reasonable agreement with the 533-nm emission maximum observed in E.P.A. glasses at 77°K. The emission spectra for $M(CO)_5$(py)ads, $M(CO)_4$(bpy)ads, and $M(CO)_4$(o-phen)ads (M=Mo,W) were also recorded. Representative plots are Figures 38,39 and all agree remarkably well with emission spectra of the complexes in various media. The emission data obtained from all complexes are summarized in Table 6.

Table 6. A Summary of Absorption and Emission Maxima for Adsorbed Complexes and Complexes in Fluid Solution.

Complex	Adsorbed Complex		Complex in Solution			
	Absorption Maxima (nm) [a]	Emission Maxima (nm)	Absorption Maxima (nm)	Ref.	Emission Maxima (nm)	Ref.
$W(CO)_5$	408 (LF)	510	440 [b]	(70)	533 [c]	(65,66)
$W(CO)_5(NH_3)$	400 (LF)		408 [d]	(82)		
$Cr(CO)_5(py)$	390 (LF)		390 [e]	(128)		
$W(CO)_5(py)$	390 (LF)	526	390 [f]	(127)	524 [c]	(127)
$W(CO)_5$(1-pentene)	300 (LF)		303 [g]	(78,79)		
$HW(CO)_5^-$	450		450 [h]	(129)		
$W(CO)_5(P(PH_3)_3)$	N.A.		347 (LF) [i]	(67)		
$W(CO)_5(EtOH)$	415 (LF)		415 [j]	(129)		
$Cr(CO)_4(bpy)$	500 (MLCT)		497 [k]	(72)		
$Mo(CO)_4(bpy)$	466 (MLCT)	644	463 [k]	(72)	669 [l]	(65,66)
$W(CO)_4(bpy)$	490 (MLCT)	683	487 [k]	(72)	680 [l]	(65,66)
$W(CO)_4$(o-phen)	567 (MLCT)	660	570 [m]	(130)	674 [l]	(65,66)
$Mo(CO)_4$(o-phen)	549 (MLCT)	644	552 [m]	(74)	647 [l]	(65,66)
$W(CO)_5$(cis-2-butene)	303 (LF)					
$W(CO)_4$(1,3 butadiene)	305 (LF)					
$W(CO)_5$(1-butene)	302 (LF)					

Table 6 Legend.

[a] Electronic transition in parentheses. [b] CH_4 matrix at 12^oK.

[c] Methylcyclohexane at 77^oK. [d] Benzene (room temperature).

[e] CH_3CN at 298^oK. [f] Isooctane at 298^oK. [g] n-hexane at 298^oK.

[h] H_2O at 298^oK. [i] hexanes at 298^oK. [j] Ethanol at 298^oK.

[k] CH_2Cl_2 at 298^oK. [l] solid at 298^oK. [m] cyclohexane at 298^oK.

Figure 35. Reaction of $W(CO)_5$ads with thoroughly degassed bipyridine (10^{-2}M/n-hexane). Reaction at 22.5 ± 1.0 °C. 1.20×10^{-5} Moles $W(CO)_6$/g PVG.

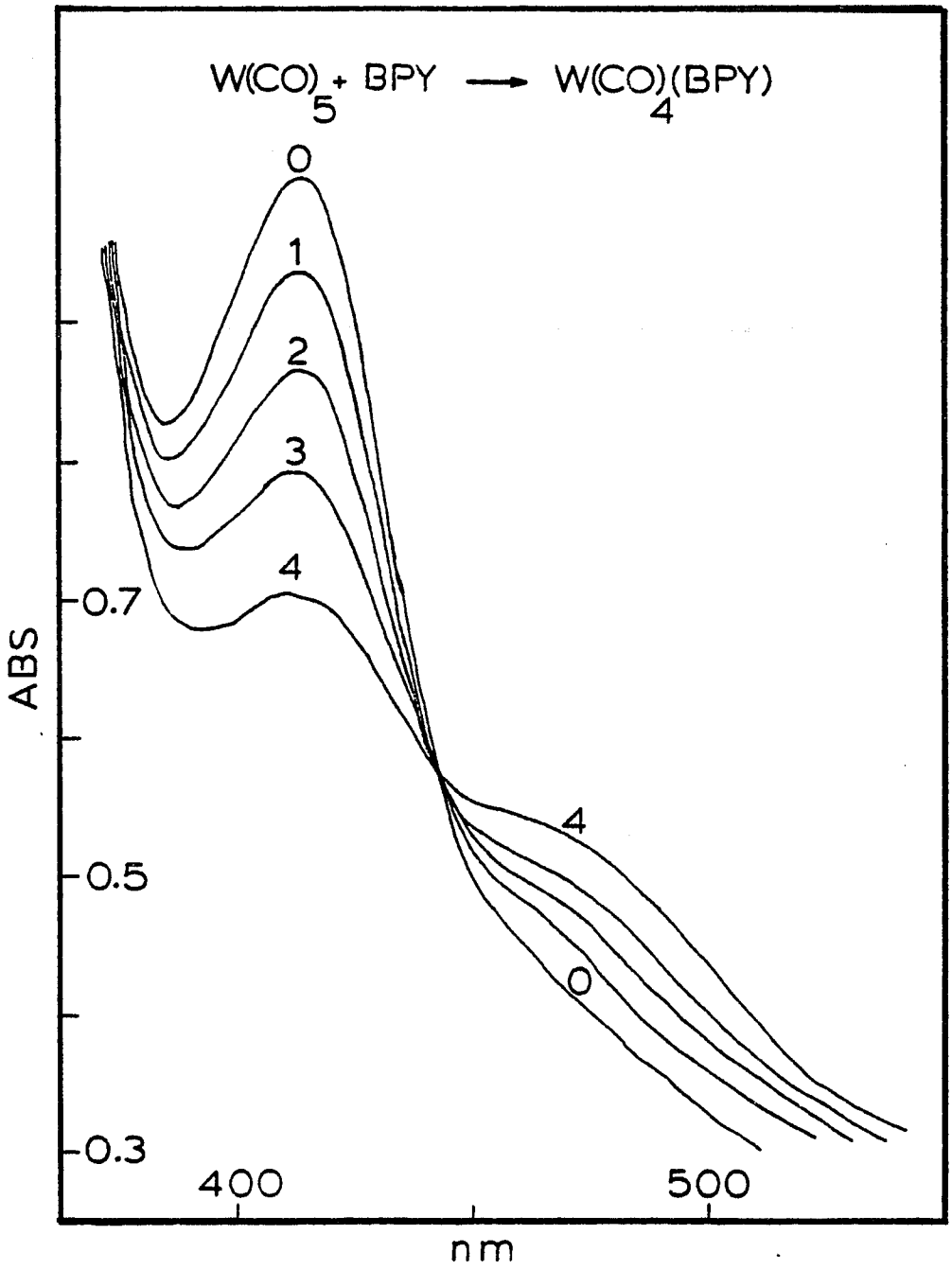

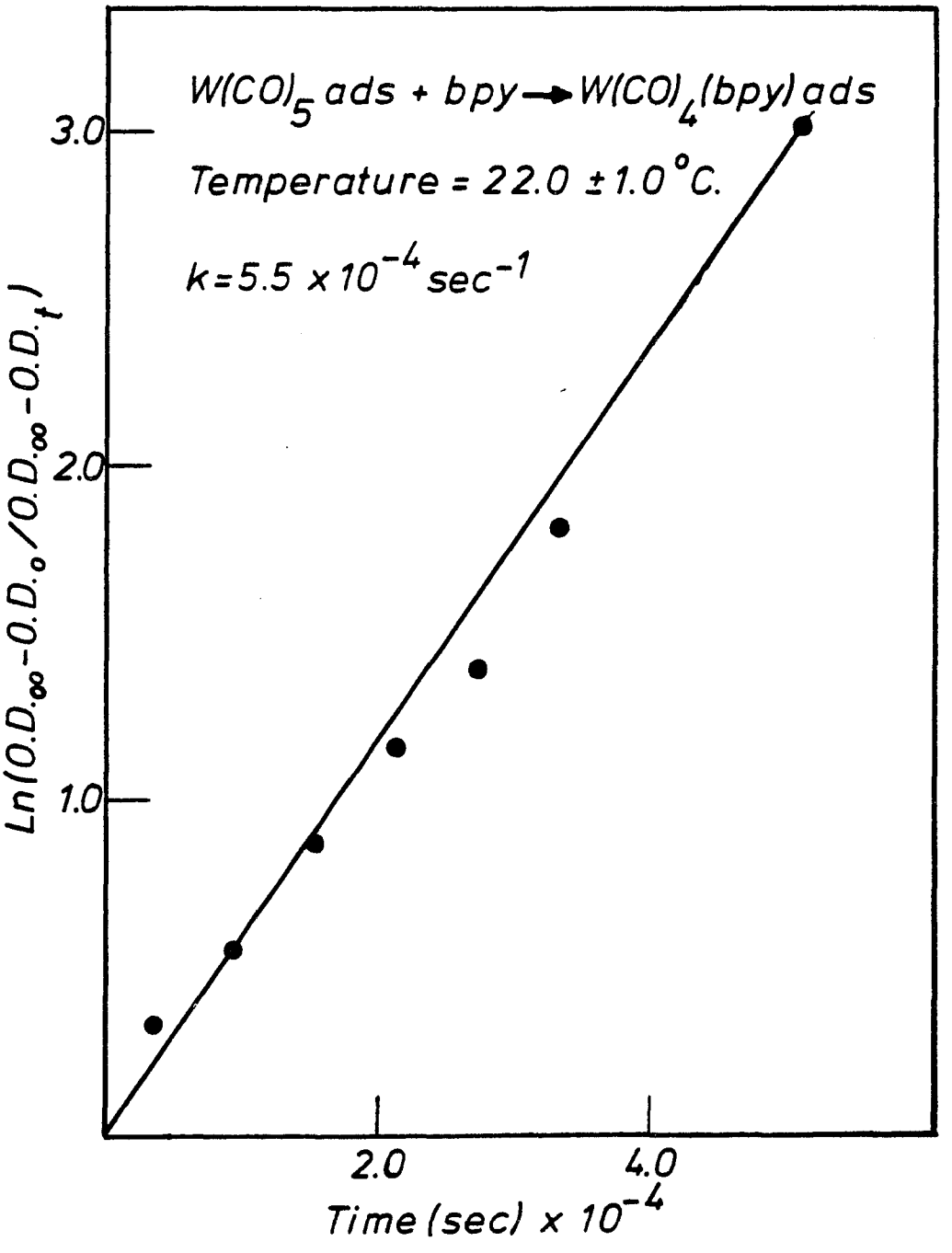

Figure 36. Pseudo first-order rate plot of $W(CO)_5$ads with bipyridine (10^{-2}M/n-hexane). 1.20 x 10^{-5} moles $W(CO)_6$/g PVG.

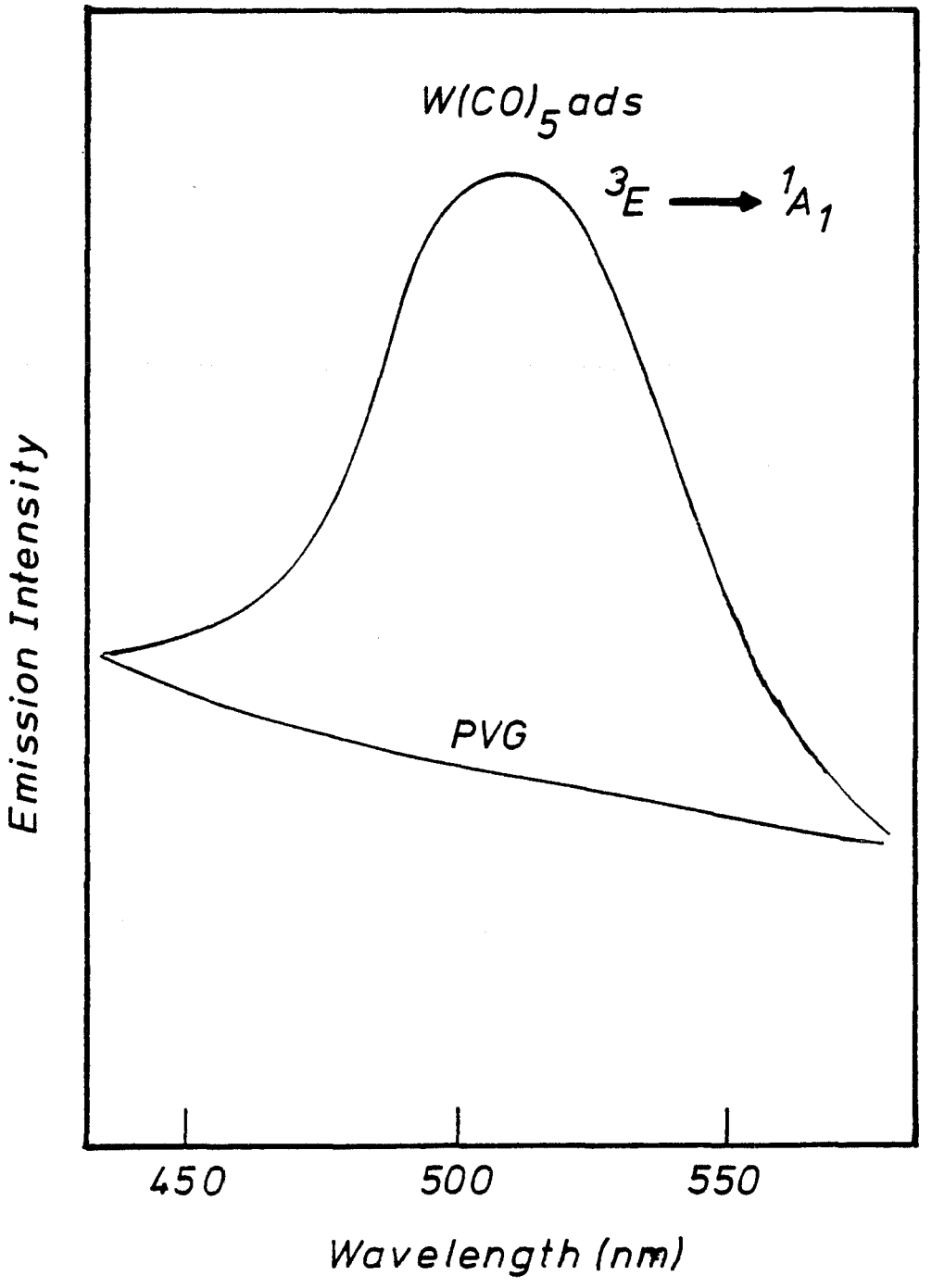

Figure 37. Room temperature emission spectrum of $W(CO)_5$ads. Excitation wavelength is 410 nm.

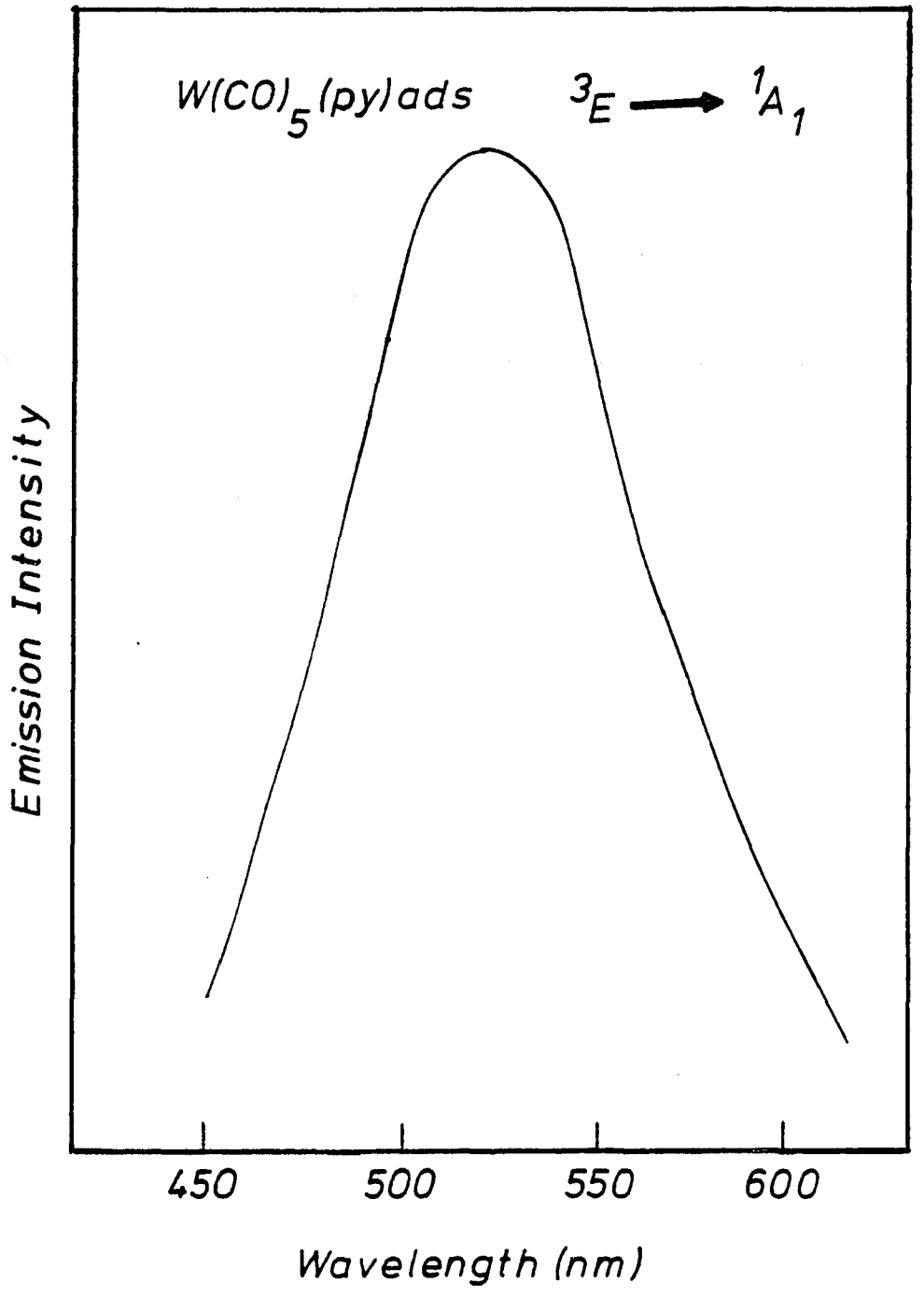

Figure 38. Room temperature emission spectrum of $W(CO)_5(py)ads$. Excitation wavelength is 457.9 nm.

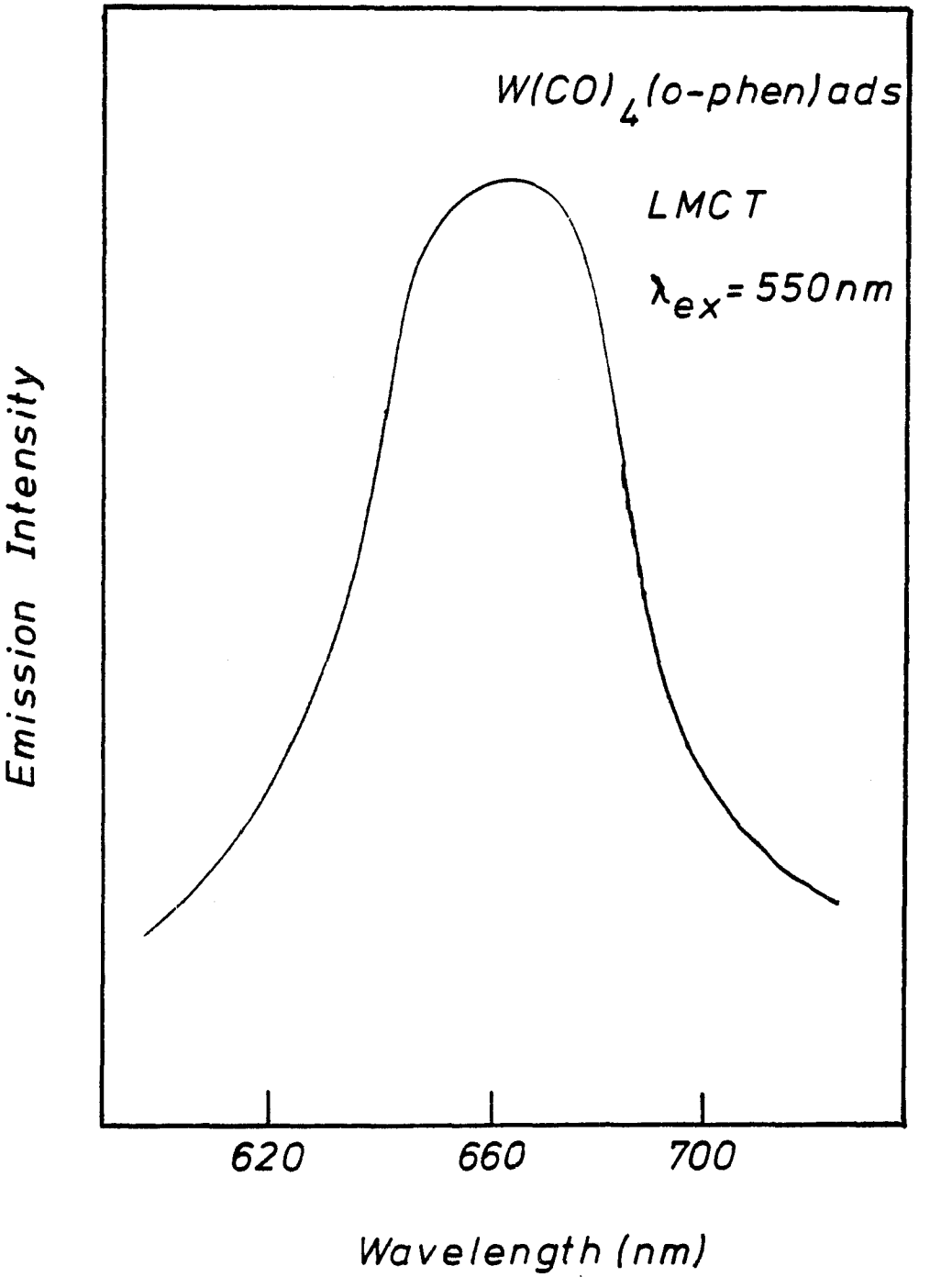

Figure 39. Room temperature emission spectrum of $W(CO)_4$(o-phen)ads. Excitation wavelength is 550 nm.

The addition of olefins to $M(CO)_5$ads was examined in detail. 1-pentene, 1-butene, cis-2-butene, and trans-2-butene, either as gases or in thoroughly degassed n-hexane solution, were exposed to $M(CO)_5$ads. The observed spectral changes, in which the low energy $^1A_1 \longrightarrow {}^1E$ LF band, corresponding to $M(CO)_5$ads, is shifted to higher energy, are consistent with the formation of the $M(CO)_5$(olefin) complex (Table 6). A detailed kinetic analysis of these reactions will be discussed in a later section.

The formation of the $W(CO)_5NH_3$ads was accomplished by exposing $W(CO)_5$ads to 1-atm of NH_3. The observed band maximum, 400-nm, is consistent with the band maximum reported by Wrighton and Morse (82) at 408-nm in benzene (ε =3.8 x 10^3 M^{-1} cm^{-1}). This band has been assigned as a $^1A_1 \longrightarrow {}^1E$ LF transition.

Because of the great potential for employing not only carbon monoxide but carbon dioxide as a feedstock in the production of reduced carbon containing molecules such as alcohols and hydrocarbons, an investigation of the addition of CO_2 to $M(CO)_5$ads was undertaken. Recently, Darensbourg and Rokicki (101), have reported on the facile reduction of CO_2 by anionic group VIB metal hydrides resulting in the formation of metalloformate derivatives (equation 14).

$$M(CO)_5H^{-1} + CO_2 \longrightarrow M(CO)_5O_2CH^{-1} \quad (14)$$

We have observed that when scrupulously oxygen free and dry CO_2 (0.153-atm;9.08 x 10^{-4} moles) is added to 1.74 x 10^{-6} moles of $W(CO)_5$ads, as shown in Figure 40, the ligand field band at 408-nm dissappears. A plot of log $O.D._t/O.D._o$ versus reaction time was constructed and is illustrated in Figure 41 which compares the rate of CO and CO_2 with $W(CO)_5$ads. The apparent rate constant for the CO_2 reaction is 6.76 x 10^{-5} sec^{-1} at 22 $\pm$ 1.0°C. Further evidence that a reaction has taken place is the observance in the decrease in the MLCT band at 245-nm, characteristic of $W(CO)_5$ads. Unreacted CO_2 was then pumped off for > 24 hours and the sample was rephotolyzed at 254nm. The gaseous effluent was isolated and analyzed for CO_2. The results showed, that within the detection limits (10^{-8} moles) of the gas chromatograph, no CO_2 evolved. The UV spectrum showed that the 285-nm band, characteristic of $W(CO)_6$ads, decreased from optical density 1.7 to 1.46 during the course of the reaction, suggesting that the CO_2 reaction product reacts, to a limited extent, with the hexacarbonyl. In an independent experiment $W(CO)_6$ads was photolyzed at 350-nm, generating 5.95 x 10^{-7} moles of $W(CO)_5$ ads, and exposed to 0.104-atm (6.0 x 10^{-4} moles) of CO_2 at 22 $\pm$ 1.0 °C, a decrease in the 408- and 245-nm bands was observed. However, there was no change in the optical density of the 285-nm until a higher pressure (1-atm) of CO_2 was added.

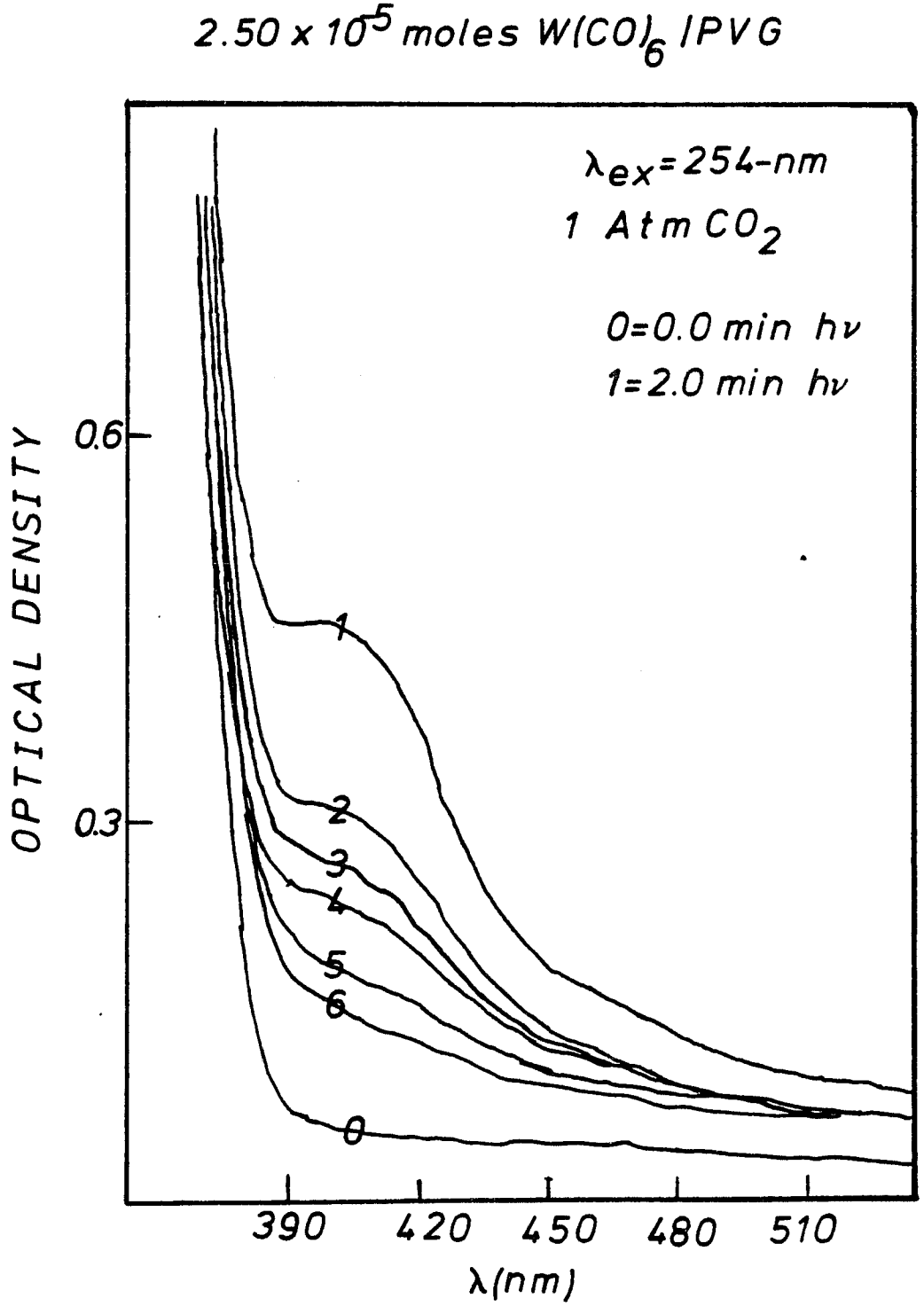

Figure 40. Reaction of $W(CO)_5$ads with 1-atm CO_2. Reaction times: 2=149.0 sec., 3=340.0 sec., 4=964.0 sec., 5=2,570.0 sec., 6=3,240.0 sec. Reaction temperature = 23.0 $\pm$ 1.0 ^{o}C.

Figure 41. Pseudo first-order plots of the reaction between CO and CO_2 and $W(CO)_5$ads. Both reactions were run at a temperature of 23.0 ± 1.0 °C.

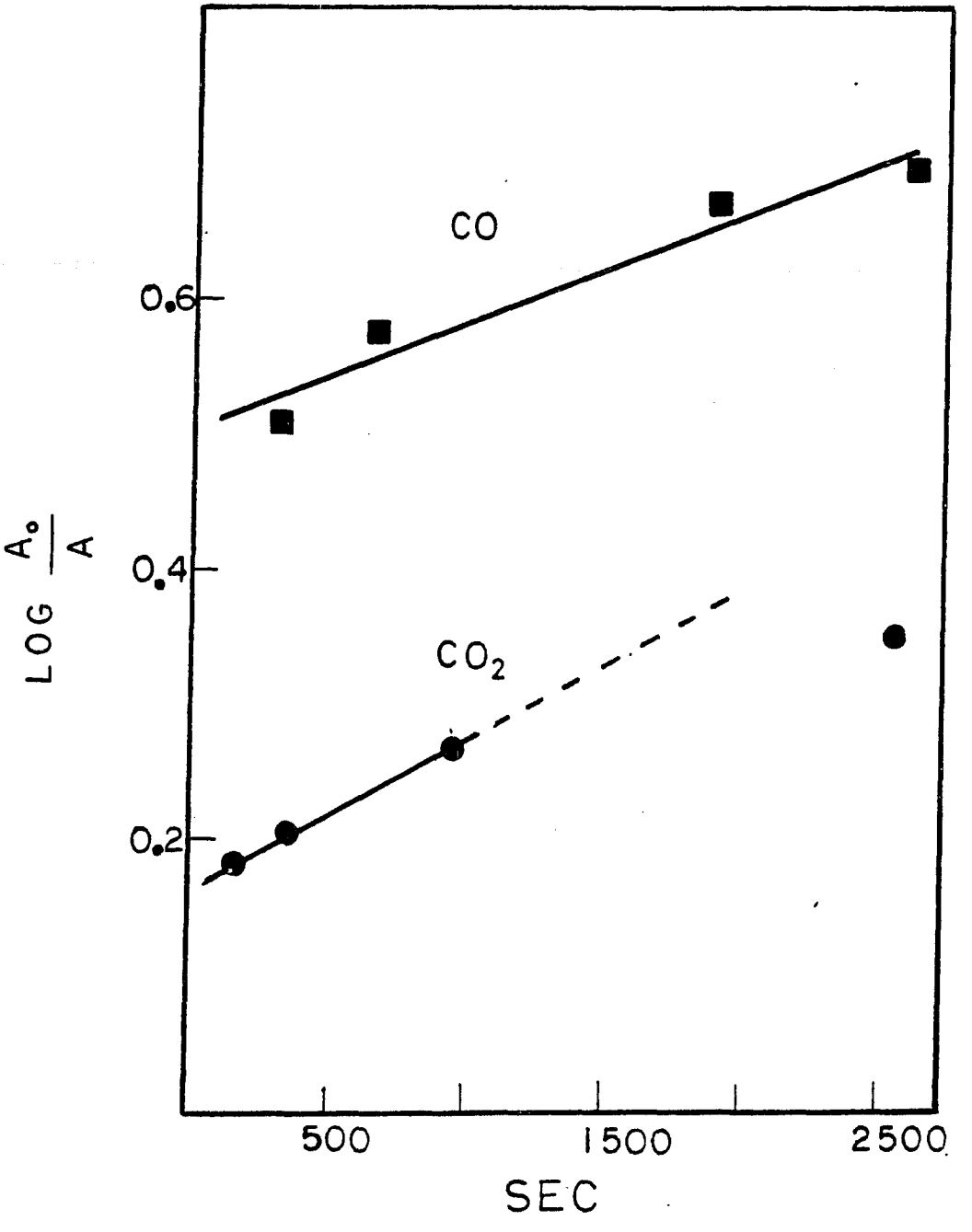

In another experiment, $Mo(CO)_5ads$ was reacted with CO_2, changes in optical density at 400-nm were observed suggesting the formation of a CO_2 complex with molybdenum (Figure 42). Although characterization of the adsorbed CO_2-$M(CO)_5ads$ reaction product will have to await further experiments, the reaction with CO_2, a species of poor complexing ability, illustrates the relative lability of the bond between $M(CO)_5ads$ and PVG.

Further characterization of the $M(CO)_5ads$ intermediate was accomplished by analysis of the gaseous effluent surrounding the piece when photolyzed at 350-nm. A sample containing 3.33×10^{-5} moles of $W(CO)_6ads$ was pumped out for > 24 hours and photolyzed, a plot of total moles of CO evolved and total moles of $W(CO)_5ads$ (determined spectrally) were plotted as a function of photolysis time (Figure 43). The plot illustrates a 1:1 stoichiometry where the moles of CO evolved is within experimental error of the moles of photoproduct determined spectrally. In some measurements, the number of moles of CO detected was less than the number of moles of $W(CO)_5$. This is attributed to the irregular desorption of CO from the PVG surface. The average stoichiometry following 3.66×10^3 seconds of photolysis is $W(CO)_5ads$, although the isosbestic point in the reaction was lost after 6.00×10^2 seconds of photolysis corresponding to 43.8% consumption of $W(CO)_6$. In spite of the stoichiometry, the loss of the isobestic point suggests the existence of a

Figure 42. Reaction of $Mo(CO)_5$ads with 0.172-atm of CO_2.
Reaction times: 1=2.09 min., 2=4.28 min., 3=6.43 min.,
4=8.72 min., 5=15.65 min., Reaction temperature = 23.0 ± 1.0°C.
7.11×10^{-6} moles $Mo(CO)_6$/g PVG.

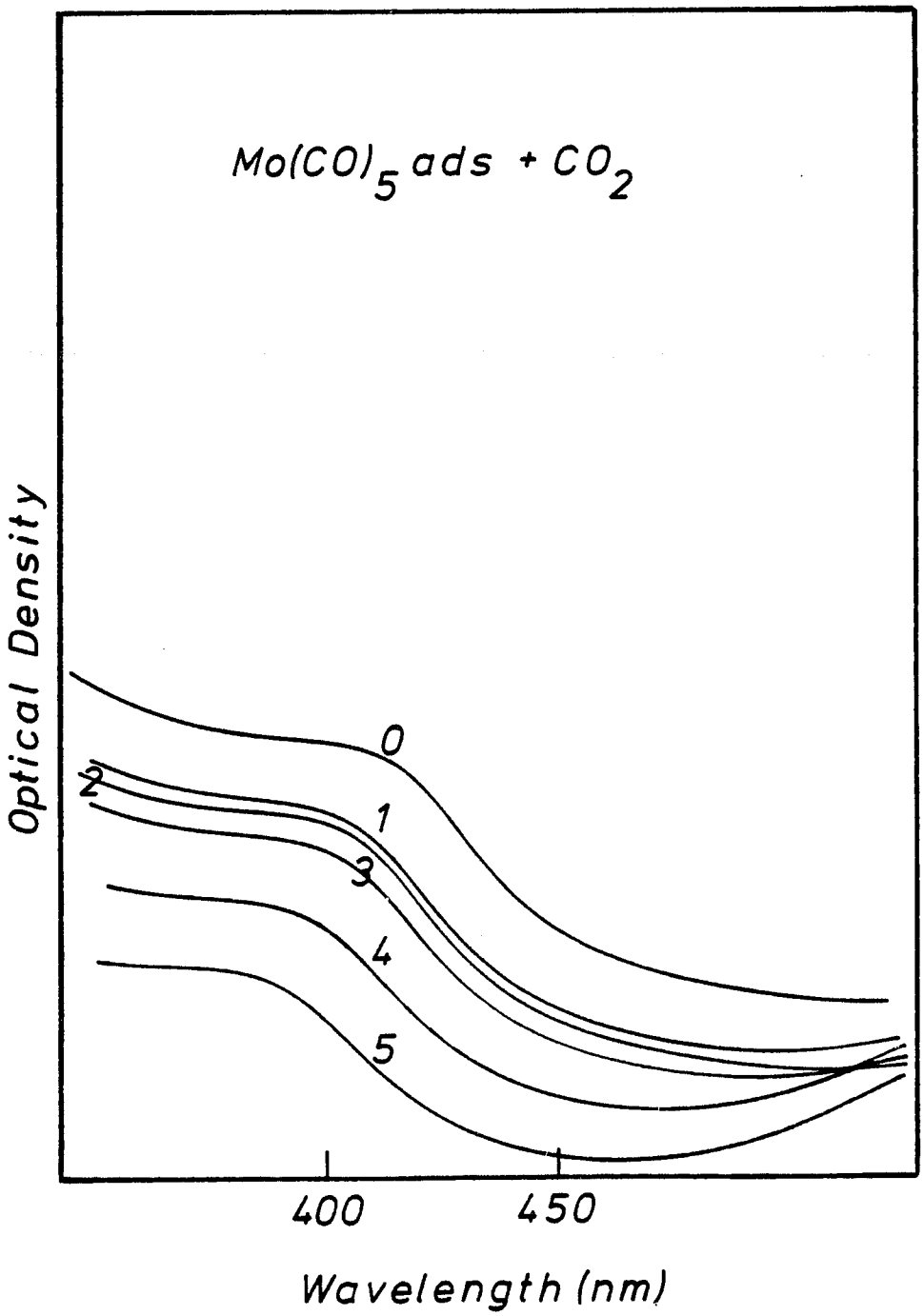

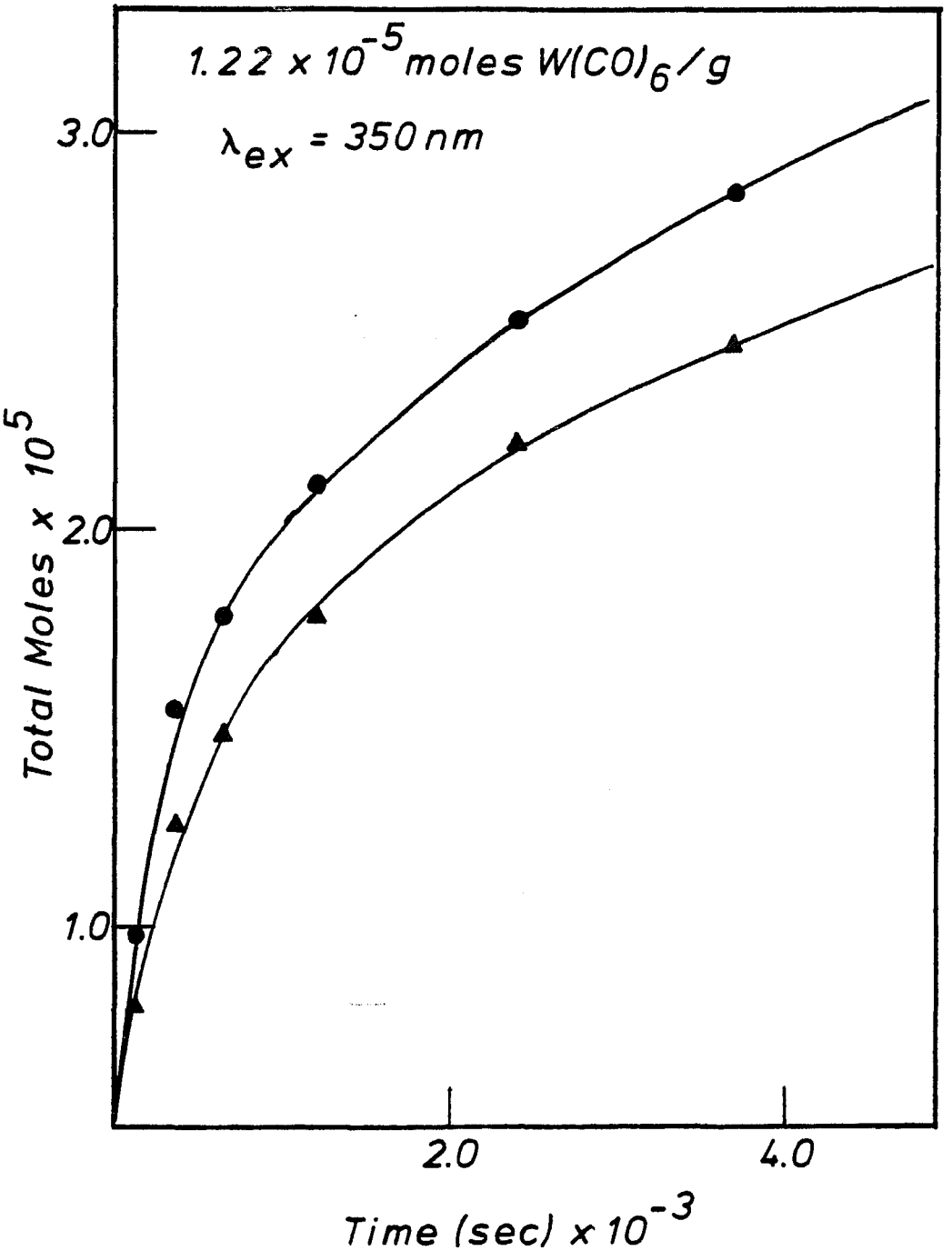

Figure 43. Comparison of the number of moles of $W(CO)_5$ads generated, determined spectrally, and the number of moles of CO evolved. ● =moles of $W(CO)_5$ads; ▲ =moles of CO.

species with average stoichiometry $W(CO)_5$ but is partially oxidized. In an independent experiment $W(CO)_6$ads was photolyzed with 350-nm light for 1.51 x 10^4 seconds. This piece contained 2.14 x 10^{-5} moles of $W(CO)_6$ads, and following photolysis, 2.79 x 10^{-5} moles of CO were evolved. This suggests an average stoichiometry of $W(CO)_{4-5}$, but both studies suggest that with 350-nm photolysis, the principle photoproduct is $W(CO)_5$ads and it is difficult to achieve lower subcarbonyls. This contrasts sharply with photolysis of $W(CO)_6$ads at higher energy (λ_{ex} < 310-nm) where, initially, $W(CO)_5$ads is in a 1:1 stoichiometry with CO but leads, as shown in Figure 44, to the formation of lower subcarbonyls. Exhaustive 254-nm photolysis (>10^6 sec) of a sample containing 2.30 x 10^{-5} moles of $W(CO)_6$ evolved 98% of the CO ligands (Figure 45). However, it was impossible to determine spectrally the existence of lower subcarbonyls. Eventually, the well resolved ligand field band, characteristic of $W(CO)_5$ads, becomes featureless and ultimately a sharp cutoff at 465-nm.

C. Photoinduced Methane Forming Reaction.

The photoinduced decarbonylation of $M(CO)_6$ads is dependent on the excitation wavelength and the extent of photolysis. Figure 43 illustrates the photolysis of $W(CO)_6$ ads at 350-nm. The spectral evidence and gas analysis establish that the principle reaction is formation of $W(CO)_5$ads with little formation of lower

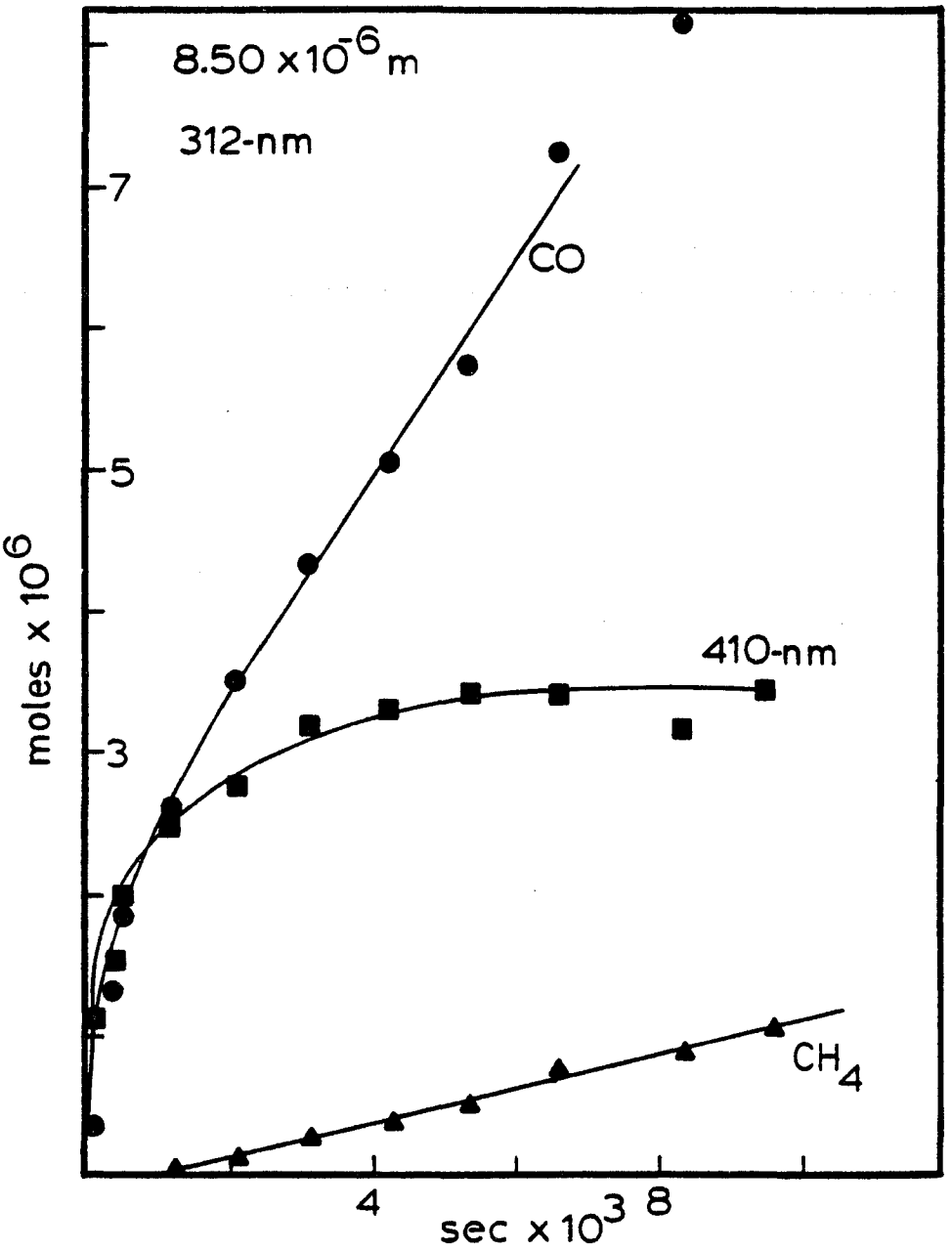

Figure 44. Photolysis of $W(CO)_6$ads at 312 nm. Plot illustrates total moles of gaseous products evolved during photolysis. (●) CO, (■)$W(CO)_5$ads, and (▲) CH_4.

Figure 45. Photolysis of 2.30×10^{-5} moles of $W(CO)_6$/PVG at 254 nm. Plot illustrates total moles of gaseous products evolved during photolysis. PVG was not baked out prior to impregnation.

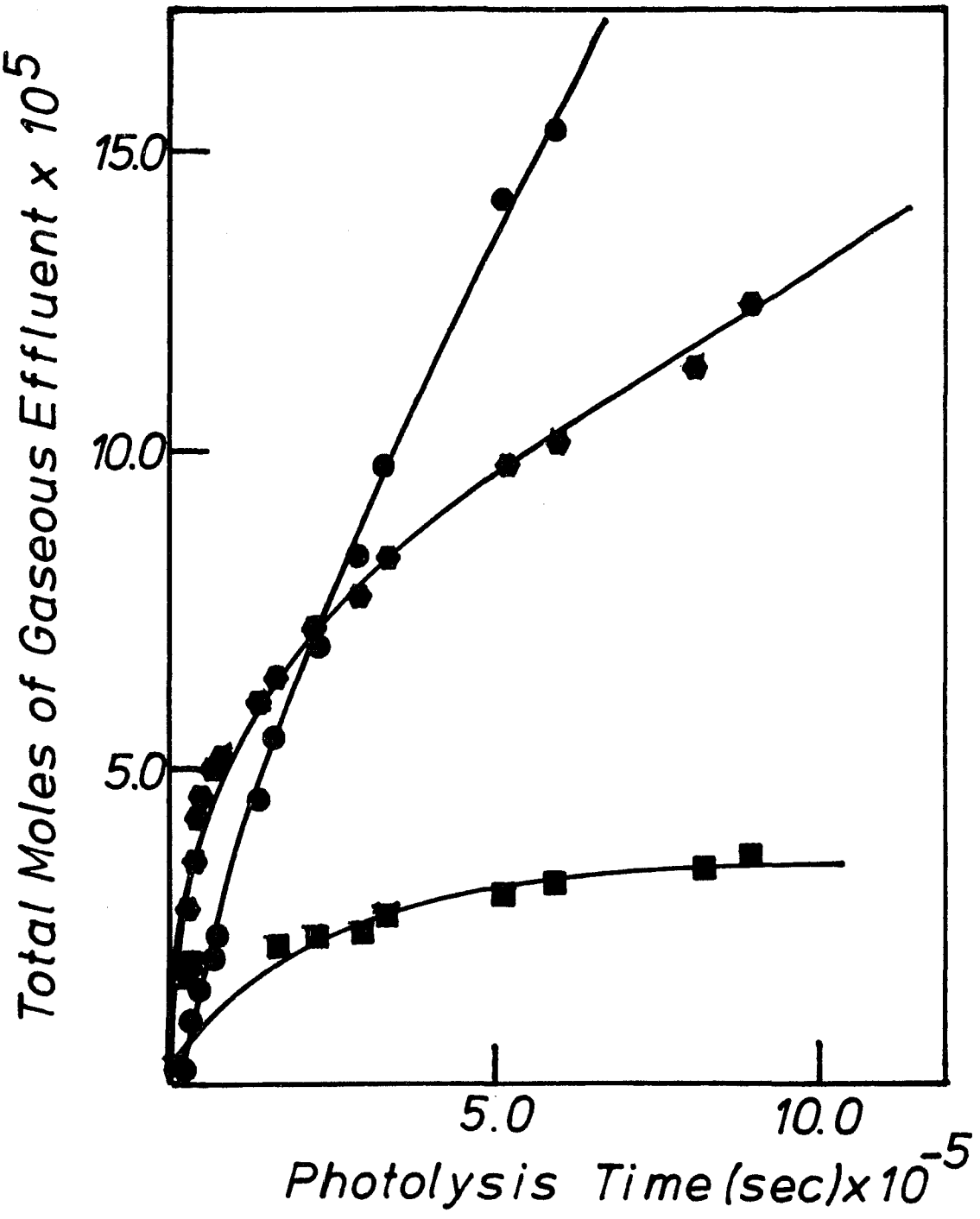

(●) CO, (●) CH_4, and (■) H_2.

subcarbonyls. However, photolysis at excitation wavelengths <310-nm results in further decarbonylation and the formation of CH_4. Gas phase analysis of a sample containing 9.76 x 10^{-6} moles of $W(CO)_6$ and photolyzed at 310-nm, for 6.74 x 10^4 seconds, shows that 1.73 x 10^{-5} moles of CO evolve, prior to this point <1 x 10^{-6} moles of CH_4 have evolved. The number of moles of CH_4 evolved at this point in the photolysis is 7.59 x 10^{-6} moles, and an average stoichiometry of $W(CO)_{4\pm0.2}ads$ is observed. These results suggest that in order to produce a significant quantity of CH_4 (>1 x 10^{-6} moles) an average stoichiometry of $W(CO)_4ads$ must be generated. This conclusion is further exemplified in Figure 44, which shows that an induction period is present at 310-nm photolysis, while no induction period is observed at 254nm photolysis. Although the quantum yields of CH_4 at these excitation wavelengths (Table 5) differ, periodically recorded spectra are similar and show that the initial changes, indicative of $W(CO)_5ads$ formation, are followed by a loss of the isosbestic point at 350-nm. Prolonged 254 or 310-nm photolysis causes the LF band, characteristic of $M(CO)_5ads$, to become featureless and eventually approach a sharp cutoff, a characteristic of semi-conductor metal oxides (102). It is noteworthy that the band gap energy of WO_3 is 2.7 eV (102) which corresponds to an energy of 21,786 cm^{-1} (459nm), the 50% transmission point observed in our featureless spectra is 465nm.

The formation of dimeric species or higher order clusters have been thought to be efficient mediators in the methanation reaction (122-124). Therefore, we will establish here whether dimeric or higher order clusters are being generated at any point in the reaction. As a model for the spectrum of a dimeric species, the absorption spectrum of $W_2(CO)_{10}^{2-}$ is used. The latter in CH_2Cl_2 is characterized by absorptions at 351-nm (ϵ=7.21 x 10^3 M^{-1} cm^{-1}) and 392-nm (ϵ=4.84 x 10^3 M^{-1} cm^{-1}). However, there is no indication in our spectra of dimer formation or visible absorption bands indicative of higher order clusters. 310-nm photolysis of PVG containing 9.26 x 10^{-6} moles of $W(CO)_6$ads, 2.83 x 10^{-6} moles/g of PVG, yields 7.54 x 10^{-6} moles of CH_4 and 1.73 x 10^{-5} moles of CO. Taking $\Delta A<0.002$ as the minimum detectable absorbance change indicative of the dimer, the spectra indicate that < 3.94 x 10^{-9} moles of $W_2(CO)_{10}^{2-}$ are formed. At a fractional surface coverage of 0.08, the mean separation between the W centers is calculated according to equation 15, where

$$d=1/(N_{av}C)^{1/2} \qquad (15)$$

N_{av} is Avogadro's number and C is the coverage in mol/cm^2. Taking $130m^2/gm$ as the surface area, a surface coverage of 0.08 yields a calculated value of d=14.4 Å, which is significantly larger than bond distances of tungsten dimers. For example, the W-W bond distance in

$K_3W_2Cl_9$ is 2.41 Å (126) while that in $W_2(CH_3)_8$ is 2.26 Å (126).

Photolysis of $M(CO)_6$ads under 0.1-atm of H_2 does not increase the rate of CH_4 evolution. Replacing adsorbed H_2O by D_2O, however yields mixtures of deuterated methanes when examined by mass spectroscopy, which establishes that the hydrogen source is adsorbed water or silanol groups since these could exchange deuteriums with adsorbed D_2O.

CH_4 evolution occurs on extensive 310- or 254-nm photolysis of $M(CO)_6$ads in vacuo, under 1-atm of CO, or under 0.25-atm of CO and 0.5-atm of H_2.
Various control experiments were performed in which a blank sample of PVG was photolyzed (254nm) in vacuo for > 24 hours and in a separate experiment in which a blank sample of PVG was photolyzed in the presence of 0.5-atm of CO and 0.5-atm of H_2. Analysis of the gaseous effluent in both studies showed that no CH_4 evolved. Although the complex is essential to CH_4 formation, isotopic labelling establishes that CH_4 does not arise from coordinated CO. Photolysis of $W(^{13}CO)_6$ads (90% enriched) yields only $^{12}CH_4$. Mass spectra of the gaseous photoproducts, Figure 8b, show that photolysis of a PVG sample containing 3.6×10^{-5} moles of $W(^{13}CO)_6$ (90% enriched) evolves the expected 90:10 ratio of photoreleased CO, but <1% $^{13}CH_4$. The absence of a hexane fragmentation pattern in the mass spectrum (minimum

detectable quantity = 10^{-9} gram) and the formation of CH_4 in solventless runs, where the complex is sublimed onto PVG, establish that CH_4 is not due to the photolyzed decomposition of C_6H_{14}. Moreover, when $M(CO)_6$ is dissolved in $CHCl_3$, and then adsorbed onto PVG, only CH_4 is evolved indicating that the reaction that is taking place is highly specific and independent of what solvent is used to dissolve $M(CO)_6$. After exhaustive 254-nm photolysis of 2.30×10^{-5} moles of $W(CO)_6$ads, 98% of the carbonyl ligands are recovered as gaseous CO in addition to 2.52×10^{-4} moles of CH_4. These results offer compelling evidence that CH_4 does not originate from the adsorbed complex, but from an extraneous carbon source present on PVG.

In addition, to the evolution of CO and CH_4, H_2 is evolved with a rate that is dependent on glass preparation. Figure 46 illustrates the evolution of H_2 for three different samples of PVG. The first sample, which was extracted and then calcined at 600° for >72 hours, was impregnated with 1.86×10^{-5} moles of $W(CO)_6$. 254-nm photolysis of this sample led to the evolution of 5.70×10^{-6} moles of H_2 or a $H_2/W(CO)_6$ ads=3.06×10^{-1}. The second sample, which was extracted but not baked, contained 2.30×10^{-5} moles of $W(CO)_6$. 254-nm photolysis evolved 5.58×10^{-5} moles of H_2 or a $H_2/W(CO)_6$=2.43. The third sample which was heated at 600°C in flowing H_2

Figure 46. Relative rates of H_2 evolution for three differently prepared PVG samples prior to $W(CO)_6$ impregnation. Photolysis was at 254-nm for all samples.

(▲) PVG was calcined in air at 600°C for > 72 hours.

(■) PVG was calcined in flowing H_2 for > 24 hours.

(●) PVG was not baked out.

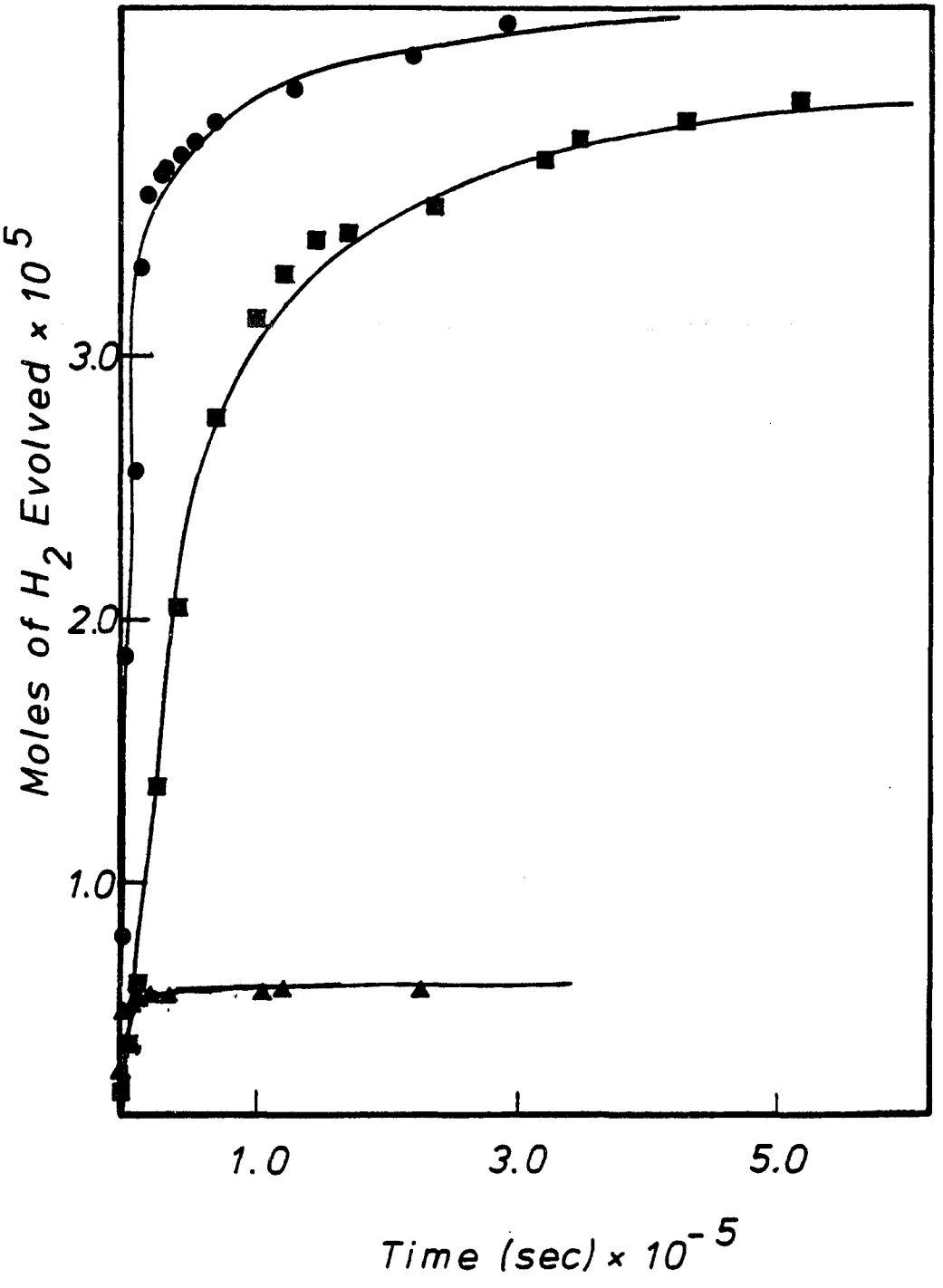

(▲) contained 1.86 x 10^{-5} moles of $W(CO)_6$; (■) contained 4.06 x 10^{-5} moles of $W(CO)_6$; and (●) contained 2.30 x 10^{-5} moles of $W(CO)_6$.

and impregnated with 4.09×10^{-5} moles of $W(CO)_6$ evolved 4.4×10^{-5} moles of H_2 or a $H_2/W(CO)_6 = 1.08$. Although each sample had a different amount of complex adsorbed to it, these results establish that the mode of pretreatment dictates the amount of hydrogen evolved. With complexes supported on γ-alumina Brenner and co-workers (12) have suggested that H_2 arises from a redox reaction between surface hydroxyl groups (σ-OH) and the metal, i.e.,

$$M(CO)_{6ads} + n(\sigma\text{-OH}) \longrightarrow (\sigma\text{-O})_n M^{n+} + (n/2)H_2 + 6CO$$

EPR experiments further confirm that H_2 evolution is concurrent with oxidation of the originally zerovalent metal.

Photolysis of crushed PVG (60-80 mesh) impregnated with 7.83×10^{-6} moles of $Mo(CO)_{6ads}$ results in the appearance of an ESR signal, Figure 47, which increases in intensity with continued photolysis. The ESR signal, which has a $g = 1.948 \pm 0.002$ and a peak width of 75 G, is in excellent agreement the ESR spectrum of $MoO_2(OH)$ recorded by Howe and Leith (21). This spectral similarity indicates that photolysis of $Mo(CO)_{6ads}$ ultimately leads to Mo(V) species.

The evolution of an oxidation product, CO_2, is also observed. Mass spectroscopic examination of the effluent following 254-nm photolysis of $W(^{13}CO)_6$ establishes that CO_2 is derived from CO (Figure 8b). The rate of

Figure 47. Room temperature EPR spectrum of Mo(V) on crushed (60/80 mesh) PVG following photolysis of $Mo(CO)_6$ at 254 nm.

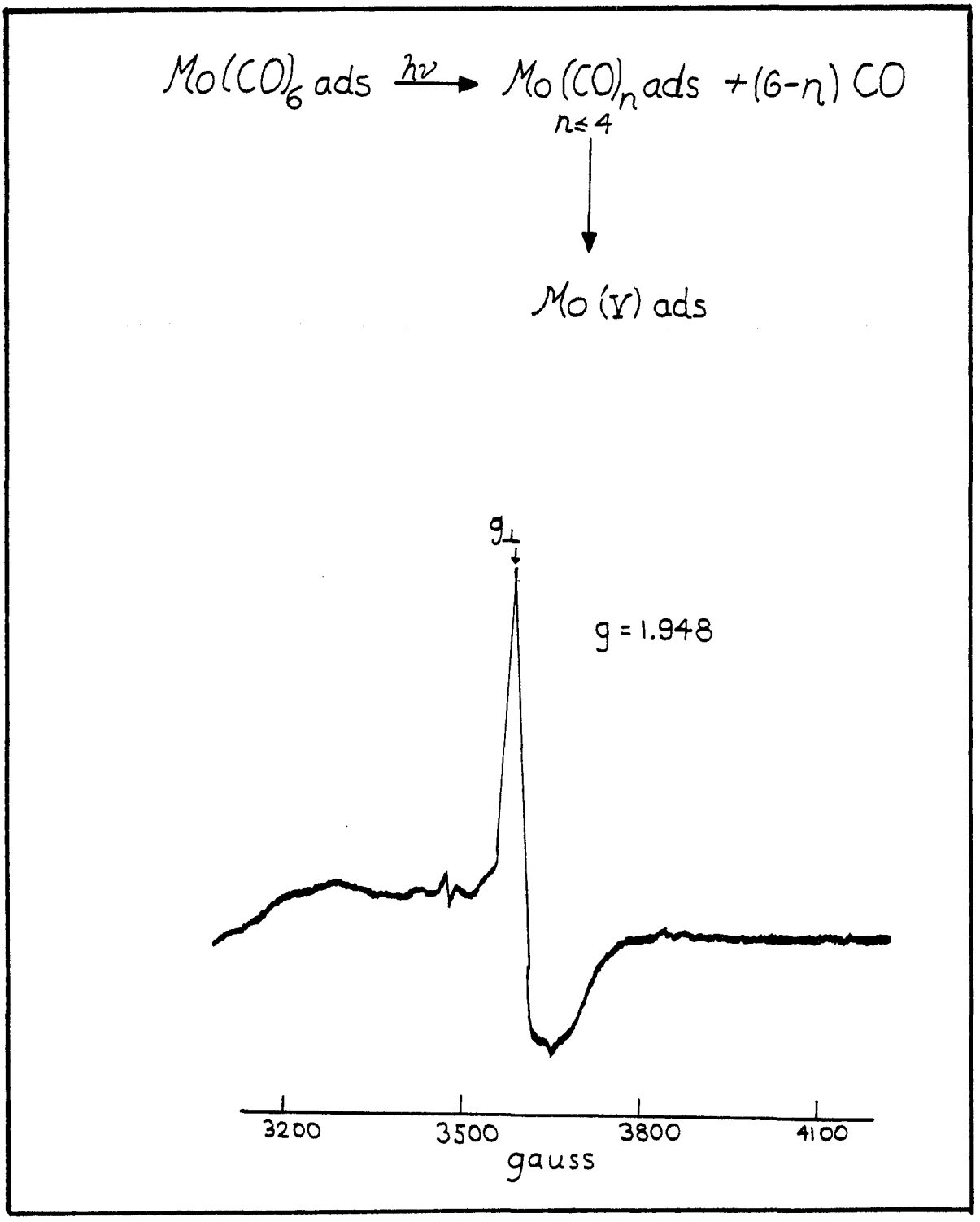

evolution of CO_2 is extremely low as compared to the rate of CO and CH_4 evolution, but is enhanced in the presence of small pressures of O_2 (Figure 48).

Since ^{13}C labelling establish that CH_4 was from a carbon source present on PVG, experiments were conducted to reduce and/or volatilize this source by calcining the sample in flowing H_2. A 2.7 gm sample of PVG was heated to 600°C in H_2 for 24 hours and then impregnated with a n-hexane solution of $W(CO)_6$. After removal of the solvent, $W(CO)_6$ was photolyzed at 254-nm and gaseous products measured. Figure 49 shows an induction period prior to CH_4 evolution, but on prolonged photolysis the rate of CH_4 evolution begins to approach the rate found for a sample that was calcined in air.

To gain further insight into the methanation reaction, $W(CO)_5P(Ph)_3$ and $HW(CO)_5^-$ were synthesized and adsorbed onto PVG. The former, $W(CO)_5P(Ph)_3$, was examined in an attempt to prevent the oxidation of the metal atom and, thus, preventing the formation of H_2. In n-hexane, the complex $W(CO)_5P(Ph)_3$ displays two absorption bands, one at 347-nm ($^1A_1 \longrightarrow {}^1E$ LF; ε=2,20 M^{-1} cm^{-1}, and another at 227-nm (MLCT; ε=6.79 x 10^4 M^{-1} cm^{-1}. It is noteworthy that this complex is adsorbed to PVG to a much larger extent than $W(CO)_6$. It was observed that 1.77 x 10^{-5} moles are adsorbed/gram using only 50 ml of a 3.05 x 10^{-3} M n-hexane solution of the complex. Using a similar

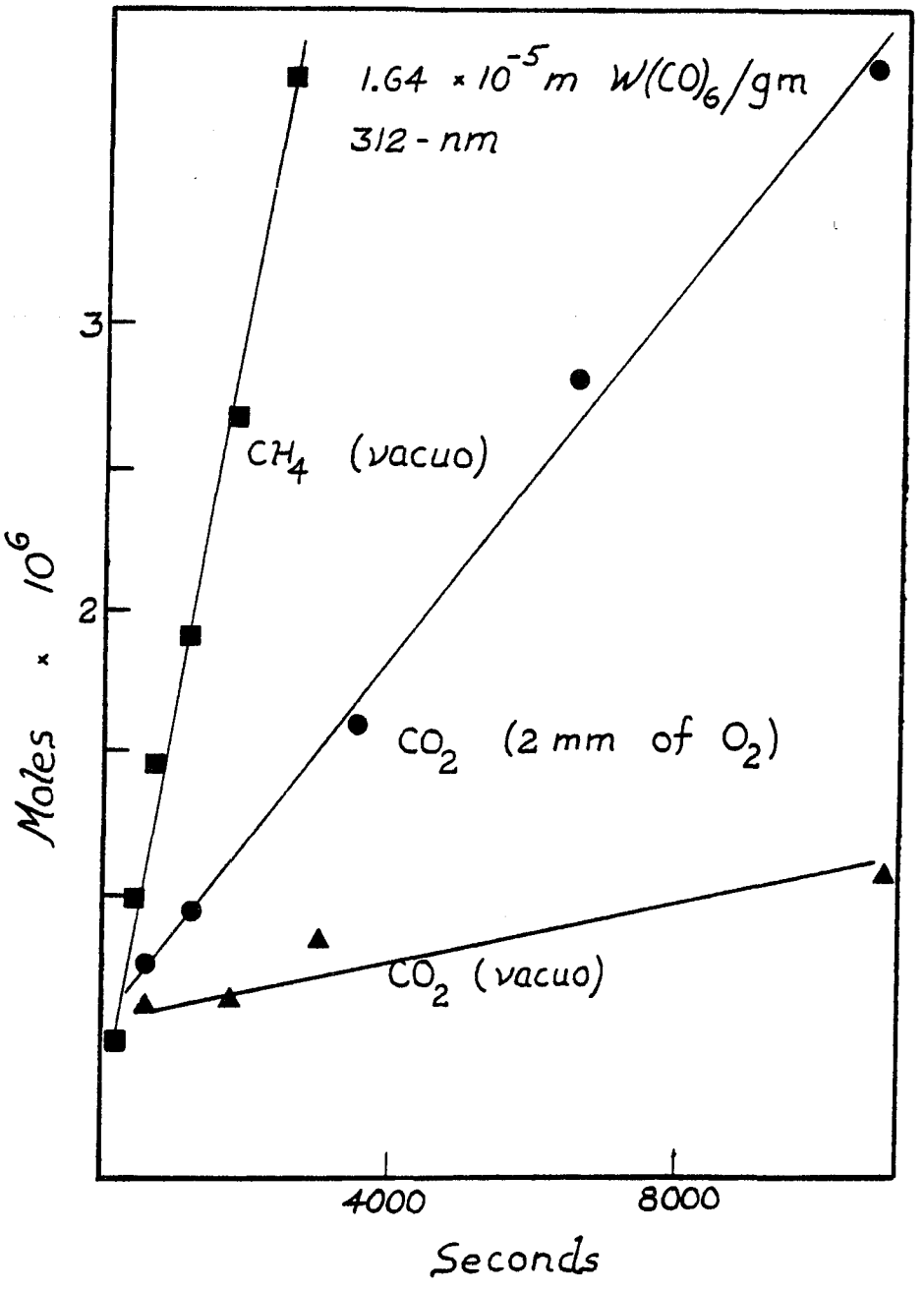

Figure 48. Evolution of CO_2 in the presence and absence of O_2 after photolysis of $W(CO)_6$ads at 312 nm.

Figure 49. Gaseous products evolved after photolysis at 254-nm of a PVG sample that was calcined in flowing H_2 at 600^{o}C prior to impregnation by $W(CO)_6$. The sample contained 4.06 x 10^{-5} moles of $W(CO)_6$. (●) H_2, (▲) CH_4, and (■) CO.

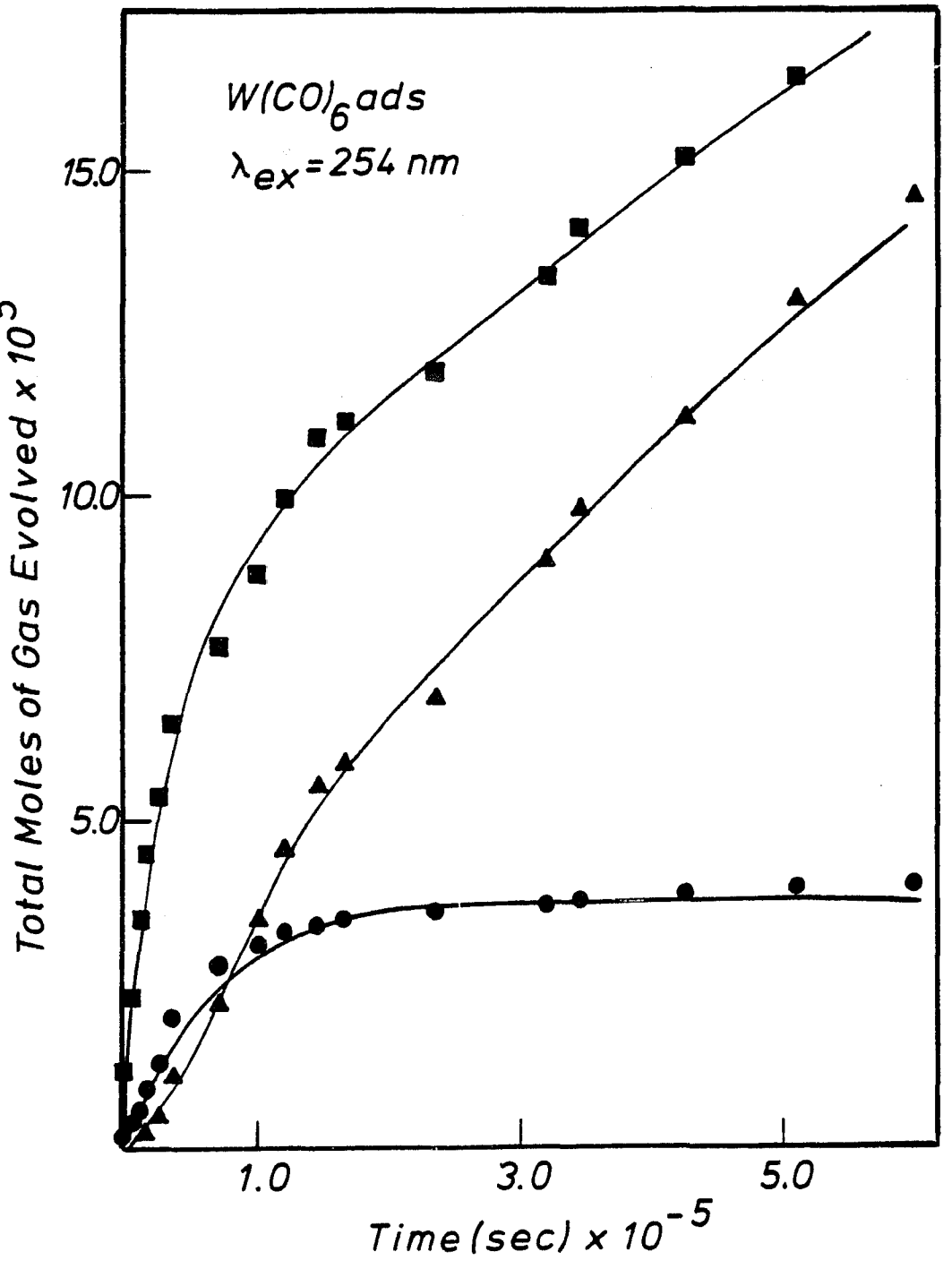
W(CO)6 ads
λex = 254 nm
15.0
10.0
5.0
Total Moles of Gas Evolved x 10^5
1.0
3.0
5.0
Time (sec) x 10^-5

concentration of impregnating solution, only 1.0×10^{-6} moles of $W(CO)_6$/gm are adsorbed. Once adsorbed, the LF band is not resolved and the region where the MLCT band occurs is masked by the absorbance of the PVG. This sample was photolyzed with 254-nm light and the gaseous products analyzed and are plotted in Figure 50 as a function of photolysis time. The quantum yields of CH_4, H_2, and CO are 0.141, 0.991, and 0.171, respectively. In an independent experiment, in which PVG was impregnated with $W(CO)_6$, the quantum yields of CH_4, H_2, and CO, after 254-nm photolysis, are 0.146, 0.044, and 0.216, respectively. These results are contrary to what was expected, particularly that ϕ_{H_2} for $W(CO)_5P(Ph)_3$ was >> than ϕ_{H_2} for $W(CO)_6$. Examination of the spectra following photolysis of $W(CO)_5P(Ph)_3$ads reveals an increase in optical density in the visible region, however, the spectra have no well resolved bands.

$HW(CO)_5^-$ was adsorbed onto PVG and examined to to determine the role of a hydride intermediate in the methane forming reaction. Because it is anionic, the salt $Me_4N^+HW(CO)_5^-$ was adsorbed onto PVG. Although the amount adsorbed is small, the PVG sample appears yellow-orange with an absorption at 450-nm, relative to a blank piece of PVG, which is similar to the spectrum of the complex in aqueous solution. The sample was photolyzed at 254-nm and the vapor phase analyzed. Following 290.0

Figure 50. Evolution of gaseous products following 254-nm photolysis of $W(CO)_5P(Ph)_3$ads. The sample was calcined (600°C) prior to adsorption of 4.64×10^{-5} moles of complex.

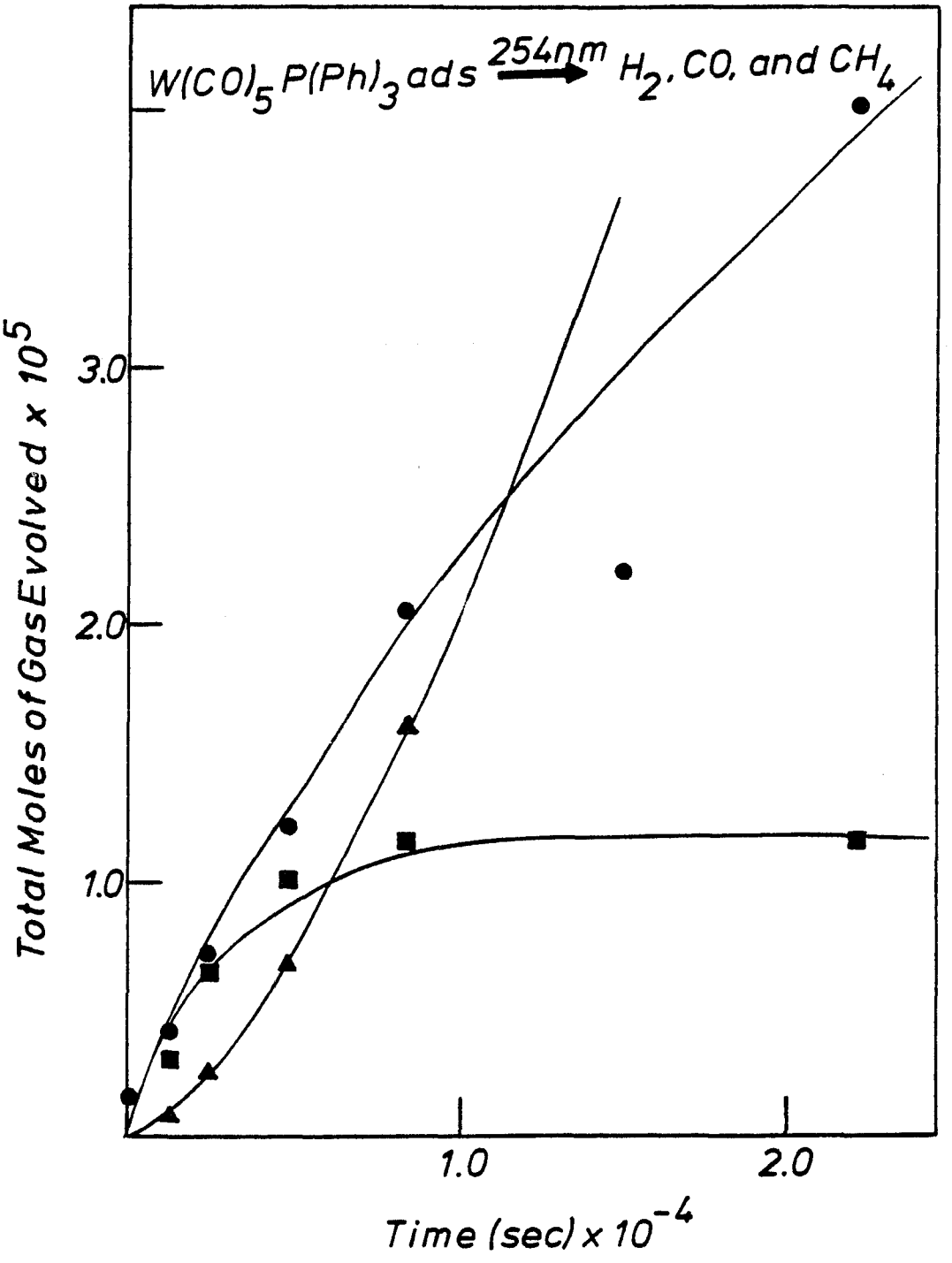

(■) H_2, (▲) CH_4, and (●) CO.

minutes of 254-nm photolysis, no gaseous products were detected. However, no spectral changes were observed either. The absence of gaseous products and the absence of spectral changes indicative of $HW(CO)_5^-$ formation suggest that hydride species are not a principle intermediate in the CH_4 forming reaction.

D. Kinetic Studies of the Addition of Various Ligands to $W(CO)_{5ads}$.

To determine the rate of reaction between $W(CO)_{5ads}$ and various ligands, $W(CO)_{5ads}$ was generated in situ by 350-nm photolysis of $W(CO)_{6ads}$. These samples were then exposed to gaseous CO, cis-2-butene, or trans-2-butene or thoroughly degassed (three successive freeze-pump-thaw cycles) n-hexane solutions of 1-pentene. A large excess of each reagent was added and and the rate of formation of $W(CO)_5Lads$ was measured under pseudo first-order conditions. As indicated in Figure 51 the reactions follow a first order dependence and the rate constants were calculated from changes in optical density at 410-nm using equation 16.

$$k = 2.303/t \log (O.D._{\infty} - O.D._o / O.D._{\infty} - O.D._t) \qquad (16)$$

The second order rate constant, k, was calculated from the slope of these plots, k_{app}, according to the relationship:

$$k_{app} = k_{true} (Ligand)$$

Ligand concentrations were taken as the moles adsorbed/g PVG and were extrapolated from the appropriate isotherm for a given applied pressure.

Figure 51. Pseudo first-order rate plots of $W(CO)_5$ads with CO, cis-2-butene, and trans-2-butene. (■) cis-2-butene (36.8°C), (▲) trans-2-butene (28.0°C), and (●) CO (28.0°C).

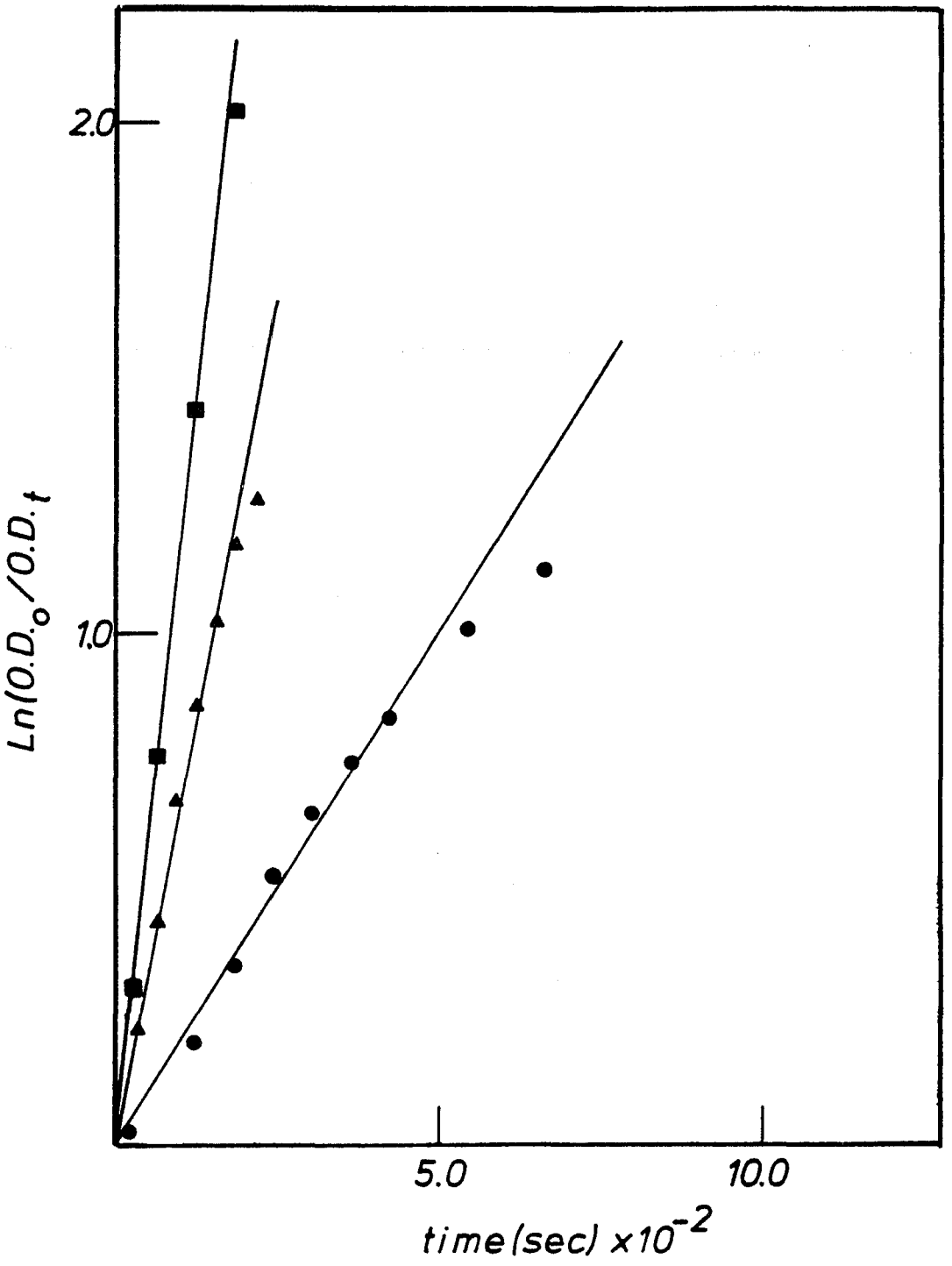

Reaction temperatures are in parentheses and the number of moles of ligand used are listed in Table 7.

The Arrhenius and Eyring activation parameters were derived from the slope of plots of k_{true} vs. temperature, Figure 52. Table 7 summarizes the rate data and activation parameters for each reaction.

E. Catalytic Reactions.

The hybrid systems composed of physisorbed Group 6B hexacarbonyls were also examined as catalysts of the hydrogenation and isomerization of olefins.

The photocatalyzed isomerization of cis-2-butene was examined by 310-nm photolysis of a sample containing 1.11 x 10^{-5} moles of $W(CO)_6$ in the presence of 1.03 x 10^{-3} moles of cis-2-butene. The UV-visible absorption spectrum shows that the initial complex, $W(CO)_6ads$, has reacted with subsequent formation of $W(CO)_5ads$, which reacts with the excess cis-2-butene. The UV-visible spectrum was monitored throughout the photolysis and after 9.3 x 10^3 seconds of photolysis and 6.12 x 10^4 seconds of thermolysis (23 $\pm$ 1.0°C) the original ligand field band of $W(CO)_5ads$ at 408-nm was shifted to 380-nm. The monoolefin complex, $W(CO)_5$(cis-2-butene) has an absorption maximum at 304-nm. However, it is likely that formation of a bis-or tris (olefin) complex would cause a red-shift in the latter bands since cis-2-butene is a weaker ligand than CO. The number of moles of CO evolved was calculated from a plot of moles of CO versus photolysis time for a sample containing a similar concentration of complex. After 9.3 x 10^3 seconds of irradiation, the calculation

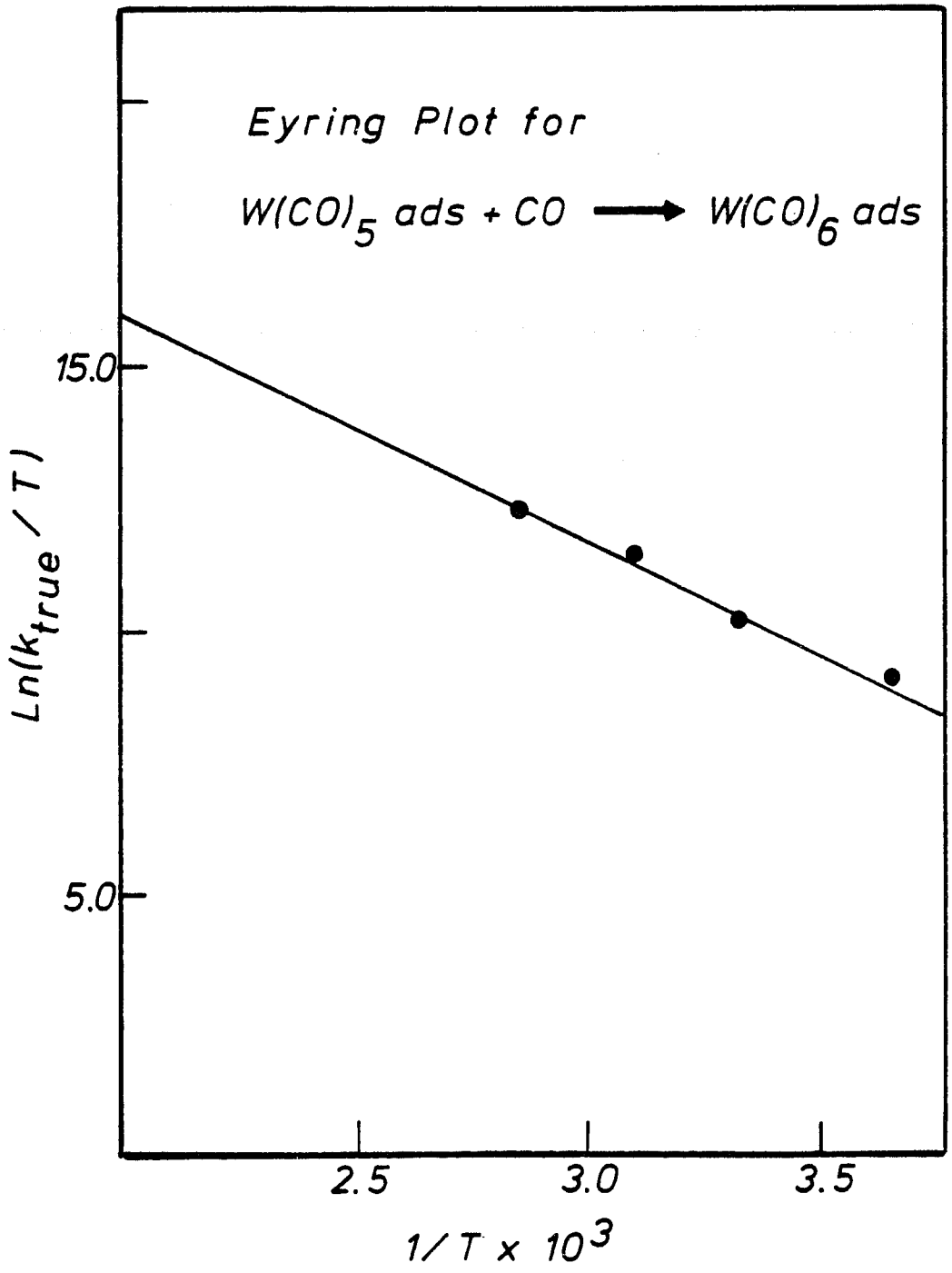

Figure 52. Eyring plot for the reaction of $W(CO)_5$ads with CO at 1.0°C, 28.0°C, 50.5°C, and 76.5°C.

Table 7. A Summary of the Kinetic Data for the Reaction $W(CO)_5$ads + L.

Temperature (^oK)	Moles of L adsorbed x 10^5	Moles of $W(CO)_5$ads x 10^6	k_{app} (sec^{-1}) x 10^4	log k_{true} M^{-1} sec^{-1}
CO				
274.16	2.58	2.20	9.80	1.58
301.16	2.58	1.51	21.20	1.91
323.66	2.30	1.24	71.83	2.49
349.66	2.15	1.82	118.67	2.74
E_a=6.97 kcal/mole A=1.32 x 10^7 sec^{-1} $\Delta H^{\neq}$=7.66 kcal/mole $\Delta S^{\neq}$=-1.0 cal/mole ^oK.				
Cis-2-butene				
278.16	1.22	2.54	4.13	1.53
301.66	0.599	2.41	75.67	3.10
318.66	0.579	2.41	103.33	3.25
339.16	0.583	2.06	241.67	4.62
E_a=20.39 kcal/mole A=5.75 x 10^1 sec^{-1} $\Delta H^{\neq}$=21.09 kcal/mole $\Delta S^{\neq}$=46.78 cal/mole ^oK.				
Trans-2-Butene				
281.16	1.15	2.13	3.20	2.45
309.96	1.16	3.09	76.20	2.82
317.66	1.12	2.41	116.50	3.02
331.66	1.11	2.34	186.67	3.23
E_a=6.05 kcal/mole A=1.35 x 10^7 sec^{-1} $\Delta H^{\neq}$=6.65 kcal/mole $\Delta S^{\neq}$=-10.33 cal/mole ^oK.				
1-pentene [a]				
304.66		2.41	16.0	
317.66		2.82	92.67	
335.66		2.61	208.33	
E_a=16.68 kcal/mole A=1.07 x 10^{11} sec^{-1} $\Delta H^{\neq}$=16.0 kcal/mole $\Delta S^{\neq}$=-10.33 cal/mole ^oK.				

[a]All 1-pentene solutions were 10^{-2} M in n-hexane.

yields a value of 3.3×10^{-5} moles of CO evolved, which suggest that the average stoichiometry, at this point in the photolysis, is $W(CO)_3$ads. However, continued photolysis was necessary before isomerization products were observed (Table 8). Specifically, a tunrnover frequency (isomerized molecules/ sec/W atom)= 5.18×10^{19} molecues/2.54×10^5sec/6.69×10^{18} atoms W = 3.05×10^{-5} sec^{-1} was obtained for the isomerization to 1-butene.

In another study a piece containing $\sim 10^{-5}$ moles of $W(CO)_6$ was photolyzed at an excitation wavelength of 350-nm for 360.0 seconds. A change in optical density of 0.49 at 410-nm was observed corresponding to the generation of 1.20×10^{-6} moles of $W(CO)_5$ads, which was subsequently exposed to 5.81×10^{-3} moles of cis-2-butene at 22$\pm$ 1.0.^oC. Following 8.90×10^2 seconds, the optical density measured at 410-nm, characteristic of $W(CO)_5$ads, went from 0.49 to 0.16 corresponding to 73.5% reaction of the latter to form $W(CO)_5$(cis-2-butene). Unreacted cis-2-butene was pumped off and GC analysis after pumping showed no residual cis-2-butene. The sample which now contains $W(CO)_6$ads and $W(CO)_5$ (cis-2-butene) was rephotolyzed with 350-nm light. Periodically during photolysis, UV-visible absorption spectra were recorded and the vapor phase was examined by GC. The visible region of the spectra showed a substantial increase in optical density although no well

Table 8. Product Distribution for the Isomerization of Cis-2-Butene.

λ_{ex} = 254 nm. Temperature = 22.0 ± 1.0°C.

Sample contained 1.11 x 10^{-5} moles/g $W(CO)_6$ ads.

Cell contained 1.03 x 10^{-3} moles of cis-2-butene.

Photolysis Time (sec)	%Cis-2-Butene	$\%CH_4$	%1-Butene
0.0	100.0	0.0	0.1
1,580.0	100.0	0.0	0.1
5,280.0	99.9	0.1	0.1
7,200.0	99.9	0.1	0.1
8,520.0	99.9	0.1	0.1
9,300.0	99.9	0.1	0.1
Thermolyzed for 17.0 hours.	99.9	0.1	0.1
14,100.0	99.9	0.1	0.1
21,480.0	99.9	0.1	0.1
90,180.0	93.78	1.91	4.31
93,180.0	94.0	2.00	4.00
98,400.0	91.82	2.48	4.73
99,120.0	94.19	1.74	4.07
101,880.0	93.24	2.03	4.73
157,860.0	91.45	3.02	5.53
165,720.0	92.17	2.49	5.34
172,200.0	90.66	3.65	5.69
254,220.0	85.48	6.16	8.36

resolved features indicative of a specific adsorbate could be resolved. After 40.0 minutes photolysis, the spectra showed that the initial increase in the visible region, O.D.=0.40 at 410-nm decreased to O.D.=0.105. Although the excess cis-2-butene was removed, this molecule is strongly adsorbed to PVG, (as evidenced by the odor from the PVG that persisted after the study). This suggests that any $W(CO)_{5ads}$ that is being regenerated is immediately reacting with adsorbed cis-2-butene. Moreover, analysis of the vapor phase after 6.0 minutes (O.D.=0.40) shows that trans-2-butene has been produced in a cis/trans ratio =4.0. This ratio remained approximately constant throughout 40.0 minutes photolysis, however, the optical density of the sample decreased to 0.105.

The isomerization of 1-butene was examined by exposing a PVG sample containing 1.15×10^{-6} moles/g $W(CO)_6$ to 6.29×10^{-3} moles of 1-butene and photolyzing the system with 254-nm light for 1.5×10^3 minutes. The formation of cis- and trans-2-butene was observed (Figure 53) in a ratio of cis/trans = 0.167. Numerous other peaks were observed in the chromatogram and their retention time suggest formation of higher molecular weight hydrocarbons or hydroformylation products (12,22,23,24,26).

Hydrogenation Reactions.

As described above, the ability of 1,3 butadiene to react with $W(CO)_{5ads}$ was investigated prior to examining

Figure 53. Chromatogram of $W(CO)_6$ photocatalyzed isomerization of 1-butene. Chromatogram was taken after 3,000 minutes photolysis. Peak 3=1-butene, peak 4=trans-2-butene, and peak 5=cis-2-butene.

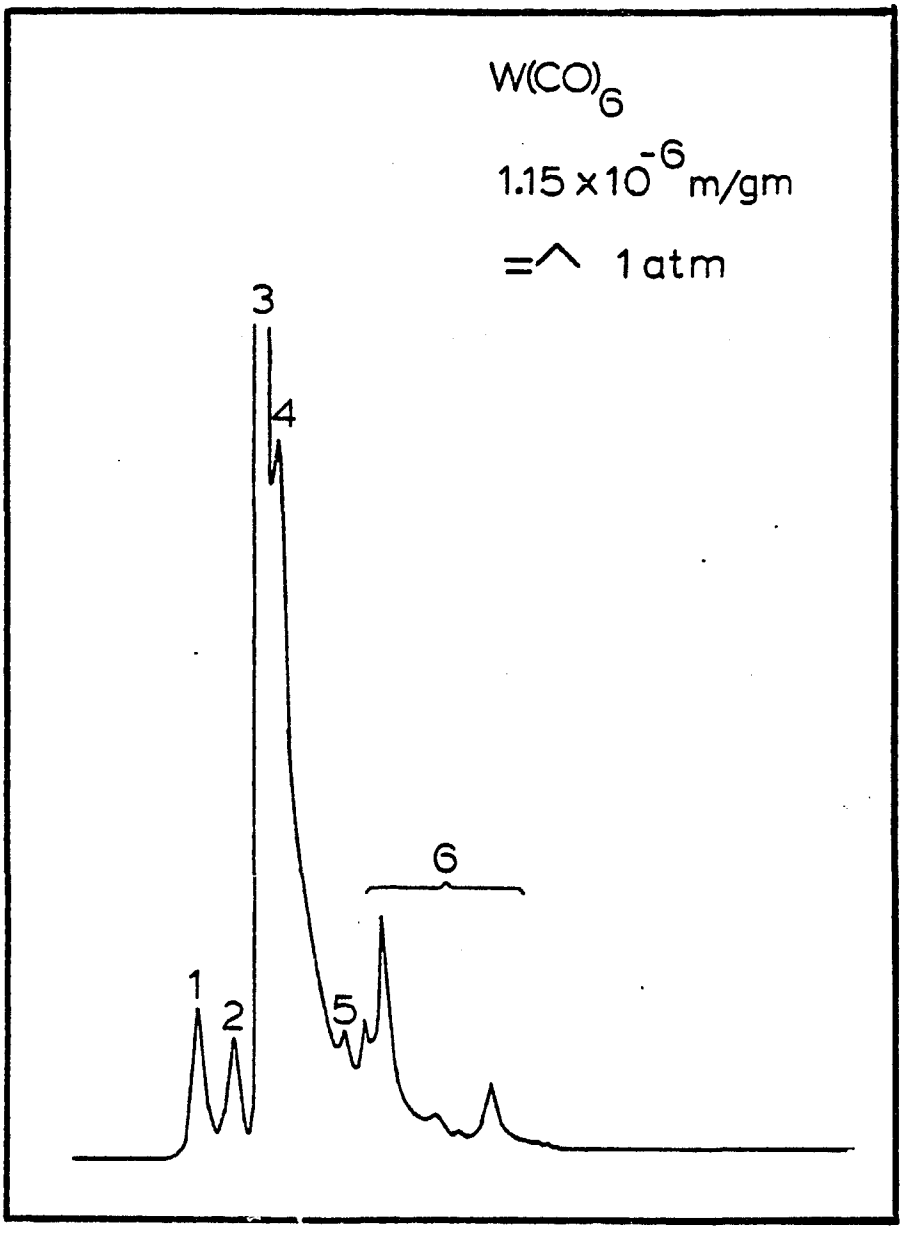

the ability of these hybrid systems, $M(CO)_6$ (M=Cr, Mo, and W)/PVG, to function as hydrogenation catalysts. A sample containing 2.39×10^{-5} moles of $W(CO)_{6ads}$ was photolyzed at 350-nm for 600 seconds resulting in the formation of 1.74×10^{-6} moles of $W(CO)_{5ads}$. The photoproduct was then exposed to 5.75×10^{-3} moles of 1,3 butadiene resulting in a spectral change from O.D.=0.505 to O.D.=0.255 at 410-nm. These spectral changes correspond to 56.5% reaction. The excess 1,3 butadiene was removed by vacuum and the sample rephotolyzed. The number of moles of photoreleased 1,3 butadiene was measured. However, no correlation was made between the observed spectral changes and the number of moles of photoreleased 1,3 butadiene. 1,3 Butadiene is strongly adsorbed, similar to what is observed for cis-2-butene, therefore it is difficult to remove by vaccum. However, this experiment did establish that 1,3 butadiene will react with $W(CO)_{5ads}$. However, it is uncertain whether 1,3 butadiene is behaving as a bidentate ligand.

The hybrid systems ability to function as a hydrogenation catalyst was also investigated. A sample containing $\sim 10^{-5}$ moles of $Cr(CO)_{6ads}$ was photolyzed with 350-nm light for 70.0 minutes in the presence of 3.01×10^{-3} moles of 1,3 butadiene and 2.94×10^{-3} moles of H_2. Gas chromatographic analysis of the vapor phase gave no indication of hydrogenated products such as cis-2-butene, 1-butene, and trans-2-butene. In another

experiment, a sample containing 5.5 x 10^{-5} moles of $Cr(CO)_6$ads was photolyzed for 126.0 minutes in the presence of 2.96 x 10^{-3} moles of H_2 and 3.05 x 10^{-3} moles of 1,3 butadiene. This experiment resulted in the formation of $\backsim 10^{-4}$ moles of cis-2-butene. The reaction mixture was thermolyzed, 22± 1.0°C, for 24 hours and the formation of trans-2-butene and 1-butene was observed as well as some unidentified higher molecular weight hydrocarbons (Figure 54). The ratio of 1,3 butadiene to cis-2-butene went up (4.1) indicating that cis-2-butene has undergone subsequent thermal reaction.

Various control experiments were conducted in order to ascertain if the hybrid catalyst is determining the formation of products in the various catalytic reactions. In one experiment, 3.05 x 10^{-3} moles of H_2 was combined with 2.97 x 10^{-3} moles of cis-2-butene in an empty cell. The cell was photolyzed, 350-nm, for 1.31 x 10^3 minutes, gas chromatographic analysis indicated that no reaction took place. Injections taken before and after photolysis were equal in intensity, indicating that the gas molecules were not being adsorbed by the cell. In another experiment, cis-2-butene, H_2, and $W(CO)_6$ads were thermolyzed, 22.0 ± 1.0°C, for 1.40 x 10^3 minutes, gas chromatographic analysis showed that no reaction took place. The system was then photolyzed for 1.09 x 10^3 seconds with the generation of 3.63 x 10^{-4} moles of trans-2-butene and 1.14 x 10^{-4} moles of 1-butene (Figure

Figure 54. $Cr(CO)_6$ photocatalyzed hydrogenation of 1,3 butadiene. Chromatogram is after 126.0 minutes photolysis and ∽24 hours thermolysis. Peak 1=trans-2-butene, peak 2=cis-2-butene, and peak 3=1,3 butadiene.

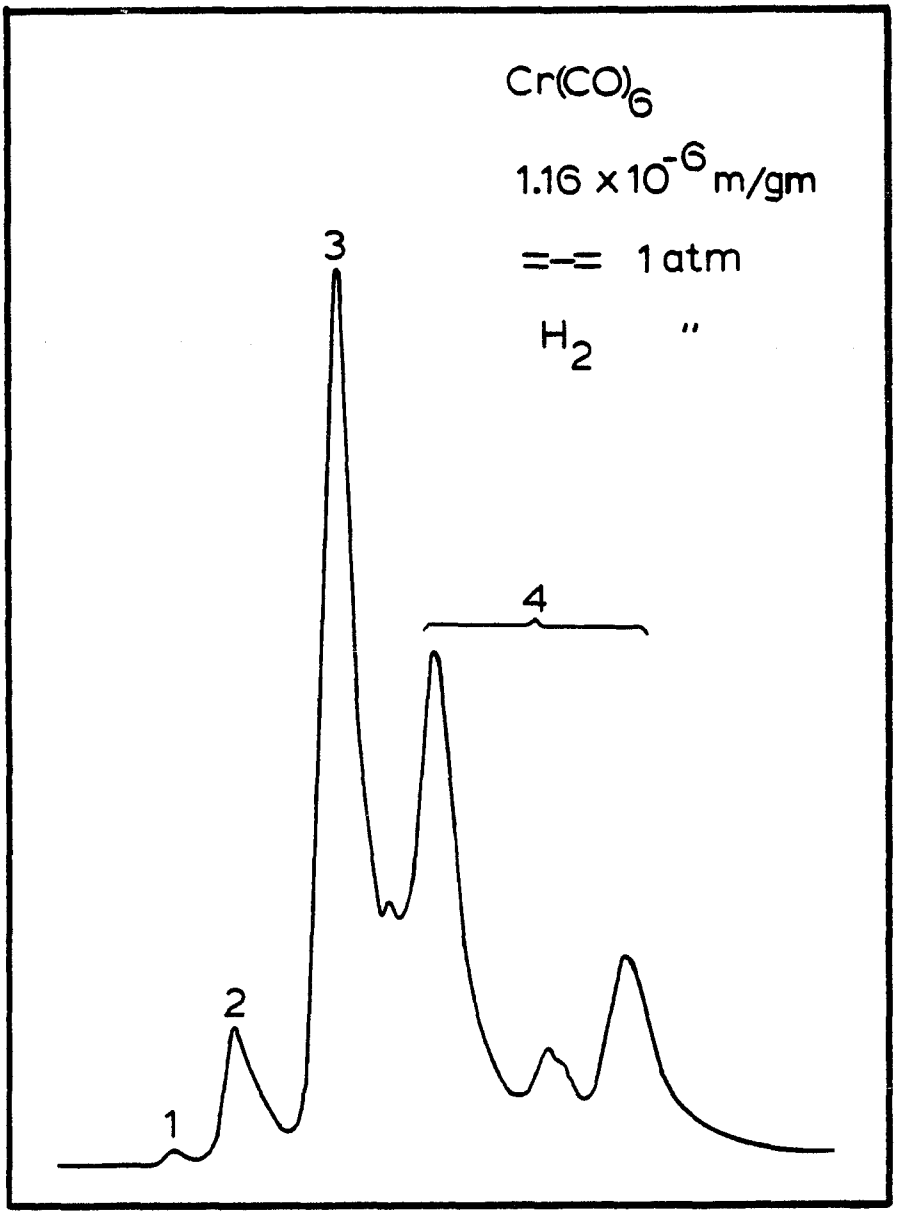

55). A blank (no $M(CO)_6$) sample of PVG was photolyzed at 350-nm for 1.21×10^3 minutes in the presence of 3.09×10^{-3} moles of H_2 and 2.91×10^{-3} moles of cis-2-butene. Gas chromatographic analysis indicated that no hydrogenation or isomerization occured.

Figure 55. Control experiment. Reactants were exposed to $W(CO)_6$ ads without photolysis. Then photolyzed for 1,087.0 minutes. Peak 1=1-butene, peak 2=trans-2-butene, and peak 3=cis-2-butene.

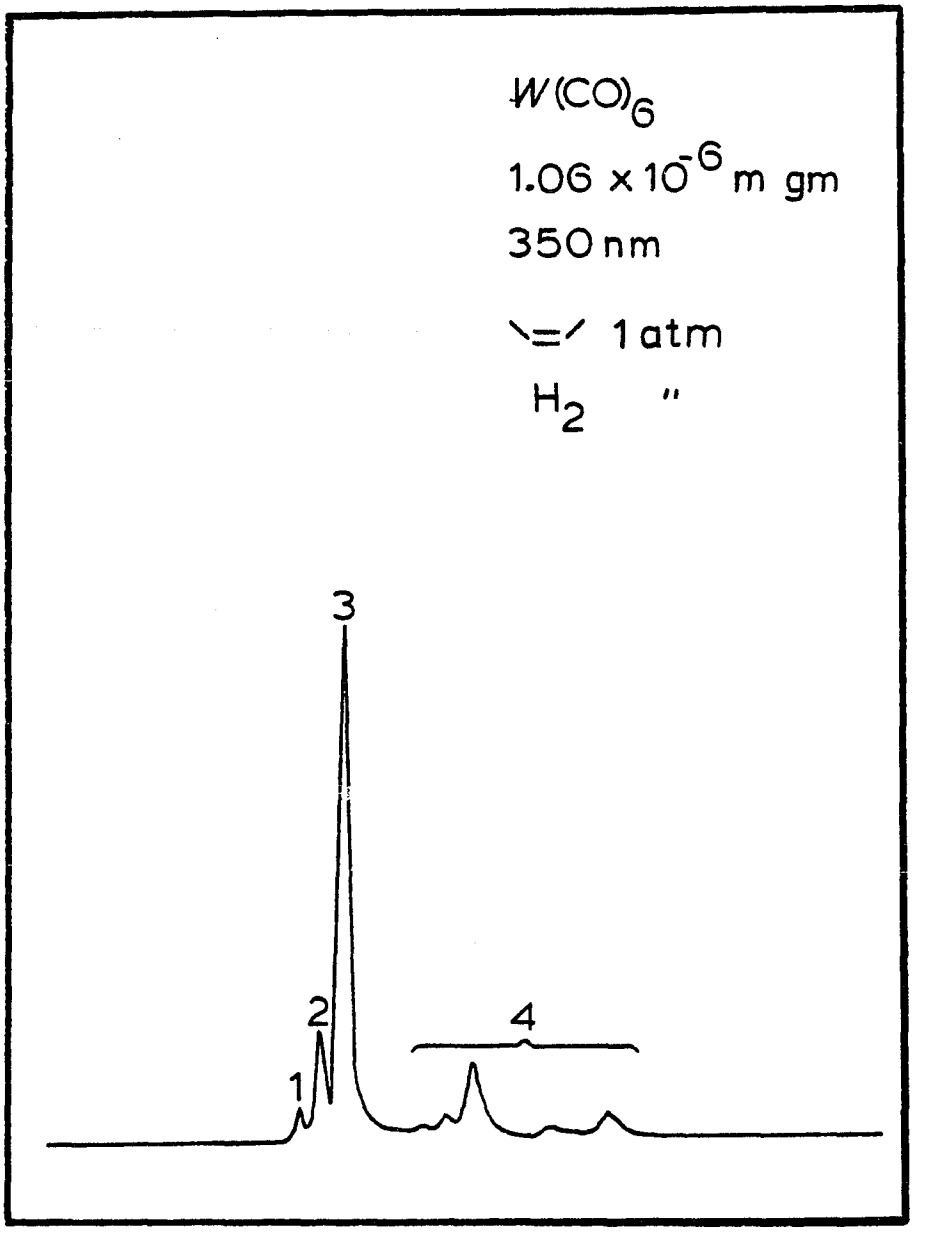

Chapter 4

Discussion

A. Physical Nature of Adsorbed Reagents.

In principle, chemical and physical adsorption are distinguishable. Physical adsorption, or physisorption, is attributed to forces of molecular interaction which involve permanent dipole, induced dipole, and quadrupole interactions (104). For this reason, it is frequently designated as van der Waals adsorption. Chemisorption, on the other hand, involves the rearrangement of the electrons between adsorbate and adsorbent, with consequential formation of chemical bonds. Experimentally, it is often difficult to distinguish between the two modes of adsorption. However, porous Vycor glass is amenable to various spectroscopic techniques and the data described below offer strong evidence that Group VIB hexacarbonyls are physisorbed.

1. Rate of Adsorption of $M(CO)_6$ onto PVG.

Previous studies in this laboratory have shown that $Ru(bpy)_3^{2+}$ is cationically bound to PVG via anionic silanol sites that are ubiquitous to PVG. Two changes in the rate of adsorption of this complex suggest that more than one type of hydroxyl group is involved. An initial rapid rate, $t<10$ minutes, appears to be an artifact of the time required to saturate the glass with the solution (105). Beyond this point, however, the rate of adsorption follows a dependence predicted by the Elovich equation, equation 17,

$$q = 1/\alpha \ln (t+t_o)/t_o \qquad (17)$$

where q is the amount adsorbed at time t, α is a constant for each system at a specified temperature. As indicated by Figure 24, the adsorption for $W(CO)_6$ follows a dependence consistent with the Elovich equation where the rate of adsorption is proportional to site availability. This suggests a competition for sites which eventually are occupied by $W(CO)_6$ and adsorption becomes independent of the concentration in the fluid phase. That is, the sites are eventually depleted, which is consistent with the observed leveling-off in the rate plot.

2. Adsorption isotherm for $W(CO)_6$.

The adsorption isotherm for $W(CO)_6$, Figure 23, establishes that a concentration gradient must be present in order for adsorption to take place. Because of the limited solubility of $W(CO)_6$ in n-hexane, however, saturation does not occur for the concentrations applied. Even though leveling-off behavior is not observed, the maximum fractional surface coverage, using the solution impregnation method, is 0.08. $Cr(CO)_6$ is slightly more soluble and therefore can be adsorbed to a greater extent, i.e., the maximum number of moles of tungsten or molybdenum hexacarbonyl that can be adsorbed is 4×10^{-5}. For chromium hexacarbonyl a maximum of 5.5×10^{-5} moles was observed, which corresponds to a fractional surface coverage of 0.09. Studies done by Jackson and Trusheim (53), in which vapor phase $Fe(CO)_5$ is adsorbed onto silica gel

established that greater than monolayer coverages could be achieved if a sufficient concentration of adsorbate could be delivered. These data, in addition to the absence of leveling-off behavior illustrated in the $W(CO)_6$ isotherm, suggest that monolayer coverages are possible for $M(CO)_6$.

3. The Distribution of $W(CO)_6$.

The distribution of $W(CO)_6$ on PVG was determined from the measurement of absorption at different points to show uniform surface distribution. Figure 18 illustrates the cross-sectional distribution of $W(CO)_{6ads}$ determined by the grinding technique described previously. The linearity of the optical density versus relative thickness indicates that the distribution is uniform throughout the regions adjacent to each surface. This study was undertaken in order to calculate the effective penetration depth of the complex. This data must be known for extinction coefficients in the glass to be calculated. Interestingly, the same penetration depth is obtained as the ruthenium tris(bipyridine) cation. Since the same depth is found with two very dissimilar complexes, which are adsorbed by different mechanisms, perhaps this depth is an indication of surface deviations rather than penetration into pores.

4. Spectroscopy of Adsorbed Reagents.

Examination of the FTIR-PAS and UV spectra of $M(CO)_{6ads}$ establishes that these complexes are physically adsorbed and the primary coordination sphere of

the complex is not disrupted. The Raman spectrum of $Mo(CO)_6$ adsorbed to porous Vycor glass has been obtained (25) and the spectrum resembles the solution spectrum of this complex, and is notably different from that of the crystalline solid (106). The higher frequency ν(CO) band (A_g in the O_h point group) is at a position (2117 cm^{-1}) intermediate between those of the solid (2112 cm^{-1}) and the vapor (2124 cm^{-1}) and comparable to a solution in a solvent of high dielectric constant, such as CH_2Cl_2. We have observed similar behavior in the photoacoustic infrared spectra of $M(CO)_6$ (M=Cr, Mo, and W) (Table 4). The data indicate that the ν(CO) stretching frequency is shifted to higher energy suggesting that PVG accepts electron density from the pi* orbital on CO, which is partially filled by backbonding from metal. This would increase the net bonding and therefore ν(CO). This explanation offers a rationale for the ease of labilization of the carbonyl ligand that is observed in the photochemical experiments.

It is known (74) that the MLCT band of $M(CO)_6$ exhibits a small solvent dependence, with the more polar solvents resulting in a higher MLCT transition energy. The solvent effect is presumably due to the change in the relative position of the metal t_{2g} and the ligand pi* orbitals. A more polar solvent lowers the energy level of the t_{2g} set, thus increasing the energy required for the metal to to ligand charge transfer. We

observed a 4-nm blue shift in the MLCT band of adsorbed $M(CO)_6$, relative to that for the n-hexane solution. This shift is consistent with the more polar environment inherent in PVG. These findings are exemplified by the slight deviations of observed extinction coefficients (Figure 19) for the adsorbed complex and the complex in n-hexane. The extinction coefficient of a given material reflects its ability to absorb light. Empirically, a relationship between refractive index of a medium and the ability of a complex to absorb light, reflected in its extinction coefficient, has been investigated. Figure 56 shows an increase in extinction coefficient with increasing refractive indices. The value predicted for PVG , which has a refractive index of 1.5 (43-52), and on the basis of this plot, is similar to the observed value of $1.52 \times 10^4 \pm 0.07$. This excellent agreement further substantiates the method used in calculating extinction coefficients on PVG.

The MLCT band associated with $M(CO)_4L$ (L=bpy, o-phen) exhibits a considerable solvent dependence. For example, when $W(CO)_4(bpy)$ is dissolved in isooctane the observed maximum is 580-nm and when dissoloved in methanol a maximum of 474-nm is observed. $W(CO)_4(bpy)ads$ displays an absorption maximum at 490-nm suggesting that the polarizability of PVG lies somewhere between isooctane and methanol. When $W(CO)_4(bpy)$ is dissolved in methylene chloride a band maximum of 487-nm is

Figure 56. A correlation plot of refractive indices and extinction coefficients for $W(CO)_6$ dissolved in various solvents and adsorbed to PVG.

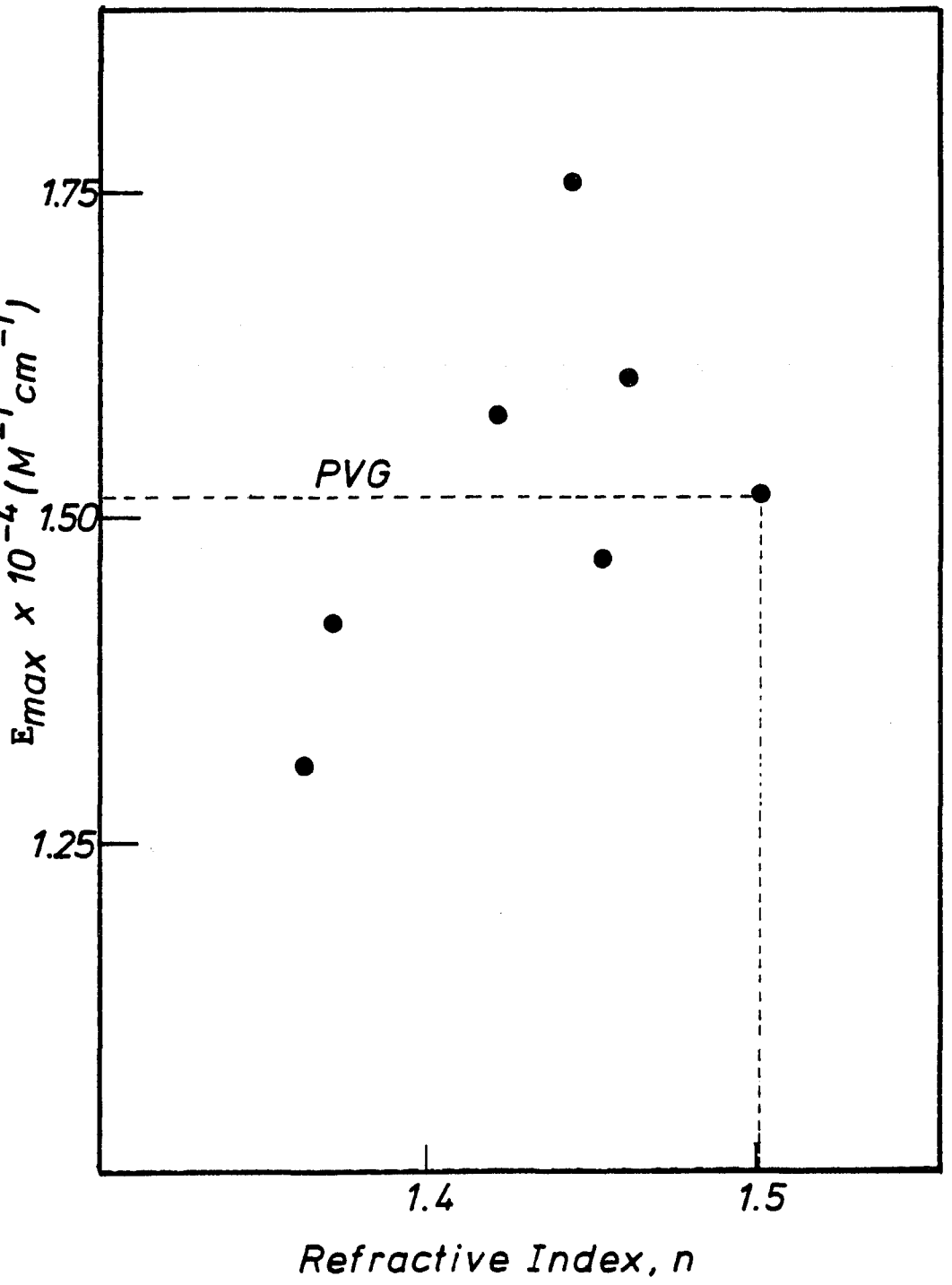

EtOH 1.3611, $CHCl_3$ 1.45, CH_2Cl_2 1.42, n-hexane 1.38, CH_3CN 1.43, CCl_4 1.46, and PVG 1.51.

observed suggesting that the polarity of this medium is very similar to PVG. $W(CO)_4$(o-phen)ads exhibits a 567-nm absorption maximum which is similar to the maximum found in cyclohexane, 570-nm. In general, the absolute polarity of PVG is not known, however, the similarity between the MLCT bands of the adsorbed complexes with those in CH_2Cl_2 or cyclohexane suggest a polarity that is similar to that found in these solvents. Moreover, the emission data for these complexes (Table 6) further substantiate this claim. The emission maximum follows a dependence on solvent polarity similar to that found for the absorption maximum. For example, when $W(CO)_4$(bpy) is dissolved in methanol the emission maximum is 563-nm, but when adsorbed onto PVG, the emission maximum is at 683-nm. This red shift is consistent with the observed red shift in the absorption maxima of the complex dissolved in methanol (474 nm) and the complex adsorbed to PVG (490nm).

The $M(CO)_5$Lads complexes (L=NH_3, py) exhibit similar maxima to these complexes dissolved in acetonitrile (Table 6). However, this transition is assigned as an $^1A_1 \longrightarrow {}^1E$ ligand field transition that does not exhibit a solvent dependence, i.e., the same band maxima are observed regardless of the polarity of the solvent.

The data gathered through these studies of adsorption, distribution, and spectra of the adsorbed complexes establish that the adsorption of $M(CO)_6$, $M(CO)_5L$, and $M(CO)_4L$ does not disrupt the primary coordination

sphere. However, the relative energy of the absorption and emission maxima suggests that the environment of PVG is analogous to media of high polarity and high dielectric constant. Even though the complexes are physisorbed there is considerable interaction between surface hydroxyls or adsorbed water in the secondary coordination sphere of the adsorbed complexes.

The density of accessible surface hydroxyls available on PVG fall within the realm of values obtained for other silica supports. These values lie between 1.4 ± 0.1 (108) to ca. 4-6 hydroxyls/100Å^2 (109,110). Taking 3 Å (100a,b) as a representative radius of $W(CO)_6$, $Mo(CO)_6$, and $Cr(CO)_6$, the total planar area of the molecule is 27 Å^2. This suggests that possibly 1-2 hydroxyl groups, in addition to physisorbed water, are within the secondary coordination sphere.

B. The Photochemistry of $M(CO)_6$ Adsorbed to PVG.

The primary photoprocess that occurs upon photolysis (λ_{ex} <350-nm) of $M(CO)_6$ads is the generation of the coordinately unsaturated intermediate, $M(CO)_5$ads. The spectral changes associated with the photolysis of $W(CO)_6$ads, illustrated in Figure 25, are consistent with the formation of $W(CO)_5$ads. The relative energy of the band maxima for $M(CO)_5$ads is a highly sensitive indicator of the extent of interaction between the pentacarbonyl and the medium. Studies by Perutz and Turner (70,71) of the photochemical generation of $M(CO)_5$ in low

temperature (<20°K) rare gas matrices have established that the matrix species occupies the vacant site and the extent of interaction is dependent on the matrix material chosen. The fact that the absorption maxima for $W(CO)_5(Et_2O)$, $W(CO)_5$(acetone), and $W(CO)_5$(EtOH) agree remarkably well with the band maximum obtained for $W(CO)_5$ads suggests that the formal coordination is via an oxygen atom. The structure of PVG, Figure 57, particularly the availability of anionic silanol groups or adsorbed water, and the relative position of the band maximum suggest that the vacant coordination site is either occupied by water or by a silanol group. These spectral similarities imply that PVG is not acting as an inert support during the photolysis of $M(CO)_6$ads. This is reasonable, since silica surface hydroxyl groups and siloxane bridging oxygen atoms should be good electron donors capable of acting as ligands toward W. The interaction of $M(CO)_5$ads is relatively weak, since, neither the surface hydroxyl groups nor the siloxane bridging oxygen atoms can stabilize the metal-ligand bond by accepting electrons back into the pi system. However, $W(CO)_5$ads does have a spectrally quantitated lifetime of > 48 hours, in vacuo, suggesting some stabilizing effect is occurring from the SiOH group. $M(CO)_5$ads might thus be modeled reasonably well by $M(CO)_{5(THF)}$ (THF=tetrahydrofuran), which is reactive toward thermal substitution. Jackson and Trusheim (53) have observed the

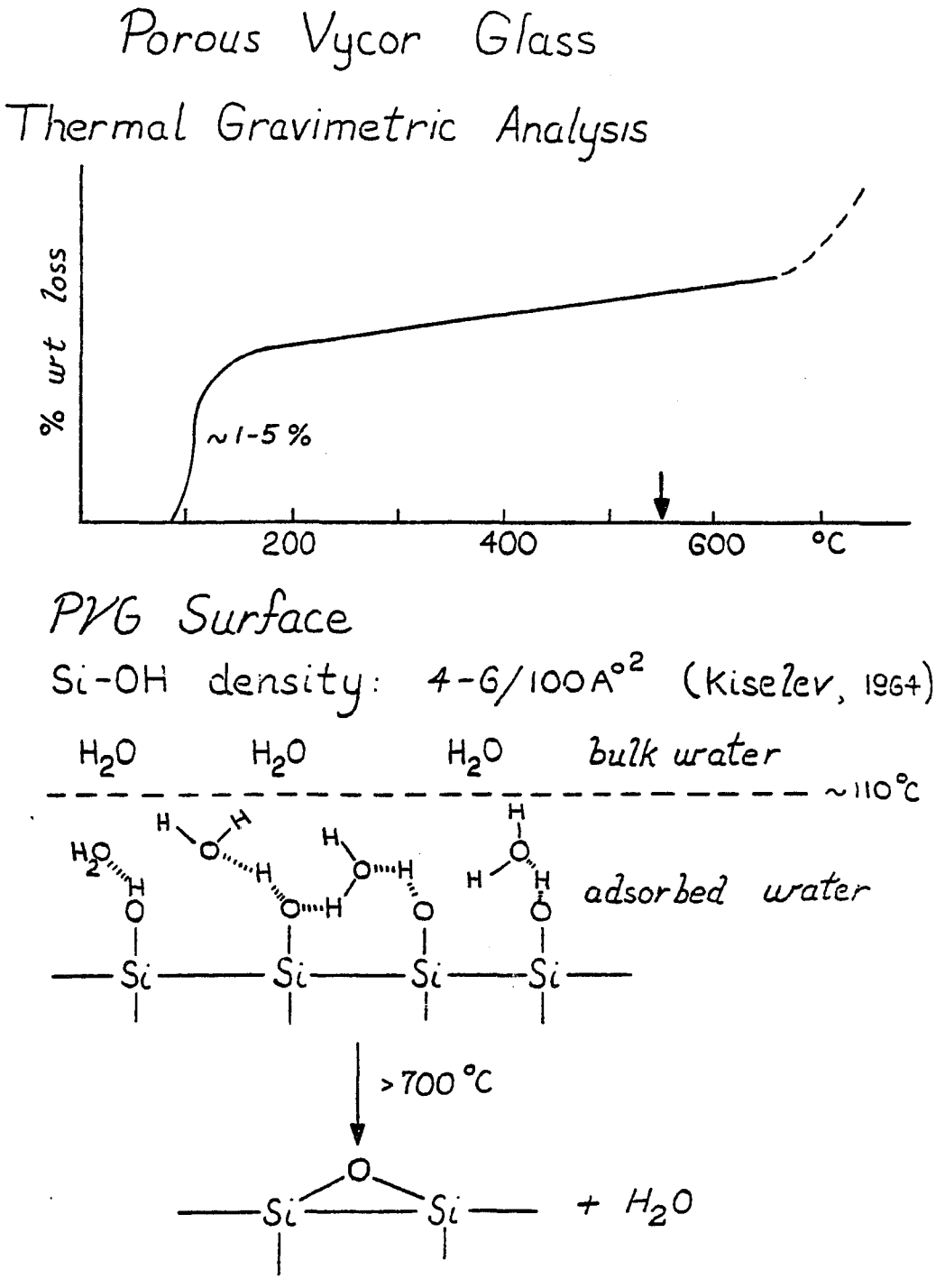

Figure 57. Figure distinguishes between the two types of H_2O present on PVG; physisorbed H_2O and chemisorbed H_2O.

vibrational spectrum of $Fe(CO)_4$ads at low surface coverages at 100°K, and have suggested that the observed shifts in the vibrational spectrum are similar to those observed for $Fe(CO)_4$(THF).

Further characterization of the $M(CO)_5$ads intermediate was accomplished by the addition of various mono-and bidentate ligands either as thoroughly degassed neat ligands or in the vapor phase. The formation of $M(CO)_5$(py)ads has been spectrally identified. Resonance Raman spectra, Figure 34, show that the 992 cm^{-1} and 1035 cm^{-1} vibrations of, py, adsorbed onto PVG shift to 1012 cm^{-1} and 1042 cm^{-1}, respectively, when pyridine vapor reacts with $W(CO)_5$ads (111). The resonance enhanced Raman effect only displays modes of vibration coupled with the electronic transition of the chromophore. In this experiment, a 457.9 nm laser line was used to excite in the ligand field region of $W(CO)_5$(py)ads. The attainment of selective modes of vibration at such low concentrations (< 10^{-5}moles) establishes that pyridine is coordinated to the metal.

The addition of bipyridine to $M(CO)_5$ads is somewhat puzzling in that it is a bidentate ligand while only one coordination site is available at the metal center. It is noteworthy that Atwood and Brown have shown that various ligands can induce a cis-labilizing effect on the dissociation of CO ligands from hexacarbonyls (112). The cis-labilizing effect spans about 8 orders of magnitude and

the ordering of ligands is the reverse of that found for the trans effect in the substitution of Pt(II) complexes. Thus the inclusion of silanol groups or physisorbed H_2O into the coordination sphere may partly explain the facile bond cleavage of the second CO necessary for the bidentate ligand to coordinate. The kinetics of this reaction, which are displayed in Figure 36, are consistent with a pseudo first-order reaction with a calculated rate constant of 5.55 x 10^{-4} sec^{-1} at 22.0 $\pm$ 1.0°C.

Many other ligands were complexed to $M(CO)_5$ads. They are listed in Table 6.

Emission spectroscopy was used to further characterize $M(CO)_5$ads, $M(CO)_5$Lads and $M(CO)_4$Lads. The room temperature emission spectrum of $W(CO)_5$ads has a maximum at 510-nm, which is considerably blue shifted, 23-nm, relative to the maximum obtained in a methylcyclohexane glass at 77°K (65,66). However, this observed blue shift in the emission maximum is consistent with the observed blue shift, in the absorption spectrum, 32 nm.

The emission spectra obtained for $M(CO)_5$(py)ads and $M(CO)_4$Lads (L= bpy, o-phen) are consistent with literature values (Table 6). The emission bands for $M(CO)_4$L (L=bpy, o-phen) are assigned as MLCT transitions and exhibit a solvent dependence comparable to what is observed for absorption.

In general, the emission maxima for all complexes discussed resemble those obtained at 77°K in EPA glasses

and those of the solid at 298 ^{o}K. It is noteworthy that the emission of many of these complexes are not detectable at room temperature in fluid solution, further suggesting a strong interaction with the solvent. The emission results offer support for the use of PVG as a room temperature matrix isolation technique.

Strohmeier and Gerlach (113) have reported that the quantum yield of decomposition of $M(CO)_6$ (M=Cr, Mo, and W) is 0.39 $\pm$ 0.03 at an excitation wavelength of 366 nm. The values obtained for the adsorbed complexes are listed in Table 5. As can be seen from Table 5, the quantum yields appear to be dependent on the excitation wavelength as well as which metals are photolyzed. Gas phase as well as spectral analysis establish that $M(CO)_{5ads}$ is being generated. The spectrally determined thermal back-reaction observed for Cr explains the low quantum yields observed relative to Mo and W (Table 5). The discrepancies between the quantum yield of formation and decomposition can be attributed to a thermal back-reaction. All quantum yields were obtained at low surface coverages, f_s= 0.005, so that the decomposition of $M(CO)_6$ could be readily detected. Spectral evidence indicates that for all metals, particularly Cr, a thermal back reaction occurs.

Nasielski and Colas have reported (114) that the quantum yield of photosubstitution of CO by pyridine (py) in $Cr(CO)_6$ is 0.67 $\pm$ 0.2 rather than 1.0. These results suggest that other deactivation pathways, e.g., radiative

deactivation, may also be present. However, the absence of unitary quantum efficiencies for the photolysis of $M(CO)_6ads$ suggests that other deactivation processes occur. Although emission was not observed for $M(CO)_6ads$ (M=Cr, Mo, and W), emission for these complexes have been reported in low temperature matrices (12°K) (75). Therefore, emission cannot be ruled out as a possible deactivation pathway and our failure to detect it may be due either to quenching by the PVG support or to inadequate sensitivity of the instrument used (see experimental section).

C. Kinetics of Gas Phase Reactions Between $W(CO)_5ads$ and Various Ligands.

Although stabilization of the $M(CO)_5ads$ photoproduct offers a means for spectroscopic examination, stability at the expense of subsequent reactivity is of little use from a catalytic point of view. To determine the lability of the $M(CO)_5ads$ photoproduct, the reactions with various gaseous ligands was examined. The kinetic parameters calculated are illustrated in Table 7. Since $W(CO)_5ads$ is anchored to the support we claim that only molecules that are in adsorption equilibrium with the surface of the PVG will react. The equilibrium concentration of molecules can be derived from their respective adsorption isotherm for a given applied pressure at a specific temperature.

1. Adsorption Isotherms.

The adsorption isotherm derived for CO exhibits Langmuir behavior (Figure 22) for the various temperatures examined. For example, the isotherm can be derived from equation 18.

$$v = v_m bp/(1+bp) \qquad (18)$$

Where v_m is the maximum rate of adsorption or cc/STP/g adsorbed at monolayer coverage, b is the ratio of the rates of adsorption, k_2, relative to desorption, k_1, and P is the applied pressure.

The isotherms derived for cis- and trans-2-butene do not exhibit Langmuir behavior, however. These isotherms reflect what Brunhauer (116) refers to as Type II behavior. This behavior is very common in the case of physical adsorption and may correspond to multilayer adsorption.

2. Rate Constants and Thermodynamic Parameters.

The calculated rate constants for the reaction of $W(CO)_5$ads + Lads were derived from plots similar to Figure 51. Second order rate constants were calculated from equation 19.

$$k_{app} = k_{true} \text{ (moles of ligand adsorbed)} \qquad (19)$$

The calculated rate constants, k_{true}, determined at various temperatures, were plotted as a function of temperature (Figure 52), and the Eyring activation parameters (Table 7) determined from the slopes.

The simplest explanation of our kinetic results appears to be the following. Assuming that the observable reactant, our stable intermediate, to be $W(CO)_5$ads, we have the following sequence.

$$W(CO)_6ads \longrightarrow W(CO)_5ads + CO \qquad (20)$$

$$W(CO)_5ads + Lads \longrightarrow W(CO)_5Lads \qquad (21)$$

It is apparent that because these reactions do not occur spontanenously, i.e., all reactions studied possess a reasonably moderate activation energy, the primary step in the mechanism is overcoming the inherent interaction between $W(CO)_5ads$ and the support.

The second important requirement of the mechanism is that the ligand must be accessible to $W(CO)_5ads$ which infers that the ligand must possess the proper steric requirements.

The values obtained for the entropy of activation establish that the reaction is not entropy controlled, i.e., the most favorable entropy of activation is associated with the highest enthalpy of activation (cis-2-butene).

Adamson and coworkers have reported (117) that the bond energy for W-S, where S=solvent, has an upper limit of 3.9 kcal/mole, using the photochemical reaction of $W(CO)_6$ with 4-acetylpyridine in methylcyclohexane. An absorption maximum of 425-nm is obtained for the transient, $W(CO)_5S$. This suggests that the matrix interaction energy of $W(CO)_5ads$ should indeed be greater as a consequence of the relatively higher energy of the ligand field band, and is consistent with the higher activation energies obtained for the heterogeneous reaction. It has also been observed that the cis isomer reacts faster than the trans isomer. This may be explained in terms of a

steric influence favoring the cis-2-butene molecule which would be more readily accomodated on the support surface (28). Moreover, the slowest rate of reaction was observed for 1-pentene due to the diffusional constraints placed on this reaction, i.e., even though the reaction was examined in the vapor phase, solvent molecules were present.

D. Methane Forming Reaction.

Periodic examination of the gaseous effluent during photolysis of $M(CO)_6ads$ at excitation wavelengths less than 310-nm results in the generation of H_2, CH_4, CO_2, and CO. The rate of evolution of these gases is dependent upon excitation wavelength and on which complex is being photolyzed. Plots of the total moles of gas evolved versus photolysis time for excitation wavelengths 310- and 254-nm are illustrated in Figures 44 and 45, respectively. 254-nm photolysis of each of the three complexes can be examined in Figures 45, 58, and 59. Interestingly, the evolution of CH_4 was not observed at 350nm, presumably due to the inability of $M(CO)_5ads$ to form lower subcarbonyls at that excitation wavelength. Moreover, the average stoichiometry of the intermediate at the onset of CH_4 evolution is determined to be $M(CO)_4ads$ (Chapter 3). The low quantum yield of CH_4 formation during $Cr(CO)_6ads$ photolysis (λ_{ex}=254-nm), relative to Mo and W, is consistent with the low quantum yield observed for the formation of $Cr(CO)_5ads$. This is established by Figure 58 which shows that CO evolution, for

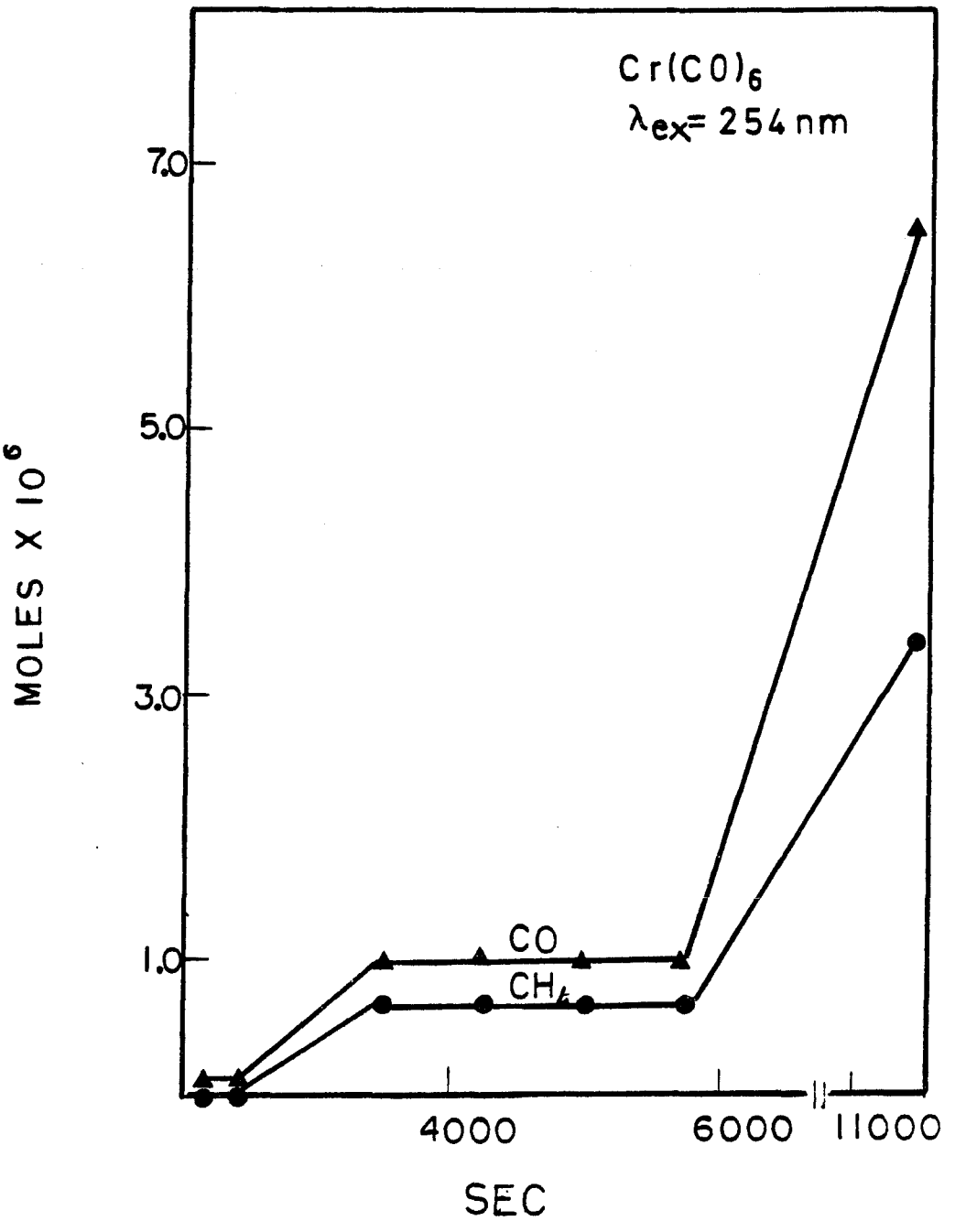

Figure 58. Photolysis of $Cr(CO)_6$ads at 254 nm. The sample was calcined (600°C) in air prior to adsorption of 1.25×10^{-5} moles of $Cr(CO)_6$.

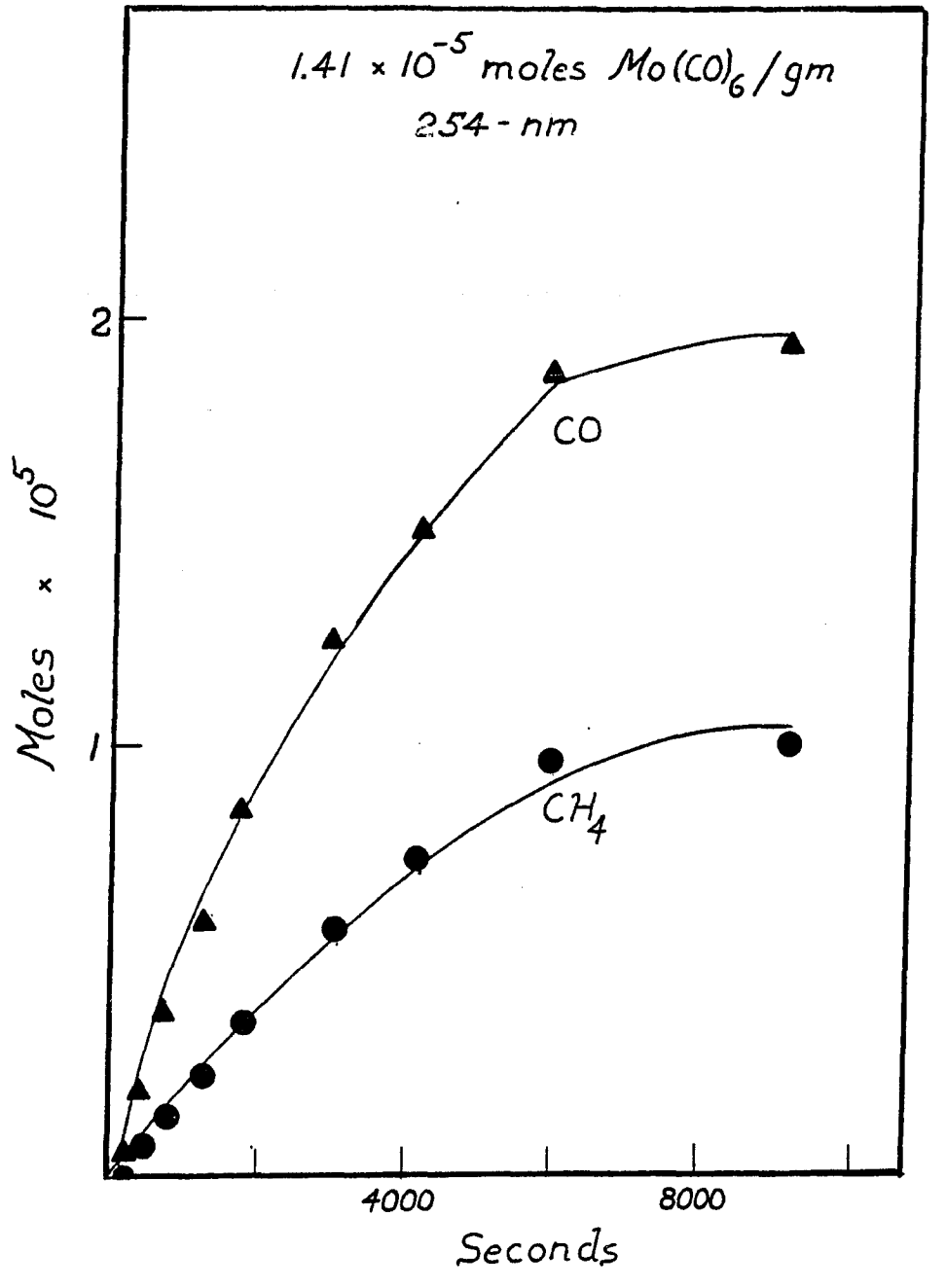

Figure 59. 254-nm photolysis of $Mo(CO)_6$ads.

the Cr complex, is less efficient than for the W or Mo analogues. However, when $Cr(CO)_{6ads}$ is photolyzed for extended periods of time, the quantum yield of CH_4 formation begins to parallel what is observed for Mo and W. An alternative explanation would be that the driving force in the methanation is the oxidation of the metal (vide supra) which provides the necessary equivalents of reduced protons. Since the oxidation potential of chromium is known (100c) to be higher than Mo and W, it is much more difficult for chromium to provide the necessary reducing potential.

As previously mentioned (Chapter 3) the carbon source for methane formation is derived from an impurity that is present on PVG. This was established by mass spectroscopic examination of the effluent following photolysis of $W(^{13}CO)_{6ads}$. The impurity may be a partially reduced carbonate, H_2CO_3 or HCO_3^-. This is reasonable because the only observed products, other than CO and H_2, are CH_4 and CO_2. Moreover, eleborate calorimetric experiments by Stone and co-workers showed that when CO_2 is adsorbed at a surface oxygen site, with a cuprous oxide support, the formation of $CO_{3ads}^{=}$ is thermodynamically favored (118-120). However, PVG is not a p-type semiconductor surface so if this reaction were to occur the carbonate species would have to be partially reduced, and would most likely be incorporated into the silica network as illustrated in equation 22.

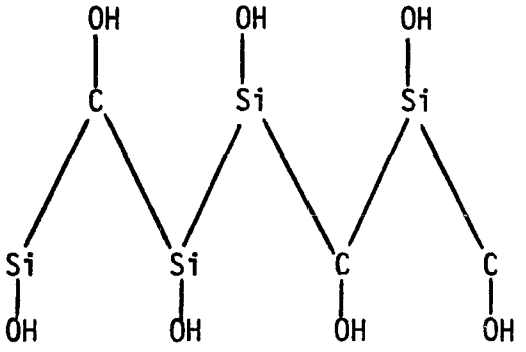

(22)

The ultimate source of hydrogen for the methanation is the adsorbed water present on PVG, either as physisorbed or chemisorbed water. This was established by treating the glass with D_2O prior to adsorption of $W(CO)_6$ followed by subsequent photolysis (λ_{ex} = 254nm). Mass spectral examination of the effluent illustrated that CD_3H and CD_2H_2 are generated. Brenner and coworkers (12) have suggested that the following reaction occurs,

$$M(CO)_6 ads + n(\sigma\text{-}OH) \xrightarrow{\Delta} (\sigma\text{-}O^-)M^{n+} + n/2\ H_2 + 6\ CO. \quad (23)$$

The evolution of hydrogen is highly dependent on the pretreatment of PVG which dictates the degree of hydroxylation and the amount of adsorbed water present. Glasses that are heated prior to adsorption have a higher degree of dehydroxylation, as well as less adsorbed water, than those exposed to the adsorbate without prior heat treatment (36). Experimentally, this has been established by heating a glass to 600°C, cooling in vacuo, and then exposing it to an n-hexane solution of $W(CO)_6$. Analysis

of the effluent after photolysis (Figure 46) afforded a rate of hydrogen evolution substantially less than that for a sample not heated prior to impregnation with $W(CO)_6$. An intermediate rate of hydrogen evolution was accomplished by pretreating the glass in a hydrogen atmosphere at 600°C. That the degree of oxidized metal can be controlled, is consistent with this model for hydrogen evolution, i.e., fully hydroxylated supports favor metal oxidation while fully dehydroxylated supports retard metal oxidation thus leading to the formation of dispersed, supported metallic particles (34,36). Thus, it is clear that the degree of hydroxylation strongly affects the rate and total amount of hydrogen evolved. Moreover, the total number of moles of methane evolved is highly dependent on the degree of hydroxylation. For example, the fully hydroxylated sample afforded a methane/W ratio = 11.39, and the partially dehydroxylated (Figure 60) (heated prior to impregnation) sample afforded a ratio of 5.94. This suggests that a sufficient amount of hydrogen must be present for the reduction to occur.

Until now it has been inferred that metal oxidation is a necessary prerequisite for methanation to occur. In order to explore this statement in a more direct manner, the following experiment was examined. At the onset of methane evolution, $W(CO)_n$ads ($n<4$), was exposed to 1-atm of CO in order to determine the extent of metal oxidation, and then rephotolyzed and the procedure repeated. The

Figure 60. Exhaustive photolysis of sample that was calcined (600°C) in air for > 72 hours prior to impregnation of $W(CO)_6$. (■) CO, (▲) CH_4, and (●) H_2.

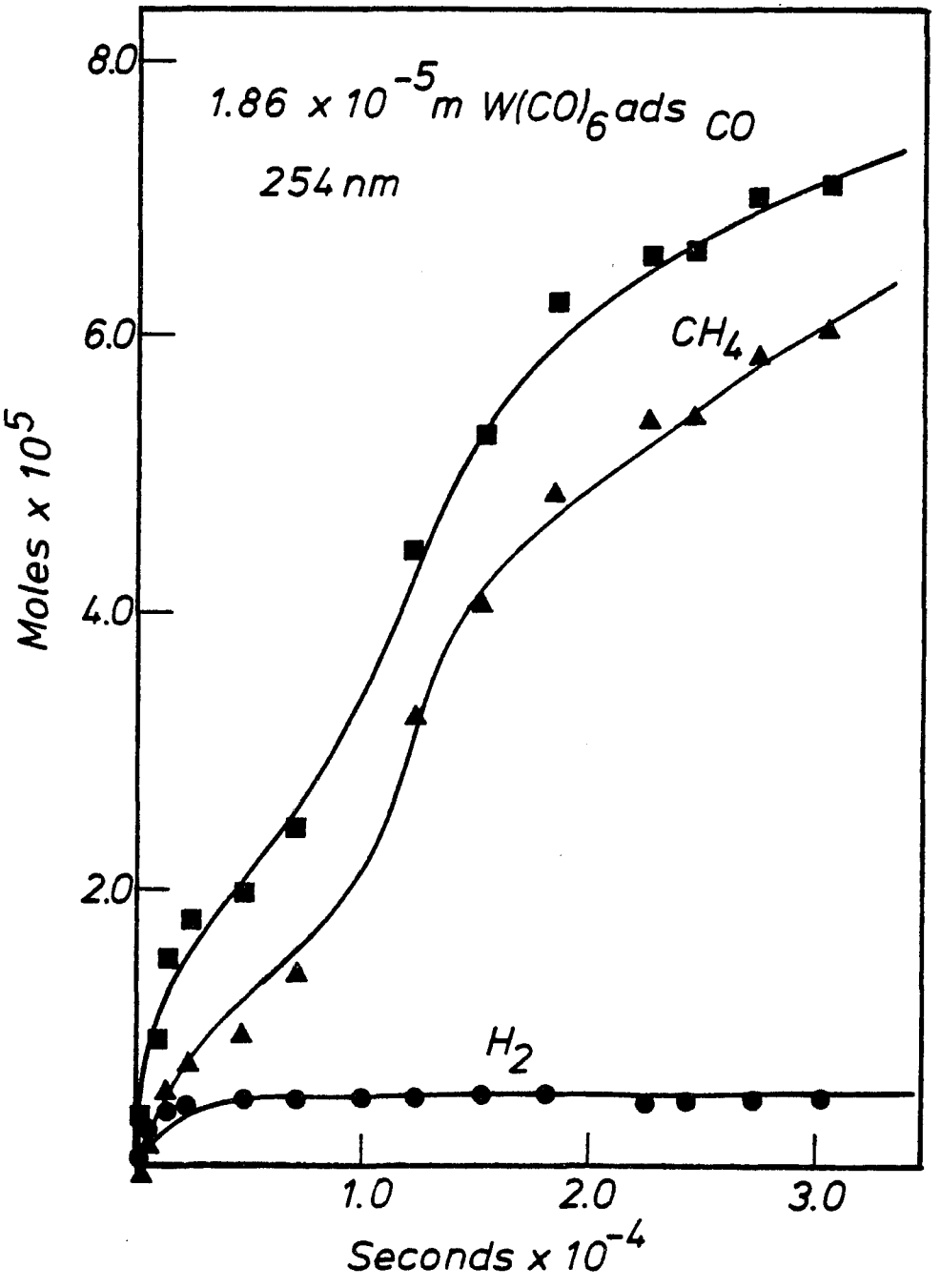

results have established that CH_4 formation is concurrent with an irreversible oxidation of the adsorbed complex. Figure 61 shows that the amount of complex oxidized, i.e., the original number of moles of $W(CO)_{6ads}$ less that regenerated on exposing the photolyzed sample to 1-atm of CO, is initially in a 1:1 stoichiometry with the moles of CH_4 evolved, and suggests that an intermediate metal oxide, perhaps a partially oxidized metal atom, is a relatively efficient mediator for the methanation. Chatt and coworkers (121) have suggested that the necessary equivalents for CO reduction may be supplied by a mononuclear complex of a metal such as Mo or W which can easily reach a high oxidation state.

EPR experiments were examined in order to characterize the metal oxide. Exhaustive photolysis of $Mo(CO)_{6ads}$, and subsequent EPR analysis of the crushed sample afforded a signal that was characteristic of Mo(V). The asymmetric signal (Figure 47) is characteristic of a species in an axially symmetric environment. An axially symmetric environment for molybdenum (V) can be achieved through surface configurations based on either tetrahedral or octahedral coordination. Exposure of this species to air for 24 hours destroyed the EPR signal along with a concurrent color change from light blue (characteristic of the hydrous oxide, $MoO_2(OH)$ to transparency (this is assumed to be MoO_3). No EPR signal was observed for

Figure 61. Plot of the correlation between the number of moles of $W(CO)_6$ads oxidized and the number of moles of CH_4 evolved. The sample was calcined (600°C) in air prior to adsorption of 4.0×10^{-6} moles of $W(CO)_6$.

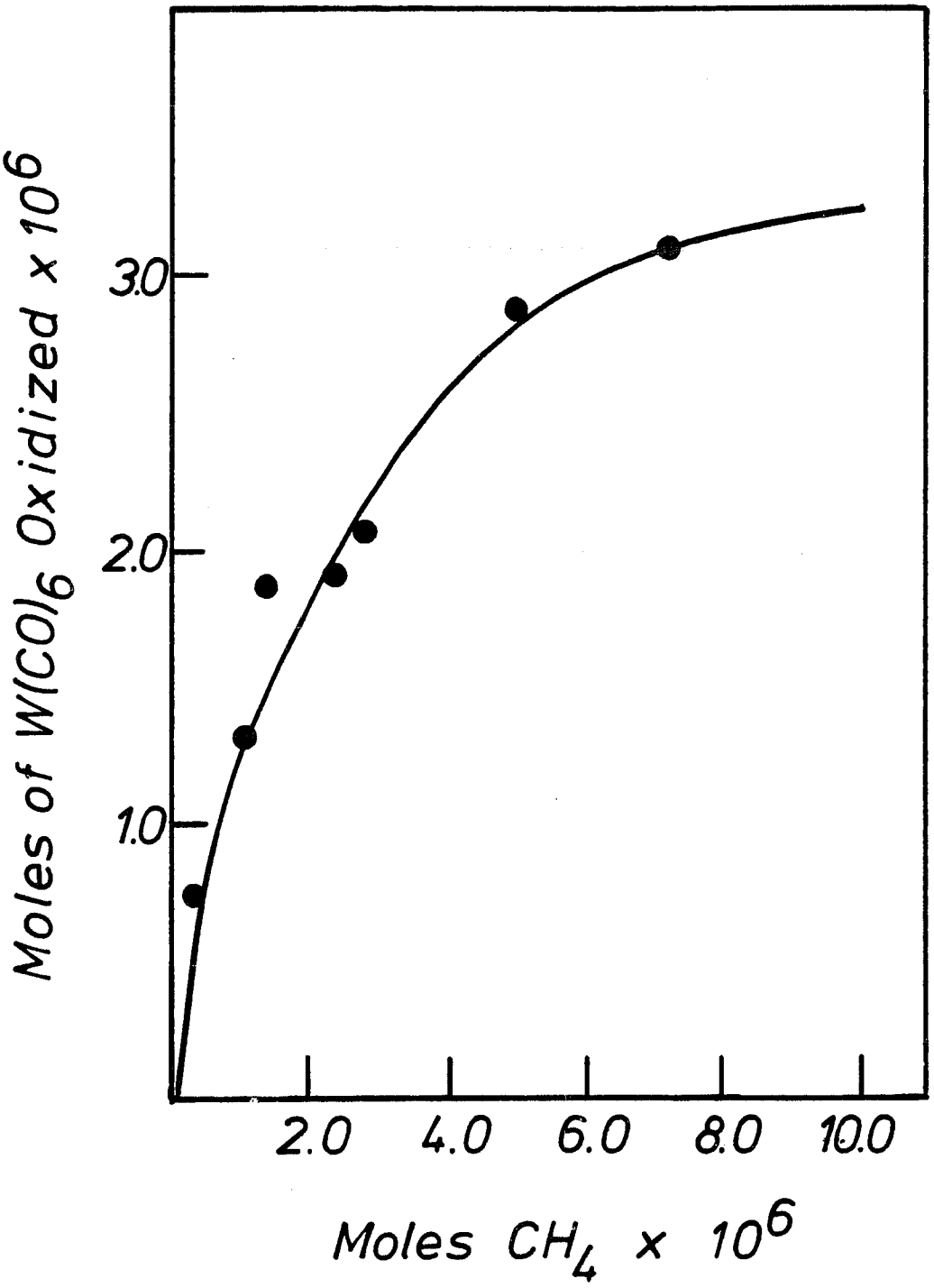

chromium or tungsten during any point of photolysis even though during the photolysis of $W(CO)_6$, on fully hydroxylated PVG a blue color was observed, characteristic of $WO_2(OH)$ or "Tungsten Blue."

Similar results were obtained by Howe and Leith, on silica and γ-alumina supports (21), however, they did not offer an explanation why Cr and W did not exhibit EPR activity.

Figure 45 illustrates the exhaustive photolysis of $W(CO)_6$ads. At an average stoichiometry $W(CO)_2$ads, methane formation begins to exceed CO evolution. This further validates the suggestion that a partially oxidized tungsten species is mediating the methanation because at this point the evolution of hydrogen begins to taper off.

An upper limit of methane formation can be calculated. Elemental analysis of PVG discloses that there is 0.72% of an incorporated carbon oxide species present. Typically, 2.5 grams of PVG are used in a particular experiment setting a maximum amount of methane formation to be 10^{-3} moles, well beyond what is observed (10^{-4} moles).

Another interesting feature in the overall mechanism of this reaction is that in order to account for the number of reduced protons relative to the number of oxidized metal centers, it must be assumed that methane formation is partially due to the addition of protons to an electron rich carbon species. For example, 1.882×10^{-3} moles of electrons are necessary to account for the number of moles

of methane and hydrogen that are evolved which far exceeds what is available from W, upon its oxidation, in particular, a sample containing 4.06×10^{-5} moles of $W(CO)_{6ads}$ evolved 4.40×10^{-5} moles of H_2 and 2.99×10^{-4} moles of CH_4. These data clearly establishes that W is not capable of supplying this many equivalents of electrons. This conclusion is based on the fact that six electrons are needed for each mole of methane that is generated. These claims are based on the premise that W is the only reductant present. The homogeneous reduction of CO to CH_4 has been reported by Shriver and coworkers (122,123) using homonuclear and heteronuclear metal carbonyls. In their mechanism, the carbonyl ligand is protonated twice followed by loss of water resulting in a coordinated carbide intermediate which undergoes subsequent protonation and the generation of methane. This mechanism offers an attractive analogy to what may be occuring on PVG in the respect that it illustrates that methane formation occurs through a combination of redox and acid-base reactions.
Subsequent studies by Whitmore and Shriver (123) have provided spectroscopic evidence for a new type of O-protonated carbonyl ligand, η^2-COH. This coordinated carbonyl hydride undergoes reduction in the presence of sufficient acid and electrons to form methane. These experiments suggest that the impurity present on PVG might be undergoing similar transformations, thus making plausible the contention that the impurity present on PVG is partially

reduced. Moreover, the introduction of an external carbinol source was accomplished by soaking a sample in CH_3OH prior to impregnation by the hexacarbonyl. The results determined for this experiment are illustrated in Figure 62. They show an overall rate enhancement for the methanation suggesting that a surface carbinol is a likely intermediate. These types of experiments were not investigated in more detail because of the deletorious effect methanol has on the gas chromatograph column.

The reduction of the carbon oxide impurity was attmpted by heating the glass, prior to adsorption, in a reducing atmosphere (H_2) at 600^oC. Analysis of the effluent following subsequent photolysis (Figure 49) displayed an initial induction period; however, prolonged photolysis led to the generation of a similar number of moles of gases as a piece that was not treated in this fashion, thus suggesting that the impurity was not reduced prior to impregnation.

Another interesting feature in the methanation reaction is the generation of CO_2. Mass spectral analysis has determined that it originates from the complex, i.e., when $W(^{13}CO)_6$ads is photolyzed a peak at m/e = 45 is present indicating that $^{13}CO_2$ is being generated. However, only a relatively small amount is generated when compared to the evolution of methane (Figure 48). Moreover, the rate of CO_2 is enhanced in the presence of low pressures of O_2 (Figure 48) suggesting that in a more powerful oxidizing environment the evolution of CO_2

Figure 62. Plot of CH_4 evolution for a sample treated with CH_3OH prior to impregnation of $W(CO)_6$. This figure illustrates the enhanced rate of CH_4 evolution versus a sample that was treated in a conventional fashion.

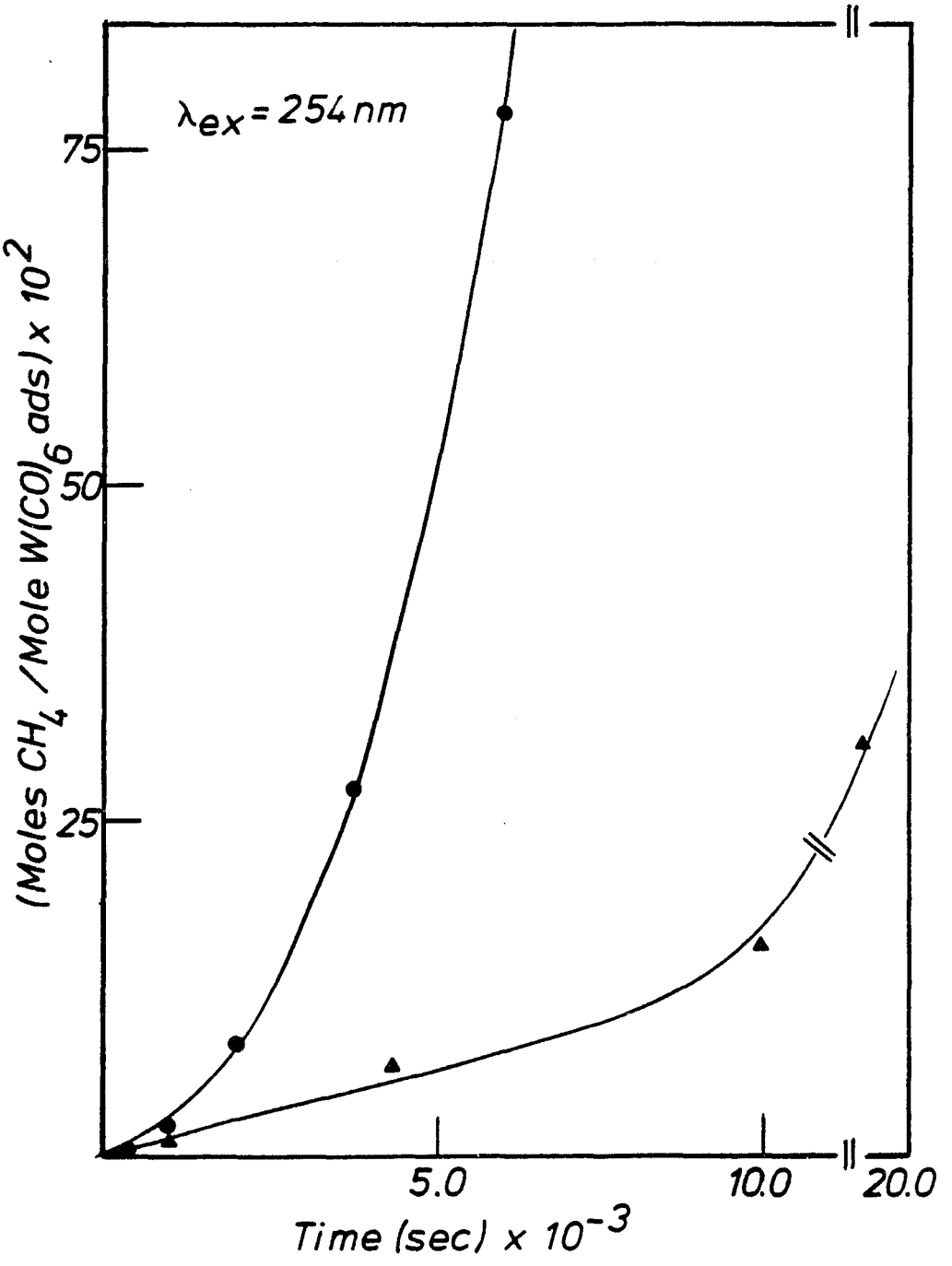

(▲) Treated in conventional manner.

(●) PVG treated with CH_3OH prior to impregnation.

might approach and even predominate over methane evolution. The classical mechanism for the methanation reaction, the Boudouard Reaction, equation 24,

$$2CO \longrightarrow C + CO_2 \qquad (24)$$

is not a likely mechanism because of the small amount of CO_2 that is evolved.

The results of the methanation reaction deviate significantly from that observed in the temperature programmed decomposition of $M(CO)_6$ bound to silica or alumina (12). When 3.183×10^{-7} moles of $W(CO)_6$ is bound to alumina and subjected to TPDE conditions 5.09×10^{-8} moles of CH_4 are evolved or the methane evolved/complex = 0.16, in our photochemical experiments a value of 11.39 is obtained. Another discrepancy is that in the TPDE of $M(CO)_6$/Alumina highly dehydroxylated supports appears to favor methane formation (12). Exactly the opposite behavior is observed in our photochemical experiments, i.e., highly hydroxylated supports lead to the greatest amount of methane evolution. The only aspect similar to the two sets of data is that a lower subcarbonyl, $M(CO)_4$ads or $M(CO)_3$ads, is a necessary prerequisite for the methanation reaction.

Bassett and Chauvin have reported (124) that when metal carbonyl clusters are supported on alumina and heated to 400°C in the presence of CO (0.380 atm), the molar ratio of CH_4/cluster is 13.3 for $Os_6(CO)_{18}$ and 10.7 for $Ir_4(CO)_{12}$. In the absence of CO the observed

ratios are 0.30 and 0.38, respectively. They concluded that the hydrogen necessary for the reduction of CO was derived from the surface water of the support. They observed higher order hydrocarbons in which the product distribution is determined by the nature of the cluster, the mode of impregnation, the nature of the support, and its water content. The photochemical results give, in the absence of CO, a molar ratio of methane/complex = 11.39 for a hydroxylated support, in accord with these systems (in the presence of CO).

In conclusion, a consistent picture has evolved which describes the methanation reaction. A full mechanistic explanation obviously requires further investigation. However, some conclusions can be drawn from the existing data. First, a subcarbonyl, $M(CO)_{4}ads$, must be generated presumably to coordinate the carbon oxide impurity so that subsequent proton transfer or reduction can take place. Second, methanation is mediated by a partially oxidized metal atom. Third, the hydrogens are derived from either adsorbed water or surface hydroxyls. Fourth, the impurity present on PVG is most likely a reduced carbonate species that is capable of forming a carbide that easily reacts with sufficient protons to form methane.

E. Catalytic Reactions.

Since our initial experiments illustrated an ability to generate $M(CO)_{5}ads$, its catalytic behavior was investigated. Current results indicate an ability to photocatalyze olefin hydrogenation and isomerization.

The catalyst, as prepared by impregnation, is simply supported $M(CO)_6$, but the photoinduced decarbonylation of this material in the absence of olefin or diene, for the times of photolysis where catalysis begins, has an average stoichiometry $M(CO)_{3ads}$ (see Chapter 3), as confirmed by gas chromatographic analysis of the effluent. In the presence of olefin or diene, the first step in the catalysis process is the absorption of substrate. This step has been confirmed spectrally. Subsequent loss of two or more carbon monoxide groups from the olefin or diene complex then generates the active catalyst. This suggests that the catalytic species is of the form $M(CO)_x(olefin)_{6-x}$ or $M(CO)_x(diene)_{6-x}$, where x is less than six and probably three or four.

The type and distribution of products offers some insight into the nature of the reaction. In the $Cr(CO)_6$ photocatalyzed hydrogenation of 1,3 butadiene in the presence of excess H_2, we observe that cis- and trans-2-butene are formed with a trans/cis = 0.13, when photolyzed for 126.0 minutes and thermolyzed for $\backsim$ 24 hours at 22.0 ^{o}C. Various other products were observed in the chromatogram, but, they were not identified. In view of the results reported by Brenner et al (12,22,23,24,26), for catalyzing similar substrates, we can assume that hydroformylation and metathesis reactions occur. Wrighton et al (78) have reported that the photolysis of

hexacarbonyls in fluid solution, yield catalysts which have a low activity for the hydrogenation of conjugated dienes (but not monolefins) at 25 °C, with a turnover frequency of 10^{-4} sec^{-1}. The low activity of the homogeneous catalyst is probably due to the dimerization of the active species (presumably a subcarbonyl species)(78). The dimerization is apparently suppressed in a supported system, e.g., $Cr(CO)_6$/alumina, which gives a much higher turnover frequency, in the hydrogenation of propylene, (N=0.08 sec^{-1} at 195°K(12). This frequency corresponds to the formation of 10^{-4} moles of product after 126.0 minutes of reaction. In the photochemical reaction, with adsorbed $Cr(CO)_6$ as a catalyst, after 126.0 minutes of photolysis, cis-2-butene was produced in a 25.14 % yield, corresponding to $\sim 10^{-4}$moles. Thermolysis of this reaction mixture afforded the previous mentioned products, i.e., trans-2-butene and higher order compounds. The yield of cis-2-butene went down dramatically (7.29%), substantiating our claim that cis-2-butene is reacting further to produce metathesis and hydroformylation products.

The photocatalyzed hydrogenation of cis-2-butene was examined by photolysis (λ_{ex}=350-nm) of $W(CO)_6$ads, in the presence of excess H_2, for 1087.0 minutes. Interestingly, no hydrogenation occurred, agreeing with what is reported for the homogeneous reaction (78,79). However, isomerization activity was observed, and gas chromatographic

analysis afforded a 13.4% and 3.7% yield of trans- and 1-butene respectively, as well as higher order compounds. Moreover, when subjected to thermolysis at 22 ± 1 °C for 24 hours, no change in the type and distribution of products was observed.

In the isomerization of 1-butene, catalyzed by $W(CO)_6$ads, cis- and trans-2-butene were generated with a trans/cis =5.71 along with other higher molecular weight compounds. Wrighton and coworkers (125) found that, using a polymer anchored iron carbonyl species, the photocatalyzed isomerization of 1-pentene in benezene, after 12 hours of near-UV photolysis, the trans/cis ratio of 2-pentene was was 2.6. Reichel and Wrighton have reported (56,57) that when $Co(CO)_4$ is bound chemically to a functionalized silca surface, in the presence of 1:1 mixture of 1-pentene: Et_3SiH, the photocatalyzed isomerization of 1-pentene to trans- and cis-2- pentene occurs with a trans/cis ratio of 4.45 (after 120.0 minutes of photolysis at 355nm). Subsequent thermolysis at 25°C did not change the type and distribution of products.

In conclusion, the hybrid systems described here possess the ability to catalyze the isomerization and hydrogenation of olefins and dienes, respectively.

References

1. Cotton, F.A.; Wilkinson, G. "Advanced Inorganic Chemistry," Interscience, New York, 3rd ed., 1972, Chapter 24, p.770.
2. Nakamura, A.; Tsutsui, M, "Principles and Applications of Homogeneous Catalysis," Wiley, New York, 1980.
3. G.W. Parshall, "heterogeneous Catalysis, Homogeneous Catalysis," Wiley, New York, 1980.
4. Wender, I.; Pino, P. "Organic Synthesis via Metal Carbonyls," Interscience, New York, 1968.
5. "Transition Metal Mediated Organic Synthesis," D.W. Slocum and O.R. Hughes, Eds., Ann. N.Y. Acad. Sci., (1980), Vol. 53.
6. Bailey, D.C.; Langer, S.H. Chem. Revs., 1981, 81, 109.
7. A "traditional" catalyst is made by impregnation with an aqueous solution of the appropriate metal salt followed by calcination and reduction.
8. Collman, J.P.; Reed, C.A. J. Am. Chem. Soc. 1973, 95, 2048.
9. Howe, R.F. Inorg. Chem. 1976, 15, 486.
10. Brenner, A.; Hucul, D.A. Prepr. Div. Petrol. Chem., Am. Chem. Soc. 1977, 22, 1221.
11. Kazusaka, A.; Howe, R.F. J. Catal. 1980, 63, 447.
12. Brenner, A.; Hucul, D.A. Hardwick, S.J. Inorganic Chem. 1979, 18, 1478.
13. Howe, R.F. J. Chem. Soc., Faraday Trans. 1 1975, 71, 1689.
14. Banks, R.L. U.S. Patent 3 463 827, 1969;

Chem Abstr. 1971, 75, 151339s

15. Banks, R.L. Belgian Patent 633418, 1963;
Chem. Abstr. 1964, 61, 1690e.

16. Howe, R.F.; Davidson, D.E.; Whan, D.A.
J. Chem. Soc., Faraday Trans. 1 1972, 68, 2266.

17. Yermakov, Y.I. Catal. Rev.-Sci. Eng. 1976, 13 77.

18. Smith, J.; Howe, R.F.; Whan, D.A. J. Catal.
1974, 34, 191.

19. Davie, E.S.; Whan, D.A.; Kemball, C. Chem. Commun.
1969, 1430.

20. Whan, D.A.; Barber, M.; Swift, P. J. Chem. Soc.,
Chem Commun. 1972, 198.

21. Howe, R.F.; Leith, I.R. J. Chem. Soc.,
Faraday Trans. 1 1973, 69, 1967.

22. Brenner, A.; Burwell, R.L. Jr. J. Am. Chem.
Soc. 1975, 97, 2565.

23. Burwell, R.L. Jr.; Brenner, A. J. Mol. Catal.
1975/1976, 1, 77.

24. Burwell, R.L. Jr.; Brenner, A. In "Catalysis
Heterogeneous and Homogeneous"; Delmon, B.
Jannes, G. Eds.; Elsevier: New York, 1975; p. 157.

25. Adams, D.M.; Gardner, I.R.; Parkyns, N.D.
J. Catal. 1976, 45, 145.

26. Brenner, A.; Burwel, R.L. Jr. J. Catal. 1978, 52, 353.

27. (a) Banks, R.L.; Bailey, G.C. Ind. Eng.
Chem. Prod. Res. Dev. 1964, 3, 170.
(b) Banks, R.L. Prepr., Div. Petrol. Chem.,

Am. Chem. Soc. 1979, 24, 399.

28. Davie, E.S.; Whan, D.A.; Kemball, C. J. Catal. 1972, 24, 272.

29. Brenner, A. J. Mol. Catal. 1979, 5, 157.

30. Alper, H.; Blais, C. J. Chem. Soc., Chem. Commun. 1980, 169.

31. Alper, H.; Patee, L. J. Org. Chem. 1979, 44, 2568.

32. Brenner, A.; Hucul, D.A. Sixth North American Meeting of the American Catalysis Society; Chicago, 1979; Abstract G 11.

33. Brenner, A.; Hucul, D.A. J. Catal. 1980, 61, 216.

34. Bowman, R.G.; Burwell, R.L., Jr. J. Catal. 1980, 63, 463.

35. Bilhou, J.L.; Theolier, A.; Smith, A.K.; Bassett, J.M. J. Mol. Catal. 1977/78, 3, 245.

36. Brenner, A.; Hucul, D.A. J. Catal. 1980, 61, 216.

37. Olsthoorn, A.A.; Moulijn, J.A. J. Mol. Catal. 1980, 8, 147.

38. (a) Heckelsberg, L.F. French Patent 1 562 396, 1969; Chem. Abstr. 1969, 71, 93357a. (b) Heckelsberg, L.F. South African Patent 68 01 707, 1968; Chem. Abstr. 1969, 70, 67557a.

39. Heckelsberg, L.F. French Patent 1 562 397, 1969; Chem. Abstr. 1969, 71, 93358b.

40. Heckelsberg, L.F. South African Patent 68 01 878, Chem. Abstr. 1969, 70, 67559c.

41. Wrighton, M.S. Chem Revs., 1974, 74, 401.

42. G.L. Geoffroy and M.S. Wrighton, "Organometallic Photochemistry," Academic Press, New York, 1979.

43. Elmer, T.H.; Fehlner, A. Corning Glass Company,

private communications, 1977 and 1978.

44. Elmer, T.H.: et. al. J. Amer. Ceram. Soc., 1970, 53, 171.

45. Sakairo; T. Hyomen 1971. 9, 115.

46. Pierce Chemical Co., Rockford Ill., General Catalogue (1976-1977), p. 215.

47. Spatorico, A.L. J. Appl. Polym. Sci. 1975, 12, 1601.

48. R.K. Iler, "The Chemistry of Silica," Wiley-Interscience, New York, 1979, p. 551.

49. Hockey, J.A. Chem. Ind. (London), 1965, 57.

50. Davydov, V.Y. Trans. Faraday Soc. 1964, 60, 2254; Russ. J. Phys. Chem. 1964, 38, 1108.

51. Kiselev, A.V. "The Structure and Properties of Porous Materials," D.H. Everett and F.S. Stone, Eds. Butterworth, London 1958, p. 195.

52. (a) Janowski, V.F.; Heyer, W. Z. fur Chemie 1979, 19, 1. (b) All, K.G. J. Organomet. Chem. 1975, 87, 203.

53. Jackson, R.L.; Trusheim, M.R. J. Am. Chem Soc. 1982, 104, 6590.

54. Liu, D.K.; Wrighton, M.S. J. Am. Chem. Soc. 1982, 104, 898.

55. Kinney, J.B.; Staley, R.H.; Reichel, C.L.; Wrighton, M.S. J. Am. Chem. Soc. 1981, 103, 4273.

56. Reichel, C.L.; Wrighton, M.S. J. Am. Chem. Soc. 1981, 103, 7180.

57. Reichel, C.L.; Wrighton, M.S. Inorg. Chem. 1980, 19, 3858.

58. Klein, B.; Kazlauskas, Romas, J.; Wrighton, M.S. Organometallics 1982, 1, 1338.

59. Beach, N.A.; Gray, H.B. J. Am. Chem. Soc. 1963, 85, 2922.

60. Beach, N.A.; Gray, H,B. J. Am. Chem. Soc. 1968, 90, 5713.

61. (a) Kelly, J.M.; Hermann, H.; Koerner von Gustorf, E.A. IUPAC Symposium on Photochemistry, Baden-Baden, Germany, 1972, Paper No. 34, p. 119 of the Manuscripts of Contributed Papers; (b) Kelly, J.M.; Hermann, H.; Koerner von Gustorf, E.A. Chem. Commun. 1973, 105.

62. Figgis, B.N. "Introduction to Ligand Fields," Wiley, New York, N.Y., 1966, p. 158.

63. Wrighton, M.S.; Gray, H.B.; Hammon, G.S. Mol. Photochem. 1973, 5, 165.

64. (a) Reference 62. pp. 234-237; (b) Cotton, F.A. "Chemical Applications of Group Theory," 2nd ed. Wiley, New York, N.Y. 1971, 363, pp. 260-263.

65. Wrighton, M.S.; Hammond, G.S.; Gray, H.B. J. Am. Chem. Soc. 1971, 93, 4336.

66. Wrighton, M.S.; Hammond, G.S.; Gray, H.B. Inorg. Chem. 1972, 11, 3122.

67. Wrighton, M.S. Ph.D. Thesis, California Institute of Technology, 1972.

68. Graham, M.A.; Rest, A.J.; Turner, J.J. J. Organomet. Chem. 1970, 24, C54.

69. Graham, M.A.; Poliakoff, M.; Turner, J.J. J. Chem. Soc. A 1971, 2939.

70. Perutz, R.N.; Turner, J.J. J. Am. Chem. Soc. 1975, 97, 4791.

71. Turner, J.J.; Burdett, J.K.; Perutz, R.N.; Poliakoff, M.A. Pure Appl. Chem, 1977, 49, 271.

72. Wrighton, M.S.; Morse, D.L. J. of Organomet. Chem. 1975, 97, 405.

73. Lees, A.J.; Manuta, D.M. Inorg. Chem. 1983, 22, 572.

74. (a) Saito, H.; Fujita, J.; Saito, K. Bull. Chem. Soc. Jpn. 1968, 41, 359-364.
(b) Saito, H.; Fujita, J.; Saito, K. Ibid. 1968, 41, 549-550.

75. (a) McHugh, Terence, M.; Narayanaswamy, Ramaler; Rest, A.J.; Salisbury, Kingsley J. Chem. Soc. Chem. Commun. 1979, 208.

75. (b) Rest, A.J.; Sodeau, J.R. J.C.S. Faraday II 1973, 73, 1691.

76. Massey, A.G.; Orgel, L.E. Nature (London) 1961, 191, 1387.

77. (a) Stolz, I.W.; Dobson, G.R., Sheline, R.K. J. Am. Chem. Soc. 1962, 84, 3589. (b) ibid., 1963, 85, 1013.

78. Wrighton, M.S.; Ginley; D.S.; Schroeder, M.A.; Morse, D.L. Pure Appl. Chem. 1975, 41, 671.

79. (a) Wrighton, M.S.; Hammond, G.S.; Gray, H.B. J. Organometal. Chem. 1974, 70, 283: (b) Wrighton, M.S.; Hammond, G.S.; Gray, H.B. J. Am. Chem. Soc. 1970, 92, 6068: 1971, 93, 3285.

80. Wrighton, M.S.; Schroeder, M.A. J. Am. Chem. Soc. 1973, 95, 5764.

81. Nasielski, J.; Kirsch, P.; Wilputte- Steinert L. J. Organometal. Chem. 1971, 27, C13.

82. Wrighton, M. Inorg. Chem. 1974, 13, 905.

83. Matthews, C.N.; Magee, T.A.; Wotiz, J.H. J. Am. Chem. Soc. 1959, 81, 2273.

84. Magee, T.A.; Matthews, C.N.; Wang, T.S.; Wotiz, J.H. J. Am. Chem. Soc. 1961, 83, 3200.

85. Gibson, D.H.; Ahmed, F.U.; Philips, K.R. Organometallics, 1982, 1, 679.

86. Hayter, R.G. J. Am. Chem. Soc. 1966, 88, 4376.

87. Darensbourg, M.Y.; Slater, S. J. Am. Chem. Soc. 1981, 103, 5914.

88. (a) Stiddard, M.H.B. J. Chem. Soc. 1962, 4712.
(b) Dobson, G.R.; Stolz, I.W.; Sheline, R.K. Adv. Inorg. Chem. Radiochem. 1966, 8, 1.
(c) Abel, E.W.; Bennett, M.A.; Wilkinson, G. J. Chem. Soc. 1959, 2323.
(d) Heiber, W.; Muhlbauer, F. Z. Anorg. Allg. Chem. 1935, 22, 337.

89. (a) Angelici, R.J.; Jacobson, S.E.; Ingemanson, C.M. Inorg. Chem. 1968, 7, 2466.
(b) Angelici, R.J.; Graham, J.R., ibid., 1967, 6, 988.

90. Ciapetta, F.G.; Plank, C.J. In "Catalysis"; Emmett, P.H., Ed.; Reinhold: New York, 1954; Vol. 1, p. 315.

91. Higginson, G.W. Chem. Eng. (N.Y.) 1974, 81(20), 98.

92. Innes, W.B. In "Catalysis"; Emmett, P.H., Ed., Reinhold: New York, 1954; Vol. 1, p. 245.

93. (a) Hatchard, C.G.; Parker, C.A. Proc. Roy. Soc. Ser. A.
(b) Hatchard, C.G.; Parker, C.A., ibid., 1956, 235, 518.

(c) Calvert, J.G.; Pitts, J.N. "Photochemistry," New York: Wiley, 1971.

94. Kennely, T., Ph.D. Thesis, City University of New York, June, 1980.

95. Wolfgang, S.W.; Gafney, H.D. J. Phys. Chem., in press.

96. Kennely, T.; Gafney, H.D. J. Inorg. and Nucl. Chem. 1981, 43, 2988.

97. Ross, S.; Olivier, J.P. "On Physical Adsorption," Wiley-Interscience, New York, 1964, Chapter 2, Section 1, p. 31.

98. Simon, R.C.; Gafney, H.D. Inorg. Chem. 1983, 22, 573.

99. Goonatillake, H.W.; Gafney, H.D. Unpublished Results.

100. (a) Colton, R.; Rix, C.J. Aust. J. Chem. 1969, 22, 305.
(b) Schid, G.; Bose, R.; Wolz, E. Chem. Ber. 1975, 108, 26.
(c) Hayter, R.G. J. Am. Chem. Soc. 1966, 88, 4376.

101. Darensbourg, D.J.; Rokicki, A. J. Am. Chem. Soc. 1982, 104, 349.

102. Nozik, A.J. Ann. Rev. Phys. Chem. 1978, 29, 189-222.

103. Gray, H.B.; Harris, D.C. J. Am. Chem. Soc. 1975, 97, 3073.

104. Young, D.M.; Crowell, A.D., "Physical Adsorption of Gases" Butterworths, London (1962).

105. (a) Elovich, S. Yu; Zhabora, G.M. Zh. Fix. Khim. 1939, 13, 1761.
(b) Taylor, H.A.; Thon, N. J. Am. Chem. Soc. 1952, 74, 4169.

106. Adams, D.M.; Fernando, W.S.; Hooper, M.A.

J. Chem. Soc. Dalton 1973, 2264.

107. Jones, L.H. Spectrochim. Acta 1963, 19, 329.

108. Navon, G.; Sutin, N. Inorg. Chem. 1974, 13, 2159.

109. Snyder, L.R.; Ward, J.W. J. Phys. Chem. 1966, 70, 3941.

110. Mouks, C.C.; Ellis, B. J. Colloid and Interf. Sci. 1973, 44, 37.

111. Zingaro, R.A.; Witmer, W.B. J. Phys. Chem. 1960, 64, 1705.

112. Atwood, J.D.; Brown, T.L. J. Am. Chem. Soc. 1976, 98, 3160.

113. Strohmeier, W.; Gerlach, K. Chem. Ber. 1961, 94, 398.

114. Nasielski, J.; Colas, A. J. of Organometal. Chem. 1975, 101, 215.

115. Langmuir, I. J. Am. Chem. Soc. 1918, 40, 1361.

116. Brunhauer, S. "The adsorption of Gases and Vapors," Vol. 1, Princeton University Press, Princeton, New Jersey, 1945.

117. Lees, A.J.; Adamson, A.W. Inorg. Chem. 1981, 20, 4381.

118. Garner, F.S.; Stone,, F.S.; Tiley, P.F. Proc. R. Soc. A 1952, 211, 472.

119. Dell, R.M.; Stone, F.S. Trans Faraday Soc. 1954, 50, 501.

120. Rudham, R.; Stone, F.S. in "Chemisorption," W.E. Garner, Ed., Butterworths, London (1957) p. 205.

121. Chatt, J. J. Organometal. Chem. 1975, 17, 100.

122. Drezdou, M.A.; Whitmire, K.H.; Bhattacharyya, A.A.; Hsu, W.L.; Nagel, C.C.; Shore, S.G.; Shriver, D.F. J. Am. Chem. Soc. 1982, 104, 5630.

123. Whitmire, K.H.; Shriver, D.F. J. Am. Chem. Soc. 1981, 103, 6754.

124. Smith, A.K.; Theolier, A.; Basset, J.M.; Ugo, R.; Chauvin, Y.; Commereuc, D. J. Am. Chem. Soc. 1978, 100, 2590.

125. Sanner, R.D.; Austin, R.G.; Wrighton, M.S.; Honnick, W.D.; Pittman, C.U., Jr. Inorg. Chem. 1979, 18, 928.

126. (a) Cotton, F.A. "Quadruple Bonds and Other Multiple Metal to Metal Bonds," Chem. Soc. Rev. 1975, 4, 27.
(b) Cotton, F.A. "Discovering and Understanding Multiple Metal-to-Metal Bonds," Acc. Chem. Res. 1978, 11, 226.

127. Wrighton et al. J. Am. Chem. Soc. 1976, 98, 4105.

128. Mitteilung, K. Z. Phys. Chem. 1961, 27, 439.

129. Simon, R.C.; Gafney, H.D., unpublished observations.

130. Cais, M.; Lundquist, R.T. J. Org. Chem. 1962, 27, 1167